AD_____

Award Number: W81XWH-06-1-0034

TITLE: Prostate Cancer in African-American Men: Serum Biomarkers for Early Detection Using Nanoparticles

PRINCIPAL INVESTIGATOR: Catherine M. Phelan, M.D., Ph.D.

CONTRACTING ORGANIZATION: Moffitt Cancer Center,
Tampa, Florida, 33612-9497

REPORT DATE: November 2009

TYPE OF REPORT: FINAL

PREPARED FOR: U.S. Army Medical Research and Materiel Command
Fort Detrick, Maryland 21702-5012

DISTRIBUTION STATEMENT:

☒ Approved for public release; distribution unlimited

REPORT DOCUMENTATION PAGE

Form Approved
OMB No. 0704-0188

1. REPORT DATE	2. REPORT TYPE	3. DATES COVERED
01-11-2009	**FINAL**	*1 NOV 2005 - 31 OCT 2009*

4. TITLE AND SUBTITLE
Prostate Cancer in African-American Men: Serum Biomarkers for

Early Detection Using Nanoparticles

5a. CONTRACT NUMBER

5b. GRANT NUMBER
W81XWH-06-1-0034

5c. PROGRAM ELEMENT NUMBER

6. AUTHOR(S)
Catherine M. Phelan, MD, PhD (PI)

5d. PROJECT NUMBER

5e. TASK NUMBER

5f. WORK UNIT NUMBER

7. PERFORMING ORGANIZATION NAME(S) AND ADDRESS(ES)

Moffitt Cancer Center

Tampa, FL 33612-9497

8. PERFORMING ORGANIZATION REPORT

9. SPONSORING / MONITORING AGENCY NAME(S) AND ADDRESS(ES)

US Army Medical Research and
Fort Detrick,
Maryland 21702-5012

10. SPONSOR/MONITOR'S ACRONYM(S)

11. SPONSOR/MONITOR'S REPORT NUMBER(S)

12. DISTRIBUTION / AVAILABILITY STATEMENT
Approved for public release; distribution unlimited

13. SUPPLEMENTARY NOTES

14. ABSTRACT We have collected blood samples from 65 African-American men with prostate cancer and 80 ethnically-matched control healthy men with questionnaire data on demographics, general health and cancer family history. We chose six biomarkers PSA, KLK2, KLK14, IL6, CAV-1, anti-p53 antibody and OPG as candidates for improved early detection of prostate cancer in plasma from the African American men with and without prostate cancer. We had technical problems with KLK2 and KLK14. Furthermore despite their biological pausability, anti-p53 levels were higher in controls than cases and OPG and CAV-1 showed similiar levels in cases and controls. Therefore only PSA was shown to be a suitable consistent biomarker. The use of nanoscale materials and devices has enhanced the lower limits of detection of proteins and other compounds in plasma and tissues. We have investigated using nanoparticles or quantum dots conjugated to proteins of interest for early cancer detection. Although sub-ELISA levels of proteins were detected, this technology is somewhat cost-prohibitive and not very robust. So we developed a gold nanowire biosensor surface with electrochemical detection on which the PSA antibody is immobilized, We proved the efficiency and sensitivity of this new biosensor for early prostate cancer detection. This study has laid the groundwork to make an impact in early prostate cancer detection through essential investigation into emerging cutting-edge technologies. In the future, the utilization of the gold nanowire microfluidic devices will impact early prostate cancer detection with more appropriate biomarkers.

15. SUBJECT TERMS
African-American, prostate cancer, biomarkers

16. SECURITY CLASSIFICATION OF: U			17. LIMITATION OF ABSTRACT	18. NUMBER OF PAGES	19a. NAME OF RESPONSIBLE PERSON USAMRMC
a. REPORT	b. ABSTRACT	c. THIS PAGE	UU	62	19b. TELEPHONE NUMBER *(include area code)*
U	U	U			

Table of Contents

Page

A. Introduction

In this study we set up a prostate cancer case-control study in order to develop new serum biomarkers for early detection of prostate cancer using Nanotechnology. In early prostate cancer when there are very few cells, we expect trace serum levels of proteins. Recent advances in nanotechnology mean that target biomarkers of prostate cancer can be conjugated to quantum dots, thereby enhancing detection characteristics and making it possible to detect very low levels of a particular protein (1-9). We collected blood samples from 65 African-American men with prostate cancer and 70 ethnically-matched control healthy men with questionnaire data on demographics, general health and cancer family history to investigate prostate cancer risk factors. Our Aims were to investigate emerging nanotechnologies for their use in early detection of prostate cancer in African American men and to test six biologically plausible candidate biomarkers. We have investigated the QD-conjugated serum biomarkers in a multiplex panel. However, we have found this technology to be cost-prohibitive when moving from the test samples to a larger sample population. We tested six antibodies as potential biomarkers. At the end of this project we have determined that the most suitable biomarker is still PSA. The most optimal and cost-effective nanotechnology was to conjugate the PSA antibody onto gold nanowire encased microfluidic devices which can detect sub-ELISA levels of PSA. This project is essential in terms of expanding research on the African American populations and vital to improve early detection of prostate cancer so as to reduce the dismal mortality rate. However, additional biomarkers must be identified to enhance specificity and sensitivity of early detection of prostate cancer. This study has shown that the technology is available for enhanced detection. This technology will translate rapidly to other cancer sites for which no good screening test is available.

B. Body

Task 1. To collect pre-treatment serum samples from a cohort of African-American undergoing screening for prostate cancer (Months 1-26 according to the Timeline in the Statement of Work)

1.1. Recruitment

Approach: In this study prostate cancer cases are defined as African American men with biopsy-proven prostate cancer. Controls are African American men with a PSA< 2.5ng/ml and no other evidence of prostate cancer by DRE or biopsy. Our case-control collection was slow but we have collected 65 African-American men with prostate cancer and 90 African-American controls into this study. Once consent was obtained, the participants were asked to fill in a short research questionnaire and two blood samples (10 ml each) were drawn. Recruitment took place at Lifetime Cancer Screening at the H. Lee Moffitt Cancer Center and Research Institute and Moffitt Cancer Center Hospital, the Radiation Oncology clinics in Tampa and Brandon and the 30th Street Clinic. All samples were transferred to the Tissue Procurement and the LCS laboratory at the H. Lee Moffitt Cancer Center and Research Institute and processed for serum and DNA, respectively, where they are stored. Original consents (Appendix) and questionnaires (Appendix) are stored in a locked cabinet in a locked office. The questionnaire data collected is scanned into an Access database by the Survey Methods Core. The risk factor database will be linked with the laboratory database, both are in Access.

Table 1: Section of the Access database regarding Decision Making

		%risk as perceived by patient		Decision making, page 13, top									
				I decide		I decide, doc opinion matters		Both decide		Doc decides, my opinion matters		Doc decides	
	N	Mean	Std	N	ColPctN	N	ColPctN	N	ColPctN	N	ColPctN	N	ColPctN
All patients	110	29.74	33.20	19	100.00	35	100.00	42	100.00	11	100.00	3	100.00
marital													
	1	50.00	.	.	.	.	.	1	2.38	.	.	.	.
A)married/cohabit	72	26.12	31.45	10	52.63	27	77.14	25	59.52	8	72.73	2	66.67
B)not married/cohabit	37	35.23	36.11	9	47.37	8	22.86	16	38.10	3	27.27	1	33.33
DM_Educ													
<6th grade	1	.	.	.	.	.	.	1	2.38	.	.	.	.

		%risk as perceived by patient		Decision making, page 13, top									
				I decide		I decide, doc opinion matters		Both decide		Doc decides, my opinion matters		Doc decides	
	N	Mean	Std	N	ColPctN	N	ColPctN	N	ColPctN	N	ColPctN	N	ColPctN
6-8	2	0.00	0.00	.	.	1	2.86	1	2.38	.	.	.	.
9-10	6	12.50	25.00	3	15.79	1	2.86	2	4.76	.	.	.	.
11-12	25	18.56	16.76	.	.	6	17.14	14	33.33	4	36.36	1	33.33
GED or equivalent	13	37.70	40.30	2	10.53	2	5.71	7	16.67	1	9.09	1	33.33
Vocational school	30	31.63	37.95	3	15.79	15	42.86	8	19.05	3	27.27	1	33.33
Some college	22	27.12	25.37	9	47.37	4	11.43	6	14.29	3	27.27	.	.
Graduated college	10	49.38	40.22	2	10.53	5	14.29	3	7.14	.	.	.	.
Post grad or prof. school	1	100.00	.	.	.	1	2.86	.	.	.	.	.	.
Has a DRE been recommended?													
No	21	31.80	30.56	3	15.79	4	11.43	9	21.43	3	27.27	2	66.67
yes	89	29.46	33.74	16	84.21	31	88.57	33	78.57	8	72.73	1	33.33
Has a PSA been recommended?													
.	1	50.00	.	.	.	.	.	1	2.38	.	.	.	.
no	14	52.83	40.38	2	10.53	3	8.57	6	14.29	3	27.27	.	.
yes	86	28.10	33.30	17	89.47	30	85.71	29	69.05	7	63.64	3	100.00
Don’t know	9	23.00	21.21	.	.	2	5.71	6	14.29	1	9.09	.	.
Do you have BPH													
no	70	28.54	30.40	12	63.16	17	48.57	29	69.05	9	81.82	3	100.00
yes	38	32.07	38.26	7	36.84	17	48.57	12	28.57	2	18.18	.	.
Don’t know	2	25.00	35.36	.	.	1	2.86	1	2.38	.	.	.	.
Have you had a biopsy													
no	68	32.33	30.11	9	47.37	17	48.57	30	71.43	10	90.91	2	66.67
yes	42	25.91	37.47	10	52.63	18	51.43	12	28.57	1	9.09	1	33.33
Have you had prostatitis													
no	100	27.76	31.78	14	73.68	31	88.57	41	97.62	11	100.00	3	100.00
yes	10	44.00	41.15	5	26.32	4	11.43	1	2.38	.	.	.	.
History of cancer													
no	101	26.97	30.28	17	89.47	31	88.57	40	95.24	10	90.91	3	100.00
yes	9	52.22	47.64	2	10.53	4	11.43	2	4.76	1	9.09	.	.
Family history of cancer													
no	61	24.44	29.71	9	47.37	17	48.57	28	66.67	5	45.45	2	66.67
yes	47	39.26	36.92	9	47.37	17	48.57	14	33.33	6	54.55	1	33.33
Don’t know	2	0.00	.	1	5.26	1	2.86	.	.	.	.	.	.
Family history of female cancer													
no	84	27.22	30.80	12	63.16	25	71.43	37	88.10	7	63.64	3	100.00
yes	24	41.00	40.35	6	31.58	9	25.71	5	11.90	4	36.36	.	.

		%risk as perceived by patient		Decision making, page 13, top									
				I decide		I decide, doc opinion matters		Both decide		Doc decides, my opinion matters		Doc decides	
	N	Mean	Std	N	ColPctN	N	ColPctN	N	ColPctN	N	ColPctN	N	ColPctN
Don't know	2	0.00	.	1	5.26	1	2.86	.	.	.	.	.	.
Family history breast cancer													
no	101	29.89	32.66	17	89.47	32	91.43	39	92.86	10	90.91	3	100.00
yes	9	28.14	41.40	2	10.53	3	8.57	3	7.14	1	9.09	.	.
Family history male cancer													
no	77	25.31	31.10	13	68.42	21	60.00	34	80.95	7	63.64	2	66.67
yes	31	44.75	36.00	5	26.32	13	37.14	8	19.05	4	36.36	1	33.33
Don't know	2	0.00	.	1	5.26	1	2.86	.	.	.	.	.	.
Family history prostate cancer													
no	97	27.86	32.78	15	78.95	29	82.86	41	97.62	9	81.82	3	100.00
yes	13	45.00	34.55	4	21.05	6	17.14	1	2.38	2	18.18	.	.
Psa Value													
	14	27.09	23.72	2	10.53	2	5.71	8	19.05	2	18.18	.	.
A)<=4	77	33.05	34.96	13	68.42	25	71.43	29	69.05	7	63.64	3	100.00
B)>4	19	18.36	31.21	4	21.05	8	22.86	5	11.90	2	18.18	.	.
Number of PSA in 5 years													
	29	41.06	33.06	2	10.53	8	22.86	13	30.95	5	45.45	1	33.33
A)<=5	71	25.65	32.43	15	78.95	23	65.71	26	61.90	5	45.45	2	66.67
B)>5	10	31.50	36.06	2	10.53	4	11.43	3	7.14	1	9.09	.	.
Number of DRE in 5 years													
	20	37.71	32.47	4	21.05	6	17.14	7	16.67	1	9.09	2	66.67
A)<=4	58	28.42	33.89	5	26.32	19	54.29	27	64.29	6	54.55	1	33.33
B)>4	32	27.48	32.99	10	52.63	10	28.57	8	19.05	4	36.36	.	.

1.1. Summary: Task 1: Recruitment was slow and we reached 65 prostate cancer cases and 70 controls in the timeframe of the award. Completed.

Task 2. To engineer a panel of quantum dot (QD) – antibody (AB) conjugates targeting established prostate cancer biomarkers (antigens). (Months 2-10 in the Timeline in the Statement of Work).

Approach: The experimental luminescent QDs will be composed of surface passivated II-VI semi-conductors such as ZnS, CdS, ZnSe, CdSe, or CdTe and their core/shell structures, e.g. CdSe/ZnS, CdTe/CdS, or CdS/ZnS. We targeted QDs to cover emission in the broad visible to infrared spectral range to achieve optimal spectral performance. The QDs will be directly conjugated to antibodies to the selected prostate cancer biomarkers: Prostate Specific Antigen (PSA), Kallikrein 2 (KLK2), Kallikrein 14 (KLK14), Osteoprotegerin (OPG), Anti p53Ab, Caveolin-1 (Cav-1) and Interleukin-6 (IL-6), with or without linker molecules, depending on the molecular structure of each antibody.
We purchased antibodies (multiple times) for the above biomarkers. Previously, standard curves were determined for each antigen/antibody using ELISA kits (CanAg, CA, USA; Figure 1). The lower limit of detection for this technique was approximately <0.1ug/l (Figure 2). Therefore we determined that the antibodies were detecting the chosen biomarker. We

have successfully conjugated antibodies to the above biomarkers to quantum dots and we have gone ahead and are characterizing them according to Task 3 below.

2.1. ELISA standard procedure.
In order to compare the QD PSA ELISA results with the established, commercially available ELISA, the regular ELISA was run with a PSA detection kit supplied by CanAg (CanAg PSA EIA 340-10). The methods sensitivity, claimed by the vendor, is above 0.1 ng/ml. The main stages of the procedure are shown on Figure 1. The method employs a classic "sandwich" ELISA principle, where the optical detection is based on the Horseradish peroxidase (HRP) enzyme, cleaving the substrate, yields to the change of color. Commercial kit includes 96 precovered with the PSA coating Antibody wells, to which the samples (PSA antigens) are added, following with the addition of detecting PSA Antibody, conjugated to HRP. Next, the substrate is added, following with the stopping solution addition, and absorbance reading at 450nm (Figure 2). All samples were run in duplicates and the results are the averages of the two. The reading was performed using a Synergy™ HT Multi-Mode Microplate Reader supplied by BioTek, at 450nm.

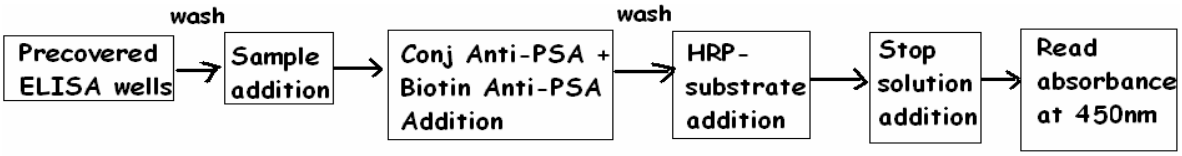

Figure 1: The brief schematic of the CanAg EIA procedure

On the Fig.2 the results of commercial ELISA are shown. As expected, among the plasma samples 0.013 and 0.093 ng/ml were undetectable (Fig 2A), as well as the whole range of the AG dilutions in PBS (Fig 2B). According to our results, 0.1ng/ml and below were undetectable in both the serum and AG dilutions samples which is in an agreement with the claimed method threshold.

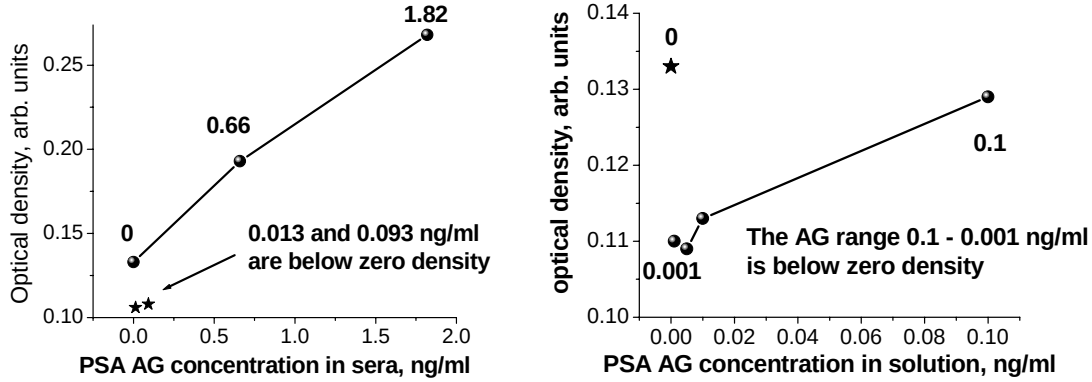

A B

Figure 2: CanAg PSA AG detection limits: A – in sera samples; B – in AG solution in PBS.

2.1. Summary: Task 2 completed

Task 3. To define the photoluminescence signatures of bound versus unbound QDs created in Aim 2, reflecting antigen-antibody complex formation. (Months 11-25 according to the Statement of Work)
Approach: High-resolution photoluminescence (PL) spectroscopy will be used to analyze antibodies and QDs separately before and then after they have been conjugated. This permits the identification of unique spectral signatures, and is based on standard PL descriptors such as: PL peak position at 400nm – 1,700nm spectral range, full width at half maximum (FWHM) of the PL band, optical/acoustic phonon frequencies, excitation wavelength dependence (different

laser sources), light polarization, te mperature quenching, a nd PL quantum eff iciency. From the PL de scriptors of th e optimized AB-QD conjugates we will ge nerate a calibration curve of the PL in tensity versus con centration of the conjugated QDs in seru m/plasma. This allows determination of the sensitivity li mit of the QD luminescence diagnostics, limits of concentration linearity and dynamic range.

3.1. Our goal was to identi fy a sensitive and specific panel of biomarkers employing reproducible and robust technol ogy at a r easonable cost so it can be applie d as a screening test to the general po pulation. W e extensively investigated the chemistry of bound versus unbound QDs in ten way s: 1. ELISA (Sections 3.1.1 and 3.1.2, Figures 3 a nd 4; table 2) ; 2. Different types of QDs (Section 3.1.3, table 3); 3. Same AB, different QDs (Section 3.1.3, table 3); 4. Same QD, different Abs (Section 3.1. 3, Fi gure 5, table 3); 5.Storage ti me (as low as 30m inutes and up to se veral months) (Section 3. 1.4, Figure 6); 6. Tem perature (as high as 250C and as low as 0C) (Section 3.1. 5, Figures 7 and 8); 7. Spectral mapping (Section 3.1. 6, Figures 9- 11, table 4); 8. Gel electrophoresi s (Section 3.1 .7, F igures 12 an d 13); 9. 'Ho me-made' QDs (section 3.1.3, table 2); 10. Ultrasonication (section 3. 1.8, Figure 14); 11. Vario us drying substrates (Si, ru bber, SiC and quarz) (secti on 3.1.9, Figures 15 and 16); 12. Various am biences (vacuum, argon, nitrogen and oxygen, increased moisture) (section 3.1.10, Figure 17); 13. TEM measurements (section 3.1.11, Figures 18 and 19).

We published a paper on the application of the b io-conjugated quantum dots (QDs) for "sandwich" enzyme linked immunosorbent assay (ELISA) (Chornokur et al. *Superlattices and Microstructures*, 2008). QD-ELISA can detect PSA antigen at concentrations as low as 0.01ng/m l w hich is ~50 times lower than the classic "sandwic h" ELISA was demonstrated. Scanning photolum inescence (PL) sp ectroscopy was performed on dried E LISA wells and the results compared with the sa me QD samples dried on a solid substr ate. We confir med a "blue" 37 nm PL spectr al shift in a case of QDs conjugated to PSA antibodies. Increasing of the "b lue" spectral sh ift was observed at lower PSA antige n concentrations. The results can be used to improve sensitivity of "s andwich" ELISA cancer antigen detection. Currentl y, the threshold of PSA AG detection for "sa ndwich"-ELISA with or ganic dyes, but for many ELISA kits the threshold i s 1 ng/ml [1-4], which is usu ally low enough for early cancer detection, but "sandwich" ELI SA with QDs could possibl y detect as low as 0.01 ng/ml of PSA AG. One of th e current pr oblems in QD usage for bi omedical applications is th at bioconjugation reactions may be incom plete and result in resid ual non-conj ugated QDs in the same bio-conjugated solution. Our rec ent exper iments de monstrated that PL spect ra o f QDs are changed b y bi oconjugation [5-9]. This is manifested as a blue or short-wavelength spectral shift of the PL maximum, which can b e cle arly obs erved as a co lor change of th e dried bioco njugated samp le. This uni que spectroscopic feature of the biocon jugated QDs may serve as a fingerprint of the bioconjugation reaction. Ulti mately, this will dramatically improve sensitivity of biomolecules detection using QDs because a background PL from the non-conjugated QDs can be spectrally separated. In this paper, we report on PL spectroscopic study of the dried "sandwich" ELISA well s, utilizing QDs to detect PSA AG at the concentration range of 0.01 – 1.0 ng/ml. The agarose gel el ectrophoresis technique w ith the organic dye fluorescamine is employed to assure the quality of the conjugate, used for "sandwich"-ELISA te chnique. A "blue" spectral shift magnitude was found to be larger for EL ISA "sandwiches" in comparison to the same bio-conjugated QDs, dr ied on a flat silicon substrate. Thi s effect can be attributed t o the elevat ed stress applied to the indi vidual QD, i nvolved int o the "sandwich" form ation, as well as more or less efficient, but probabl y not complete, nonconjugated QD eli mination caused by t he washing procedure. T he PL signa l from the bio-conju gated QDs wa s foun d in all wells, containing AG, with differ ent concentration but was und etectable in the control w ell without AG. It is ex pected that the results can provi de strong benefits for early cancer detection and forensic technology.

3.1.1 ELISA QD procedure

Uncoated polystyrene ELISA wells were purchased from NUNC. All buffers in stock solutions (coating, stopping and washing) were purchased from Immunochemistry Technologies LLC. The scheme of the "sandwich"-ELISA method is shown in Fig. 3.

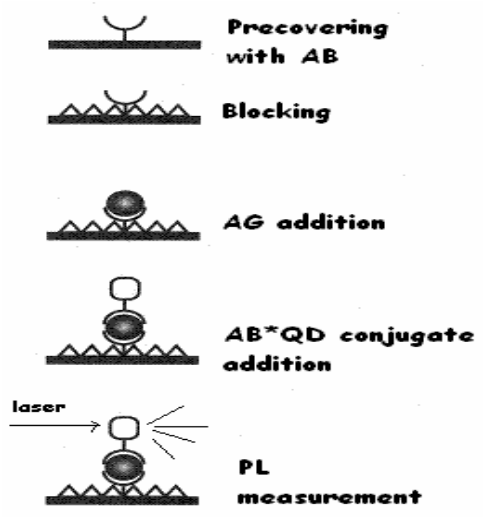

Figure 3. "Sandwich"-ELISA method schematic.

Wells were coated with capture PSA AB by adding 50ul of 5X diluted coating buffer mixed with AB in concentration 7.5 µg/ml. The wells were then covered with aluminum foil to prevent light exposure and incubated overnight at 4C. After that coated wells were washed 3 times with washing buffer and incubated with blocking buffer (300µl/well) at the same conditions to ensure blocking of all unused sites on the well, available for further protein bonding. This stage was also followed with 3-times washing, and immediately proceed to the AG solution/sera addition. 50 µl of PSA AG solution or sera was added to wells #2- 4 in the following concentrations: well #2 – 1.0 ng/ml; well #3 – 0.1ng/ml; well #4 -0.01 ng/ml; and well #5 was a control – pure PBS (pH 7.4) added, no AG. The wells were incubated in the same conditions for 12h, washed 3 times with washing buffer, and the 50 µl of 2X diluted AB*QD solution was added immediately, incubated for 12h at the same conditions, washed 3 times and let dry on air until the further spectroscopic analysis. The 2X dilution of a conjugate with QD incubation buffer was used in the effort to lower the expenses, associated with the experiment. QD*AB conjugated is very concentrated in ABs (the AB solution used for conjugation is 1mg/ml), therefore, they are taken in excess even if the conjugate is diluted 2 times. The 2X dilution of a conjugate with QD incubation buffer (obtained from Invitrogen Inc) was used in the effort to lower the expenses, associated with the experiment. QD*AB conjugated is very concentrated in ABs, therefore, they are taken in excess even if the conjugate is diluted 2 times (Table 2):

Table 2: AB concentration estimate

Main stage of conjugation	Brief description	Estimated AB concentration and volume
Initial	Stock AB solution	1 mg/ml, 300µl [inv]
Mixed with QD	125ul of QD solution	0.7mg/ml, 425µl
Separation column	To get rid of unconjugated ABs; Assuming no AB losses	0.6mg/ml, 500µl
Final volume	Assuming 50% of AB losses	0.3mg/ml, 500µl
	Assuming 90% of AB losses	0.06mg/ml, 500µl, or 60ug/ml, 500µl
	Assuming 99% of AB losses	0.003mg/ml, 500µl or 3ug/ml, 500µl

Therefore, even assuming 99% of all AB losses we still have 3µg/ml AB solution, which diluted 2 times gives us 1.5µg/ml solution, which is 1000-100000 times more than target AG concentrations.

3.1.2 QD ELISA is more sensitive than the regular PSA ELISA

The regular, commercially available and QD modified PSA ELISA's were performed on the same set of samples, which included four female serum samples with known PSA concentrations (1.82, 0.66, 0.093 and 0.013 ng/ml) and four PSA AG solutions in PBS (0.1, 0.01, 0.005 and 0.001 ng/ml). As for the serum samples, the two lowest concentrations were prepared by dilutions of other samples with greater concentrations. The samples in commercially available ELISA were run in duplicates, and the samples in QD ELISA were run in just one sample each. This was done in order to minimize the

cost of the experiment, which is at the moment high, especially for the QD ELISA. The main goal of the experiment was to determine if the QD ELISA can lower the current threshold (0.1ng/ml).

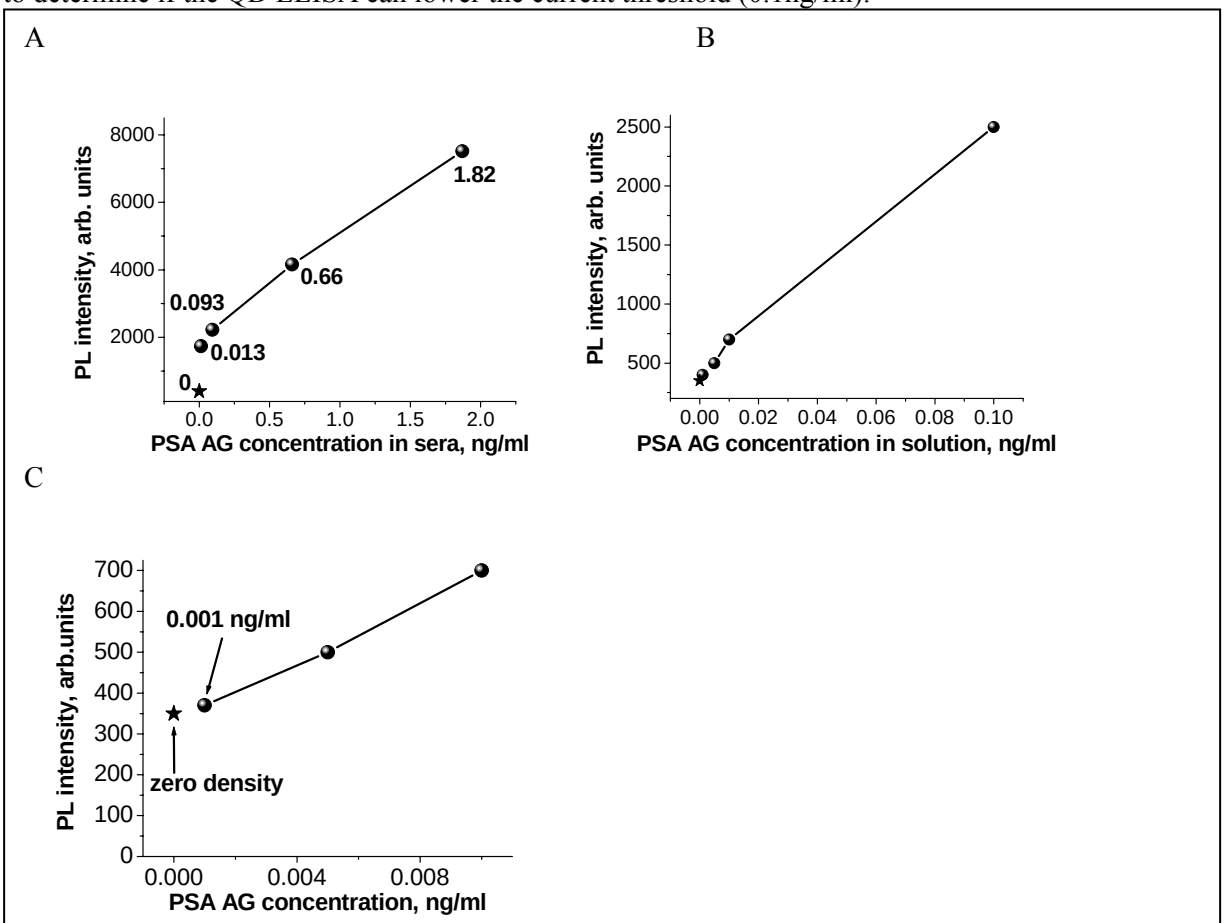

Figure 4. QD ELISA detection limits: A – in sera samples; B – in AG solution in PBS; C – the range 0 – 0.01 ng/ml for the AG solution in PBS, to better see the lowest (0.001 ng/ml) concentration.

In Fig.2 the results of commercial ELISA are shown. As expected, among the plasma samples 0.013 and 0.093 ng/ml were undetectable (Fig 2A), as well as the whole range of the AG dilutions in PBS (Fig 2B). According to our results, 0.1ng/ml and below were undetectable in both the serum and AG dilutions samples which is in a good agreement with the claimed method threshold.

Different results, however, were obtained with the QD ELISA using same set of samples (Figure 4). As obvious from the Figure 4A, all plasma samples were successfully detected, including the 0.013 and 0.093 ng/ml dilutions. As for the AG in PBS solutions, the lowest 0.001ng/ml concentration was almost at zero level (Figure 4C), so it is considered undetectable, however, the next dilution – 0.005ng/ml, was detected (Figure 4B) and therefore may be considered as a new threshold for the PSA AG detection with the QD ELISA method.

So, based on the mentioned above results, the authors conclude that ELISA, which utilizes bioconjugated QDs as detection markers is at least 20 times more sensitive that the currently available commercial ELISA (0.005 vs 0.1 ng/ml). This is attributed to a very efficient mechanism of QD emission, so that just a relatively small amount of QDs, which are engaged into the sandwich formation, is enough to create a detectable PL signal.

3.1.3 Different antibodies and QDs - summary

For the most part, 705nm QDs were used, because after conjugation and drying they exhibit the largest "blue" spectral shift. This effect is attributed by the fact, that bigger QDs have more spaces for the antibody attachment, resulting in the increased elastic stress which is applied to such QDs. For instance, if the smaller ("blue") QDs with the size 3-6nm could attach 1-2 antibodies, the relatively big 705nm QDs with the size up to 12nm, could possibly attach 3 or more biomolecules. In the scope of this research, about 80% of all effort was put into the 705nm QDs, conjugated to PSA antibodies. This is motivated by the fact, that PSA is an important (and the one reliable so far!) prostate cancer biomarker.

Table 3: The summary of QDs, antibodies and spectral shifts of all experiments, performed in the scope of this work.

Antibodies	705 (CdTeSe)	655 (CdSe)	605 (CdSe)	580 (CdSe) – home made
IL-10	Time-induced shift ~27nm during storage at room	Time-induced shift ~10nm during storage at room	Time-induced shift ~7nm during storage at room	~4nm initial shift; up to ~65nm temperature induced shift (190C, 12h); ~ 14nm room T aging shift (12 days)
PSA	Time-induced shift ~27nm during storage at room	No experiment	No experiment	No experiment
KLK19 (CAV1)	No experiment	~3nm initial shift; ~10nm temperature induced shift (190C, 12h); ~ 14nm room T aging shift (12 days)	No experiment	No experiment
P53	No experiment	~5nm initial shift; ~15nm temperature induced shift (190C, 12h); ~ 18nm room T aging shift (12 days)	No experiment	No experiment
IL-6	~4nm initial shift; ~20-25nm temperature induced shift (190C, 8h); ~21nm room T aging shift (12days);	No experiment	No experiment	No experiment
OPG	~10nm initial shift; ~36nm room T aging shift (12days); ~32-36nm temp induced shift (190C, 10h)	No experiment	No experiment	No experiment

The influence of a biomolecule's molecular weight

We extended this study to other types of cancer related antibodies. In this experiment the identical type and size of QDs with the PL maximum at 705 +/- 2nm was used. The bioconjugation and subsequent PL spectroscopic analysis was performed on 6 monoclonal ABs, currently being considered as cancer biomarkers. They are: IL-6, IL-10, PSA, P53, OPG

and CAV-1. 705nm QDs, conjugated to all ABs, mentioned above, perform "blue" spectral shift of different magnitude with the IL-6 giving the smallest shift, and OPG – the largest approaching 36 nm after 11 days of room temperature sample storage (figure 5).

The different magnitude of the blue spectral shift for different ABs, is repeatable and observed in samples dried at room or higher temperatures. For instance, we previously observed an approximately 40 nm spectral shift for IL-10 antibody after 12 days drying at room temperature or after annealing at 140C for 12 hours [123]. In figure 3.16 we present data of the maximum PL spectral shift for different ABs after room-temperature drying and correlated this shift with the AB molecular weight. It occurred that the AB molecules with larger molecular weight show a larger "blue" shift of the conjugated 705 nm QDs. For instance, molecular weight of the IL6 AB molecule is 22-26 kDa [139], while OPG AB molecule weights 48 kDa [140], which corresponds to 27 and 36 nm PL shifts.

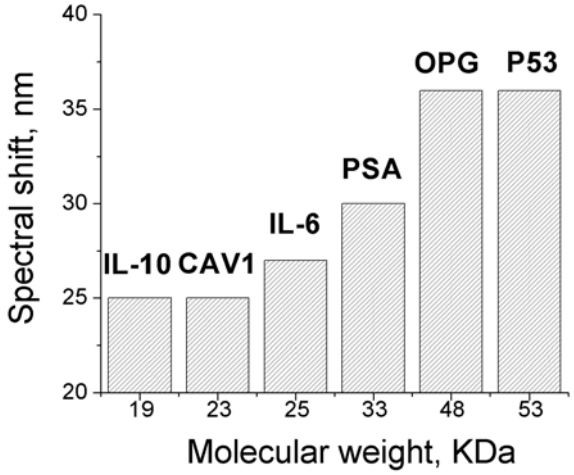

Figure 5: Dependence of the QD "blue" spectral shift on the molecular weight of the AB molecule, used for bioconjugation. The samples were deposited on silicon and dried at room temperatures for 11 days.

3.1.4. Time dependence of the "blue" spectral shift

As soon as the initial shift of bioconjugated QDs was discovered, it was necessary to research, if it changes with the time of storage of the dried sample. To do this, the dried sample was stored in the clear plastic box at room ambience and the spectra were taken once a day to monitor the peak positions. It was discovered that the blue spectral shift of bioconjugated QDs increases with time: the PL spectrum of bio-conjugated spot gradually shifts to the short-wavelength region, while the pure QDs retain the same peak position within 2nm accuracy threshold (Figure 6A). As could be seen from the Figure 6B, for this particular 705nm QDs + PSA sample, the blue shift increased from 6-7nm up to ~27nm in 11 days of storage. This effect was also observed and documented for other QDs and Antibodies as described above (table 2). The average spectral shift after 12-14 days of storage at room ambience is usually 22-35nm. We have examined the spectral shift of the samples after 3 months of storage, however, no substantial increase was noted compared to the 14 days shift. This is attributed to finishing of the drying process in 14 days, and thus stabilizing of the "blue" spectral shift that is speculated to be of a moisture-related stress-induced nature.

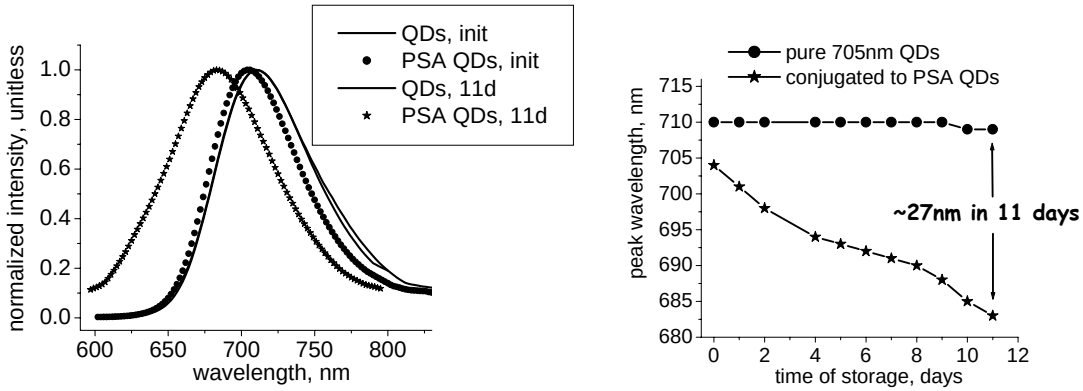

A B

Figure 6: The blue shift dependence on the sample storage time at room ambience: A – PL spectra of pure 705nm QDs and conjugated to PSA QDs, initial and after the 11 days of storageas room T; B – PL peak positions on a daily basis for pure 705nm QDs and same 705 nm QDs conjugated to PSA.

3.1.5 The influence of drying temperatures

In order to establish the influence of the a mbient temperature on the blue shift, two identical dried samples were stored at the room (+22 - +23C) and fridge (+0 - +4C) a mbiences for 13 days and the spectra w ere taken daily. The fridge sa mples were kept in a fridge for the whole time, except for the m easurement which did not exceed 10mins a day . Each sa mple had a pure 705nm QD drop and bioconjugated to PSA QD drop. The results are shown on Fig 7. It is clear that conjugated sample which was kept i n a fridge e xhibits sm aller blue shift than the one which was kept in the room a mbience, suggesting t hat lower tem peratures slow down t he blue sh ift formation. The relative difference bet ween the shift magnitudes is ~26%.

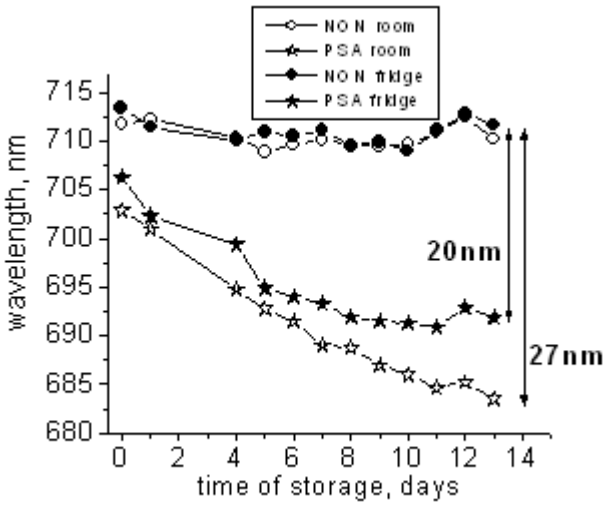

Figure 7: The blue shift of the conjugated to PSA sample (stars) in comparison to pure QD sam ple (rounds) after the 13 da ys of storage. The average shift of the room conjugated sample (open shapes) is ~ 26% bigger in co mparison to the fridge conjugated sample (closed shapes). Because the low er storage temperatures show a dim inishing effect of the shift for mation, the assumption was made that the higher te mperatures may speed its formation. To test this, conjugated a nd refe rence samples wer e dried in a temperature stabilized oven at air a mbient atmosphere at various temperatures up to 245 °C. It is realized that high-t emperature processing may produce a deco mposition of the protein structure. However, it was used to facilitate PL shift process for exploration purposes. The kinetics of the annealing process w as monitored using PL spectra at roo m tem perature. Figure 8 depicts the kinetic curves of the P L spectral shift versus annealing ti me at different tem peratures over a period of 12 h. At annealing temperatures of 140 and 1 90 °C, the kinetic curves reveal an exponential growth with saturation of t he relative PL spectral shift allowing for an e stimate of the time constan t of this process at 5 hrs and 8 hrs for 190 ^{o}C and 140 °C, respectively. The spectral shift rate was much higher for 250 °C drying temperature, while for 115 °C observable shift change does not show full exponential saturation level even after 12 hours of storage. The observed results may be described by the influence of temperatures on the proteins, attached to QDs. At lower temperatures, the proteins dry and denature slower, which may reduce the tension on the QD-substrate surface or have the chemical effect of the QD (See Discussion section).

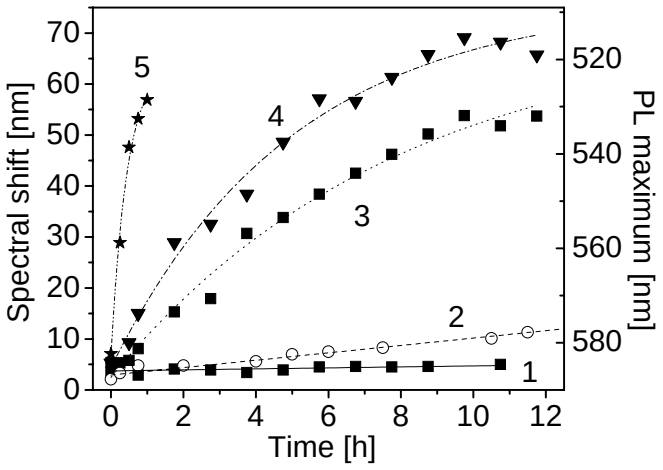

Figure 8: Kinetics of the PL spectral shift enhancement in the bio-conjugated sample due to annealing at different temperatures: 1 – room, 2 - 115°C, 3 - 140°C, 4 - 190°C and 5 – 250°C. Non-conjugated QD samples retain a PL band spectral position within experimental accuracy of ~1 nm.

3.1.6. Spectral mapping measurements

In order to more carefully examine the "blue" shift pattern across the dried spot of QDs, the PL mapping technique was utilized. Silicon wafers with deposited QD spots were mounted on a computer controlled *X-Y* moving stage with a smallest step of 0.1 mm. The typical mapping area was 3 mm x 3 mm with a step of 0.25 mm. PL system, shown on the Figure 9, was employed to make the spectral maps.

Figure 9: Photoluminescence setup for room temp measurements of quantum dots The PL mapping experiment was done with the use of an X-Y computer controlled moving stage (Velmex 8300) with 10 μm step precision and (Klinger CC 1.2) for 1 μm resolution maps.

PL spectral mapping technique has several important advantages over a "one spectra per spot" measurement, because it allows:

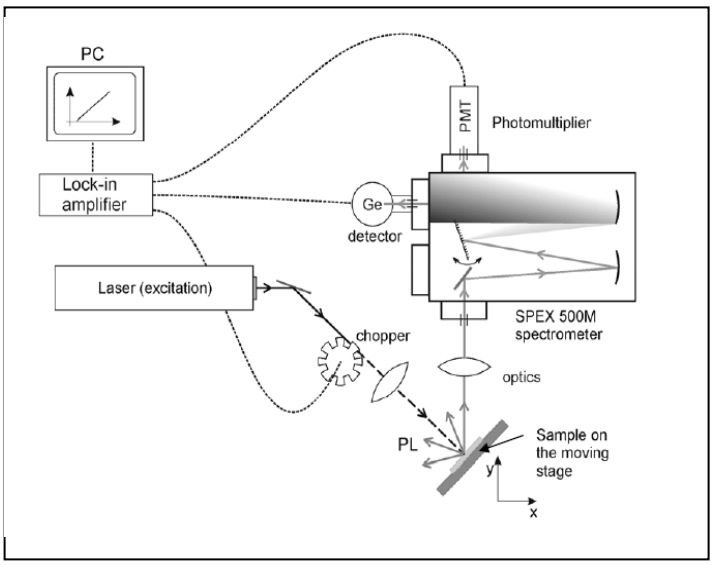

A. track the spectral peak position inhomogenities across the dried spot;
B. obtain the lowest, the highest and the average peak positions for one spot;
C. compare the highest, the lowest and the average peak positions of bioconjugated spot vs the nonconjugated control, or the bioconjugated spot at a certain amount of time with the same spot at the different amount of time and/or after treatment;
D. helps to identify possible mechanism of the shift appearance, because of certain physical mechanisms (discussion);

The following advantages are illustrated in the Figure 10.

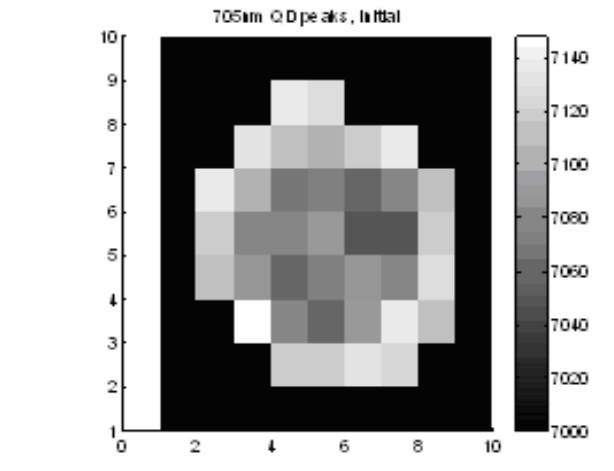

A

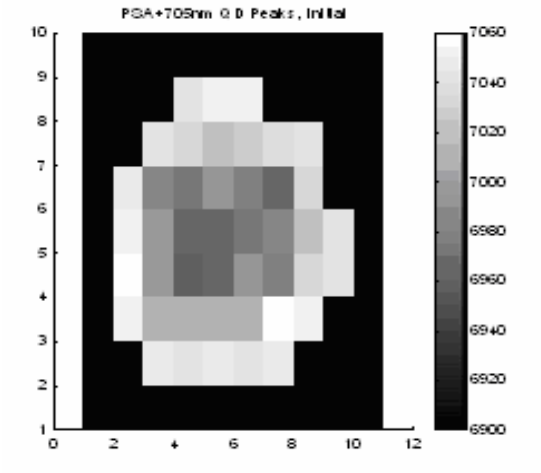

B

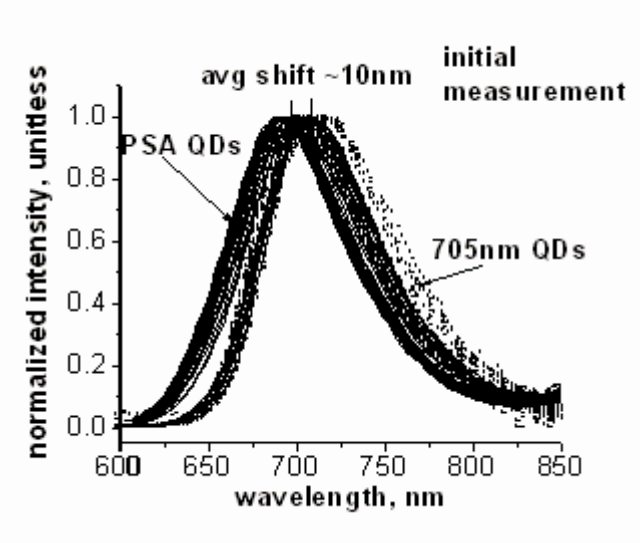

C

Figure 10: Initial spectral maps of the 705nm QDs, bioconjugated to PSA Antibody: A. peak position – pure QDs; B. Peak position – bioconjugated QDs; C. spectra of the maps, presented above. Each spectra co rresponds to one spot on the spectral map.

Figure 10 illustrates the spectral mapping of the same 705nm QD sample, bioconjugated to PSA Antibodies. As could be seen from the A and B parts of both figures, the spectral peak positions differ from one spot to another even within the same sample (lighter spots correspond to higher PL intensity and more "red" PL peak positions). This spectral inhomogenity exists for both pure and conjugated QD, and the magnitude increases with time of storage.

Having a spectral mapping data gives us an opportunity to calculate the C- average peak position for each spot, along with the spectral range. Therefore, such terms as an average spectral shift, or a maximum (minimum) spectral shift are becoming available. For instance, for the initial nonconjugated spot, the maximum high spectral position is 714nm, the lowest minimal is 702nm, therefore, the peak positions range for this spot is 702-714nm. The average peak position for the whole spot is calculated by simple summation of all peaks and dividing the sum on the number of spectra, which for this spot equals to 708nm. This number is in a good agreement with the one spectrum per spot measurement. The summary of the average spectral peak positions for each sample, along with their magnitudes, are shown in Table 3.

Table 3: The summary of the average spectral peak positions for each sample, along with their magnitudes.

	Minimal position, nm	Maximal position, nm	Average position, nm	The shift compared to pure QD sample, nm	The shift com pared to initial conjugated sample, nm
Initial 705nm QD	702	714	708	N/A	N/A
Initial PSA QD	694	703	702	Max: 20 Average: 10	N/A
Stored 705nm QD	701	712	704	N/A	N/A
Stored PSA QD	673	700	681	Max: 40 Average: 35	Max:30 Average:25

3.1.7. Agarose gel electrophoresis represents an easy, inexpensive and reli able method to verify the conj ugation of QDs to different monoclonal ABs. One QD molecule, covered with all lay ers, has a molecular weight about 750 KDa, which is larger in comparison to A B molecules being in the weight range of 20- 55 KDa. One QD molecule could attach 2-3 AB molecules, therefore we should see a d ifference in the elect ric fi eld drift and separation of the 750KDa pure QDs and 800-850KDa conjugated QDs This task requires careful optim ization of the experim ental conditions to im prove the separation distance in gel.

We used 2% agarose gel, applied voltages up to 1.5V and running time up to 2 hours. In figure 12 the agarose gel im age is shown after 120 m in of running time. Here the retarda tion in m ovement between the pure 705nm QDs and conjugated 705nm QDs is evident (co mpare wells #1 and #2; #5 and #6). In this i mage pure ABs mixed with Fluorescamine (wells #3 and #7) have already run out of the gel, and only the trace PL from them could be seen in well #3. Molecular weight of the PSA molecule is 32-33 kDa, while the one for IL6 is 22-28kDa. It is logical to assu me that QDs conjugated to IL6 molecule will move fast er than these co njugated to PSA, b ecause of the size di fference. Th is hypothesis is confir med (wells 2 and 6): the PSA movement is retarded in com parison to IL6 m ovement. Als o, the trace of the PSA + Fluorescamine PL i s visib le in w ell 3, while no P L could be observed for t he Il6 molecule, where there' s an IL6 + Fluorescamine mixture. Therefore, the separation capacity of the agarose gel is high enough for this type of application.

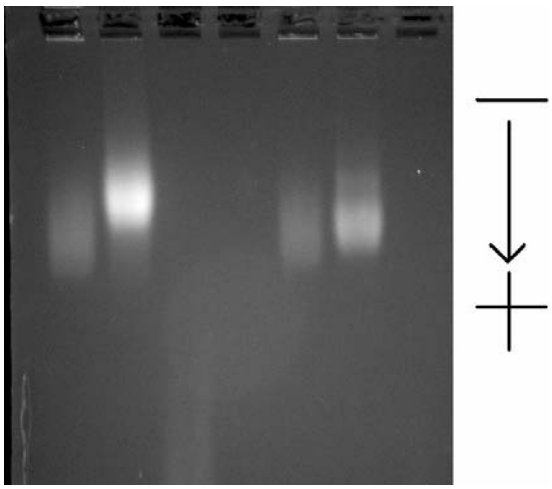

Figure 11: Agarose gel electrophoresis photograph, 2% agarose gel, 1.5V, 120 mins running time, 0.5xTBE running buffer. Wells are as follows: (1) non-conjugated 705nm QDs; (2) PSA conjugated to 705nm QDs; (3) PSA pure protein + Fluorescamine, (4) empty, (5) non-conjugated 705nm QDs, (6) IL6 con jugated to 705nm QDs, and (7) IL6 pure pr otein + Fluorescamine.

In every bio logical procedure, tim ing is an im portant optio n, a nd it is highly desirable to minimize the running time. Therefore, the gel which is shown on Figure 11, was analyzed 30mins after the run cycle started. The result is shown on Figure 12.

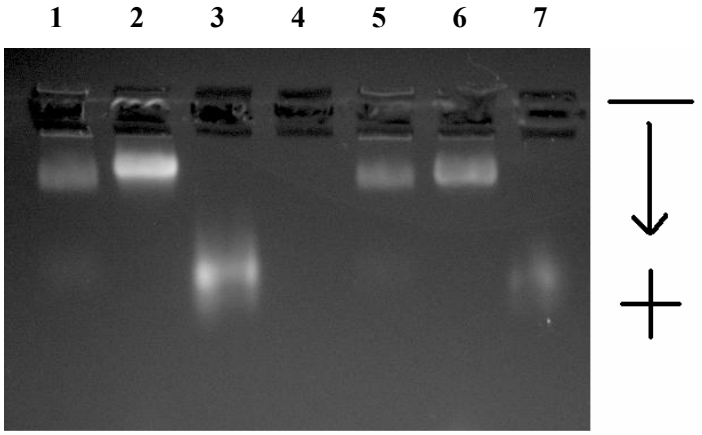

Figure 12: Agarose gel electrophoresis photograph, 2% agarose gel, 1.5V, 30 mins running time, 0.5xTBE running buffer. Wells are as follows: (1) non-conjugated 705nm QDs; (2) PSA conjugated to 705nm QDs; (3) PSA pure protein + Fluorescamine, (4) empty, (5) non-conjugated 705nm QDs, (6) IL6 conjugated to 705nm QDs, and (7) IL6 pure protein + Fluorescamine.

By comparing wells # 1 and 2; and # 5 and 6, it is evident that 30mins is not enough for the complete separation of conjugated and nonconjugated QDs. However, the 30mins gel allows the clear visualization of pure PSA (well #3) and IL6 (well #7) antibodies, mixed with fluorescamine. It is evident, that because of their smaller size they run much faster in a gel.

So, the following agarose gel specifications are proposed to be optimum for CdSe/ZnS QDs + various antibodies conjugation verification: 2% agarose gel, 1.5V, 120 mins running time, 0.5xTBE running buffer. The amount of time may be increased 15-30 mins if the satisfactory enough separation is not achieved within the 120 minutes slot.

3.1.8. Ultrasonication

We have exposed dried conjugated to anti-PSA and non-conjugated (pure) 605nm QDs to ultrasonication, in an attempt to speed up formation of the "blue" spectral shift. As seen on the Figure 13, no significant difference was noted between the ultrasonicated and non-ultrasonicated QDs in a relevant category. It is noteworthy, however, that there was substantial (~50nm) overall spectral shift between conjugated and pure QDs.

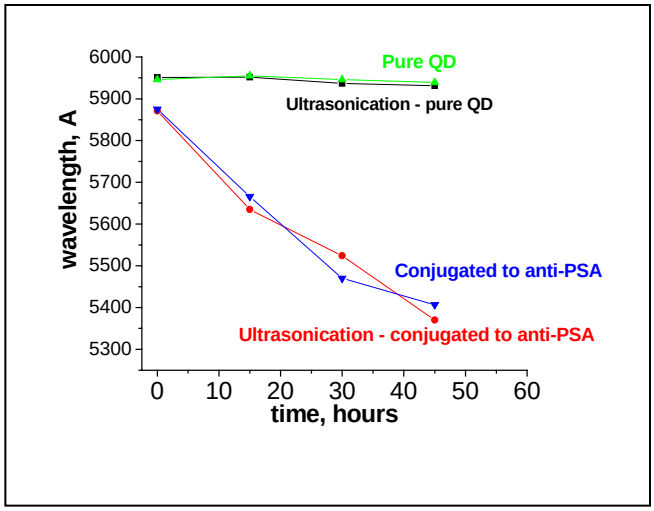

Figure 13: The influence of ultrasonication on the conjugated to anti-PSA and pure (non-conjugated) 605 nm (6050 A) QDs, obtained from Invitrogen.

3.1.9. QD samples dried on the other substrates

Different substances were tried as substrates for drying of QD samples. In every case, the silicon sample served as a control. The initial hypothesis was such that more porous, less dense substrates may influence the spectral shift magnitude, as they influence the drying kinetics of the drops. The first experiment included four substrates – Si, SiC, Quartz and rubber. All samples were dried at room ambience for 12 days. The increased temperature was not used to enhance the shift, as rubber may melt. From the Figure 14 it is obvious that rubber sample had a very small (at most 4nm) blue shift in comparison to the three other substrates which developed a standard "blue" sift of the comparable magnitude.

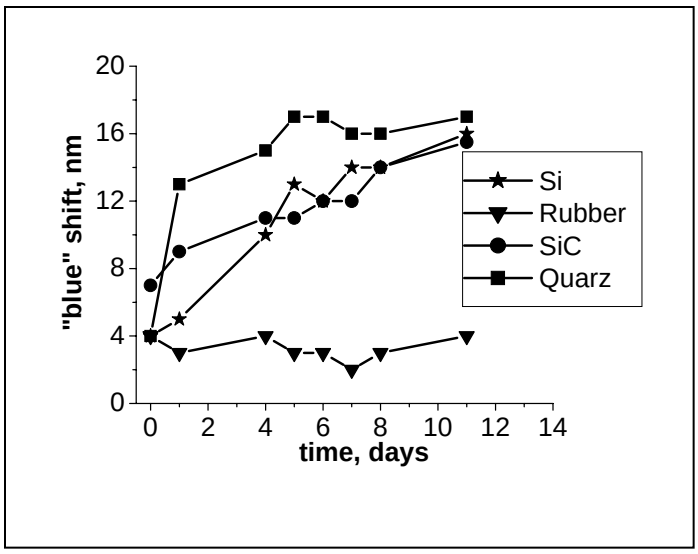

Figure 14: The relative "blue" shift of the 705nm QDs, bioconjugated to PSA antibodies, dried on the different substrates.

Similar results were obtained with the CMP pad which has a continuous porosity in its structure and is therefore similar to rubber (Figure 15). The conjugated to PSA 705nm QD sample, dried on silicon, developed approximately 28nm "blue" shift, while the CMP pad sample is just about 4-5nm in comparison to pure 705nm QD sample. The difference between the silicon and CMP samples is, therefore, about 23nm. These experiments allowed us to make a conclusion that the substrate's porosity, density and possibly other qualities have a noticeable effect on the shift magnitude. This data, along with the high and low temperature data, allows to draw a conclusion that the "blue" shift of bioconjugated QDs is probably caused by the particularities of the drying process.

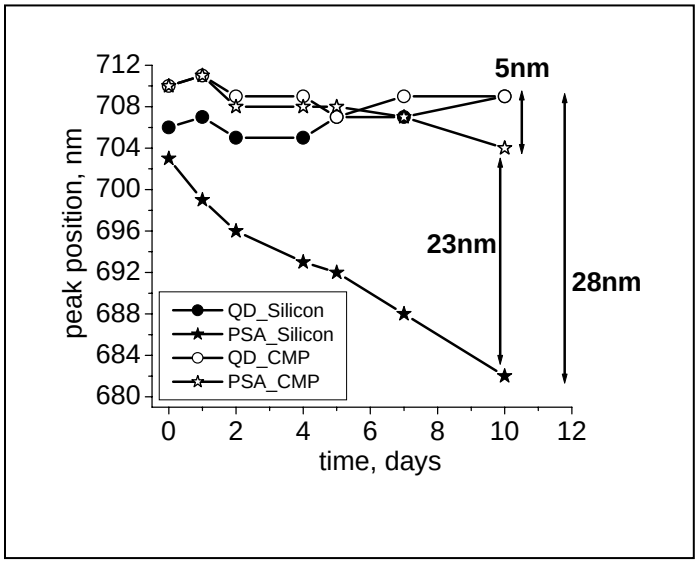

Figure 15: The blue shift of the conjugated to PSA sample (stars) in comparison to pure QD sample (rounds) after the 10 days of storage at room ambience. The silicon (closed shapes) conjugated sample performed a 23nm bigger "blue" shift in comparison to the rubber (open shapes) conjugated sample.

3.1.10. Various ambiences - vacuum, argon, nitrogen and oxygen, increased moisture In order to establish the possible influence of some environmental conditions on the shift, the two identical QD samples, pure and conjugated to CAV1 antibodies, were stored for 10-13 hours and measured hourly or every other hour. In order to speed up the shift development and shorten the experiment time to hours instead of days, the 50C storage temperature was applied. This temperature is not enough to denature the proteins, but it is good in elevating the shift development. The room controls were stored at room ambience, under constant 50C temperature, and the samples were held in closed metallic boxes in constant gas/moisture/vacuum environments and under constant 50C temperature. The samples were taken out for the measurement which did not take longer than 10mins a day. The results are shown on Figure 16. It is clear, that no statistically important influence of the oxygen, moisture, argon, nitrogen and vacuum on the blue spectral shift was recorder. Nonconjugated, pure 705nm QDs don't seem to be affected as well. Based on these results, we conclude that chemical interaction of the QD-AB with gas molecules plays a negligible role in the observed effect.

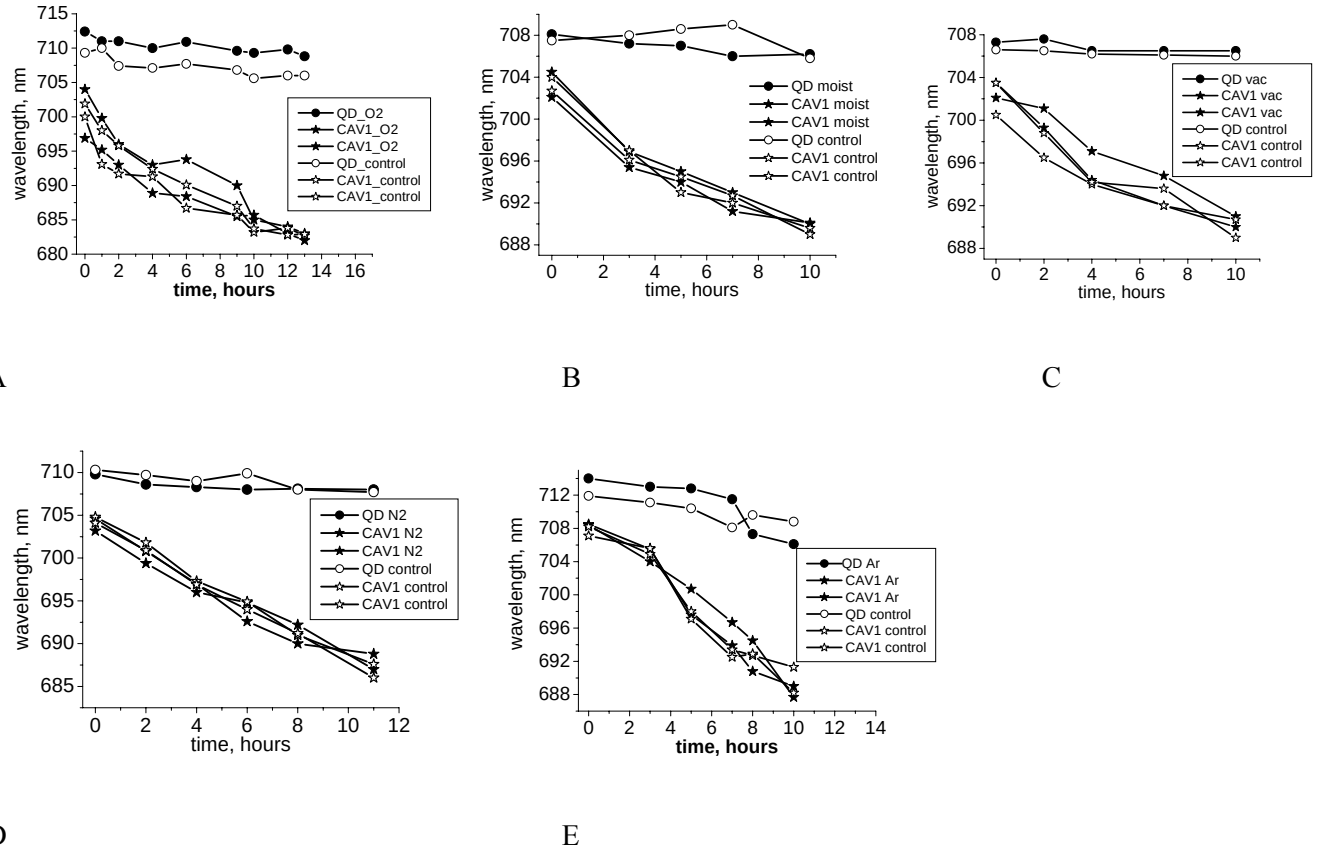

Figure 16: The blue shift of the conjugated to CAV1 sample (stars) in comparison to pure QD sample (rounds) after the 10-13 hours of storage under 50C. No noticeable influence of the following conditions (closed shapes) on the "blue" spectral shift was noticed in comparison to identical room ambience controls (open shapes): A – oxygen; B – increased moisture; C – vacuum; D – nitrogen; E – Argon.

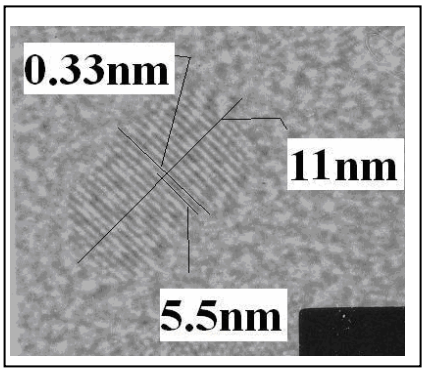

Figure 17: TEM image of the individual 705nm CdSeTe/ZnS core/shell quantum dot.

3.1.11 TEM visualization of pure and bioconjugated 705nm QDs

Quantum dots, possessing the size of at most 12nm, are hard to visualize with other techniques, however, with the TEM technique they can successfully be visualized. In this work, Transmission Electron Microscope Tecnai T20 with the line resolution of 1.2 A and electronic images captured using Orius 831 7 MP CCD camera. The TEM analysis of pure and conjugated 705nm QDs was conducted. It revealed an ellipsoid shape approximately 11x6 nm +/- 0.5nm (Fig 17).

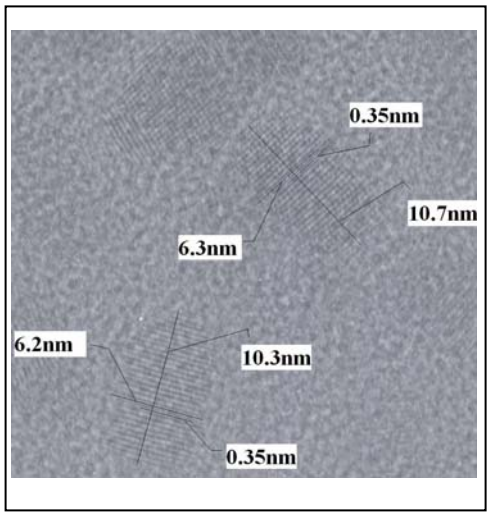

TEM analy sis of conjug ated to Ca veolin-1 (CAV-1) Anribodies was also performed in order to est ablish any size/ shape diff erences with the pure QD s. The Figure of bioconjugated QDs is shown on Fig 18.

Figure 18: 705nm QDs, conjugated to CAV-1 antibodies.

According to the pictures, no significant differences betwe en pure and bioconjugated QDs was found . This a nalysis, however, provides im portant data that the short wavelength "Blue" spectral shift of bioconjugated QDs is no t because of the size decrease or shape change resulting from the bioconjugation reaction directly.

3. 2. Conclusions "Sandwich" ELISA bimolecular tool enhanced with conjugated 705nm QDs instead of commonly used luminescent dy es was e mployed to detect a PSA A G in th e concentration range from 0.01 to 1.0 ng/ml. Three ELISA wells with AG concentrations 1.0, 0. 1 and 0.01 n g/ml s hows the PL peak, originated from the conjugated QDs in the sandwich structure with correspondin g AG (PSA). The cont rol well without AG molecules shows a negligible QD PL intensity. A short-wavelength, blue PL spectral shift was observed on all ELISA wells, utilizing conjugat ed QDs, and th e values of this spectral shift (13-37 nm) were enhanced in comparison to the same QDs, conjugated to PS A AB, dried o n silicon substrate (2-26nm). This fact was attributed t o e ffective washing of nonconjugated QDs fro m th e ELISA wells, which are always present in a conjugate mixture and therefore c ontribute to a n average PL of the dried QD s amples. In addition, a negative correlation was observed between an av erage "blue" PL spectral position and AG concentration. The origin of t his effect is under investigation and pr esumably attributed to decreasing of elastic stress at higher AG concentrtaions. If confir med, this will benefit the ultralow limits of detection for biom olecules, because "blue" spectr al shift will increase with AG concentration decreasing, making it easier to distinguish between PL com ing fro m "sandwiches" and possible traces of nonconjuga ted QDs or other contam ination at ultralow concentrations of a target molecule. Th is effe ct wil l also be us eful in predicting the unknown biomolecule concentration based on the spectral shift position alone, eli minating a ne ed for P L intensity assess ment. The results of this rese arch could lead to critical i mprovements for *in vitro* cancer antigen detection sensitivit y using the QD luminescent tagging technique.

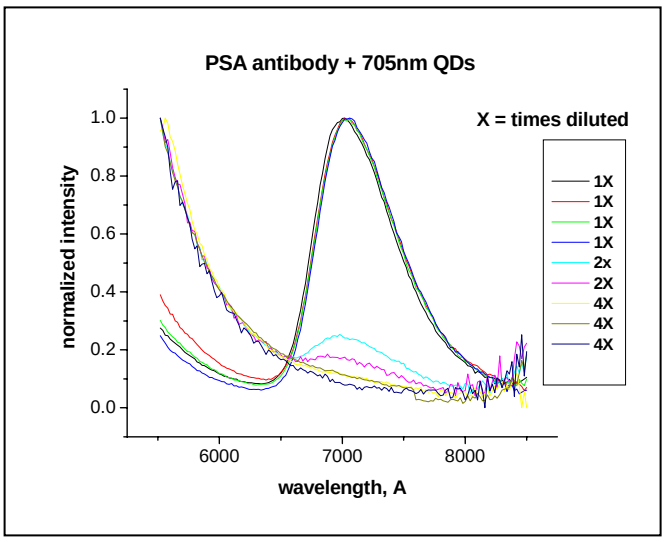

Figure 19: Normalized plot of ELISA signals perform ed with 1x, 2x an d 4x diluted conjugated 705nm QDs and PSA antibody. Wells incubated with 1X diluted (no diluti on) conjugated QD produce a well-defined, recordable signal. However the wells incubated w ith 2X diluted conj ugated QD does not pro duce a reliable si gnal (althoug h some signal is visible, the low signal-to-noise ratio renders it use less). The wells incubated with 4X di luted conjugated QD do not produce any recordable signal.

However, the cost of QDs and antibodies together is approx. $800. From this two conjugations can be performed. This results in only a small volume of conjugated QD-AB and we can assay only about six samples. We performed experiments with different dilutions of the QD-AB conjugate of 1:4 and 1:2 to determine if the QD-AB solution could be diluted but would still reveal detection of the proteins. However, the results were inconsistent and 2x dilutions or greater showed limited conjugation (see Figure 19).

3.3. Utilization of additional nanotechnologies: In the last annual report we revealed our interest in exploring two additional nanotechnologies. Microfluidic devices and Surface enhanced Raman scatteri ng (Zhang Lab.). We have proceeded with the former technology. We have included two very experienced and well published researchers Dr. Shekhar Bhansali who also previously integrated PSA into a microfluidic device for prostate (and other) cancer detection [10-16] and Dr. Weihong Tan who is already performing the Cell-SELEX in prostate cancer and has identified aptamers to prostate cancer cell surface proteins. We have been awarded funds to perform research with Dr. Tan. However, in this study we focused on the utilization of microfluidic devices. This is within the scope of the Specific Aims in this proposal and we modified the Statement of Work to reflect this new direction.

3.4. Testing of candidate biomarkers: We had chosen six candidate biomarkers based on the literature (PSA, KLK2, KLK14, OPG, anti-P53 antibodies, IL6 and CAV-1). We tested these biomarkers for their ease of conjugation to nanoparticles and nanowires as well as their effectiveness as biomarkers for early prostate cancer detection in plasma from the African American men using classical ELISA as well as QD-associated ELISA.
KLK2 and KLK14 antibodies proved technically difficult to conjugate and were not available in an ELISA kit so we excluded them from the analysis.
Anti-P53 antibodies were easy to conjugate but unfortunately were identified at higher levels in controls compared to cases (see Table 4). The most suitable biomarker would be one which is increasing in concentration as the stage of cancer increase and increases compare to control levels.
OPG, IL6 and CAV-1 showed very similar levels in the plasma from cases and controls so cut-off points could not be determined (see Table 4 and 5).

Table 4: Serum concentrations of candidate biomarkers

#	PCa status	PSA, ng/ml	P53, U/ml	OPG, pg/ml
1	+	**2.4**	**n/d**	**756**
2	+	**2.6**	**n/d**	**958**
4	+	**3.93**	**n/d**	**1141**
5	+	**4.4**	**n/d**	**842**
7	-	1.6	n/d	840
8	-	<0.5 (n/d)	n/d	699
9	+	**5.93**	**4.1**	**483**
10	+	**2.63**	**15.4**	**951**
12	+	**0.8**	**n/d**	**771**
13	+	**40.67**	**n/d**	**1002**
14	+	**4.13**	**n/d**	**1116**
15	+	**1.47**	**n/d**	**2484**
16	+	**4.27**	**5.2**	**822**
17	+	**4.8**	**n/d**	**876**
18	+	**5.27**	**n/d**	**1050**
20	+	**4.47**	**n/d**	**1926**
21	+	**14.27**	**n/d**	**1095**
22	-	3.53	n/d	972
23	-	4.4	n/d	1491
24	-	0.6	n/d	987
25	+	**2.27**	**n/d**	**1299**
26	+	**12.87**	**n/d**	**1020**
27	+	**4.4**	**4.8**	**720**

28	+	**14.8**	**3.7**	**1524**
29	-	<0.5 (n/d)	8	558
30	+	**3.8**	**n/d**	**630**
31	+	**2.8**	**n/d**	**717**
33	-	2.27	n/d	1254
34	-	0.47	n/d	417
35	+	**1.4**	**n/d**	**669**
36	-	1.8	n/d	882
37	+	**3.87**	**3.6**	**612**
38	+	**12.1**	**n/d**	**1170**
39	-	2.93	n/d	849
42	+	**2.0**	**n/d**	**864**
43	-	0.87	n/d	942
45	+	**2.92**	**n/d**	**943**
46	-	<0.5 (n/d)	n/d	876
48	-	0.9	n/d	861
49	-	1.13	141.7	633
50	-	0.67	4.2	804
51	-	0.80	n/d	1074
52	-	0.53	35.7	879
53	-	N/A	n/d	492
54	-	<0.5 (n/d)	n/d	2001
55	-	<0.5 (n/d)	n/d	612
56	-	1.07	n/d	384
57	-	<0.5	n/d	789
58	-	<0.5	4.1	846
59	-	1.4	n/d	915
60	-	<0.5 (n/d)	n/d	936
61	-	1.13	N/A	N/A
62	-	0.67	4.6	648
68	+	**2.93**	**5.7**	**714**
81	+	**4.67**	**5.1**	**678**
83	-	5.27	n/d	1116
85	+	**4.27**	**n/d**	**705**
86	-	<0.5 (n/d)	n/d	930
87	-	<0.5 (n/d)	7.8	804
88	-	0.6	3.6	489
90	-	<0.5 (n/d)	N/A	N/A
91	-	3.1	5.7	N/A

Table 5: Expression of biomarkers

	PSA	**P53**	**OPG**
Total tested	**61**	**60**	**59**
Cases +	29	28	29
Controls -	32	32	30
Expression detected (ED) total	**52 (85%)**	**15 (25%)**	**59 (100%)**
ED cases	29 (100%)	8 (29%)	29 (100%)
ED controls	24 (75%)	7 (22%)	30 (100%)
Average cases	**6.1 ng/ml**	**6.12 u/ml**	**0.984 ng/ml**
Average controls	**1.1 ng/ml**	**25.99 u/ml**	**0.866 ng/ml**

Test case of 29 cases and 33 controls, 62 total

P53: 60 samples tested, 15 have detectable p53 expression, including 8 cases and 7 controls. The average expression for cases is 6.12 u/ml, and 25.99 u/ml for controls (see Table 5).

OPG: 59 samples tested, 59 (all) have detectable p53 expression. The average expression for cases (29) is 984 pg/ml, and 866 pg/ml for controls (30) (see Table 5).

PSA: 61 samples tested, 9 have no detectable PSA (<0.5 ng/ml), all controls. Average PSA for cases (29) is 6.1 ng/ml, and 1.1 ng/ml for controls (32), including those with undetectable PSA levels (see Table 5).

Statistical analysis was performed on patient data obtained from the questionnaire. Results can be found in Table 1.

3.5. To develop microfluidic device biosensors: The chosen antibodies will be immobilized onto a gold nanowire biosensor surface with electrochemical detection. Upon protein binding, changes in the electrical properties in the vicinity of an electrode are detected.

Electrochemical sensors is a new and promising group of sensing devices, allowing increased sensitivities in conjunction with lower cost, low analysis times, miniaturized and affordable platforms [17-24]. There are numerous detection techniques, currently being researched towards an application in electrochemical sensors, which are described in detail elsewhere [25-34]. Among them, Electrochemical impedance spectroscopy (EIS) is a powerful and sensitive technique to characterize surface-modified electrodes and for the investigation of electrochemical systems and processes [35-37]. In this paper, we report on a successful fabrication of an impedance-based miniaturized biosensor (Imp-sens) and its application for an ultrasensitive PSA detection in standard and real human plasma solution, spiked with different PSA concentrations. The Imp-sens exhibited the sensitivity of 1 pg/ml for PSA which is at least 10 times lower than any most sensitive commercial ELISA on the market. An average detection time with Imp-sens for one sample is ~45 minutes, compared to at least 2.5 hours with a standard ELISA. Successful approach to minimize the non-specific binding (NSB) issue has been attempted. The Imp-sens novel technique may open an era of research geared towards ultransensitive, inexpensive and convenient testing procedures.

3.5.1. Chemicals and reagents

Dithiobis(succinimidyl propionate) (DTSP) and sodium borohydride ($NaBH_4$) were purchased from ThermoFisher Scientific. Purified PSA protein (product # 7820-0604), Monoclonal PSA antibody (anti-PSA, Mab, product # 7820-0217) and monoclonal cortisol antibody (product # 2330-4839) were procured from Abd Serotec. Phosphate buffered saline (PBS) tablets were purchased from Sigma Aldrich. SU-8 resist was purchased from Microchem Corp. All other chemicals were of analytical grade and were used without further purification. PBS solution (10 mM, pH 7.4) was prepared by dissolving 1 tablet in 200 ml of deionized water. Working solutions of both the PSA, anti-PSA and anti-cortisol were prepared by dilution in PBS (10 mM, pH 7.4).

3.5.2. Measurement and apparatus

Electrochemical impedance spectroscopy (EIS) was utilized to characterize the -EA/Mab/DTSP/IDμE bio-electrodes and to estimate PSA concentration. EIS measurements were carried out at equilibrium potential without external biasing in the frequency range of 0.5–10^5 Hz with a 5 mV amplitude using Autolab Potentiostat/Galvanostat (Eco Chemie, Netherlands). EIS measurements were carried out using 65 μl of PBS solution (10 mM, pH 7.4) containing a mixture of 5 mM $Fe(CN)_6^{4-}$ (Ferrocyanide) and 5 mM of $Fe(CN)_6^{3-}$ (Ferricyanide) i.e. 5 mM $Fe(CN)_6^{3-/4-}$ as a redox probe. Using the redox probe (5 mM $Fe(CN)_6^{3-/4-}$), change in charge transfer resistance (R_{ct}) at electrode/electrolyte interface has been investigated in electrochemical impedance.

3.5.3. Test chip fabrication

The Imp-sens chips were fabricated on an oxidized 4" silicon wafer using standard photolithography techniques [36]. Briefly, Cr/Au (200/2000 Å) layers deposited using e-beam evaporation and were patterned through lift off. IDμE with 5μm wide electrode fingers at a pitch of 10 μm were used. As a final step, SU8 chamber patterned around the electrodes using the SU8 50 to create a sample well around these electrodes (Fig 20A). Further SU8 was hard baked at 200 °C to

improve its resistance against hard solvents like acetone. Figure 20B reveals the actual photograph of an Imp-sens reagent chamber under optical microscope (10X).

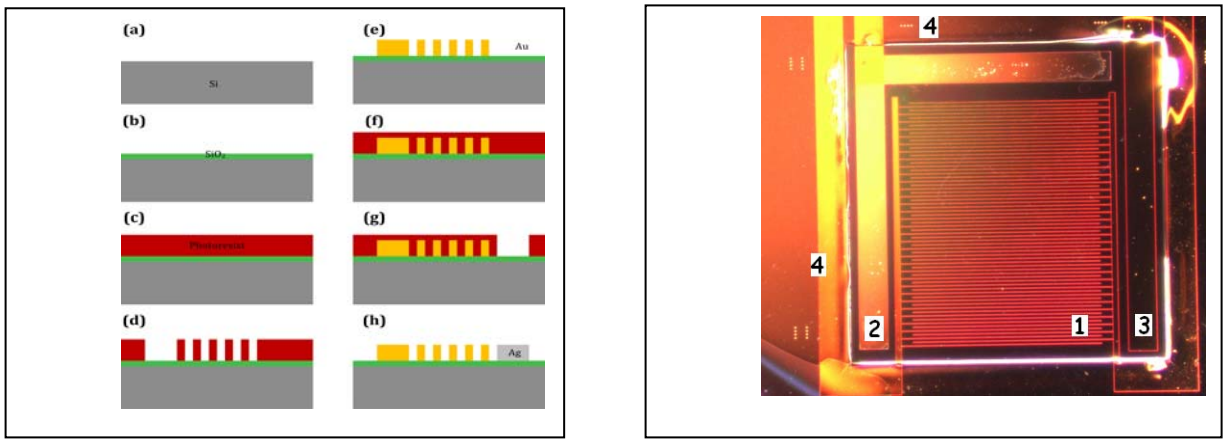

A B

Figure 20: A: Imp-sens fabrication process flow: (a) RCA clean Si wafer, (b) thermal oxidation to grow 500 nm SiO_2 as an insulation layer, (c) apply photoresist, (d) expose and pattern photoresist, (d) deposit Au using electron beam (e-beam) evaporator with thickness of 200 nm and then lift- off photoresist to get pattern Au electrodes, (f) appl y photoresist, (g) pattern photoresist, and (h) finall y despite Ag using e-beam evaporator with thickness of 300 nm and lift-off is used to remove photoresist and metal on top of it.
B: Imp-sens actual view under the microscope (10 X): 1. gold working interdigitated electrodes; 2. silver reference electrode; 3. gold counter electrode; 4. the SU8 reagent chamber.

3.5.4. Self-assembled monolayer (SAM) preparation and antibody immobilization

The Imp-sens chips were pre-cleaned with acetone, isopropyl alcohol, and de-ionized water, and exposed to 2 mg ml^{-1} solution of DTSP in acetone for 1hr for SAM formation. DTSP solution was first reduced using $NaBH_4$ and then dispensed on the pre-cleaned chips at room temperature. The DTSP SAM modified electrodes were then rinsed with acetone to remove any unbound DTSP followed by water rinsing and utilized for antibody immobilization. PSA antibodies were covalently attached to DTSP self-assembled monolayer by incubating the electrode in 65 µl of 1 µg ml^{-1} antibody in PBS solution (10 mM, pH 7.4), for 1 hr. Covalent binding (amide bond formation) results from the facile reaction between amino group of antibody and reactive succinimidyl group of the DTSP on the SAM surface. The sensor (Mab/DTSP/IDµE) was washed thoroughly with PBS (10 mM, pH 7.4) to remove any unbound

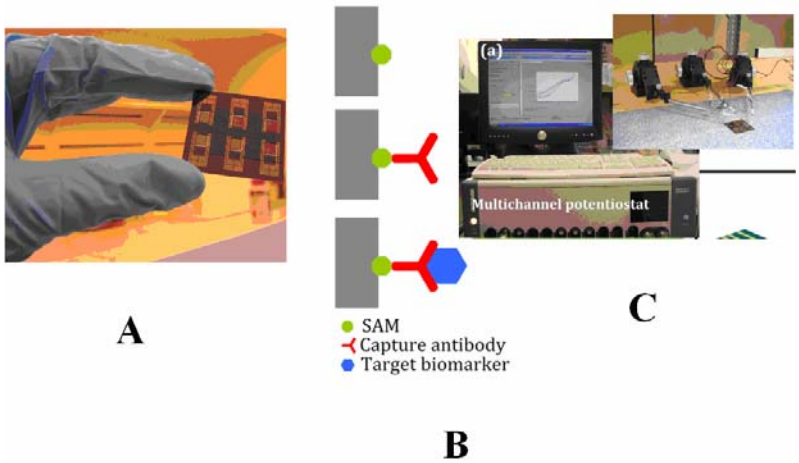

Figure 21 schematically illustrates (a) IDµE chip, (b) Schematic illustration of step-by-step immunochemical reaction on the electrode surfaces, and (c) Proposed detection system. The fabricated bi o-electrodes were characterized using the electrochemical impedance technique. Each sample was run in triplicates to ensure repeatability, and an average result of three runs was used.

biomolecules followed by a 10 min washing with ethanolamine (EA) (1%) EA was used to block unreacted succinimidyl group on DTSP SAM and to remove extra unbound antibodies onto the electrode surface.

3.5.5. Electrochemical impedance studies

Electrochemical impedance spectroscopy (EIS) is a powerful and sensitive technique to characterize surface-modified electrodes and for the investigation of electrochemical systems and processes [35, 38]. It uses periodic small amplitude AC signal over wide frequency range to measure resistive and capacitive response of materials [39-40]. EIS respond to change caused by binding of analyte to bio-recognition elements immobilized on the surface of the electrodes. Nyquist plots of impedance spectra in present studies have been exploited to study (i) change in charge transfer resistance (R_{ct}) at sensor-solution interfaces after DTSP SAM formation, Mab binding and EA blocking, (ii) the change of charge resistance with changing concentration of PSA. All EIS spectra were recorded in PBS (10 mM, pH 7.4) containing 5 mM $Fe(CN)_6^{3-/4-}$ as a redox probe.

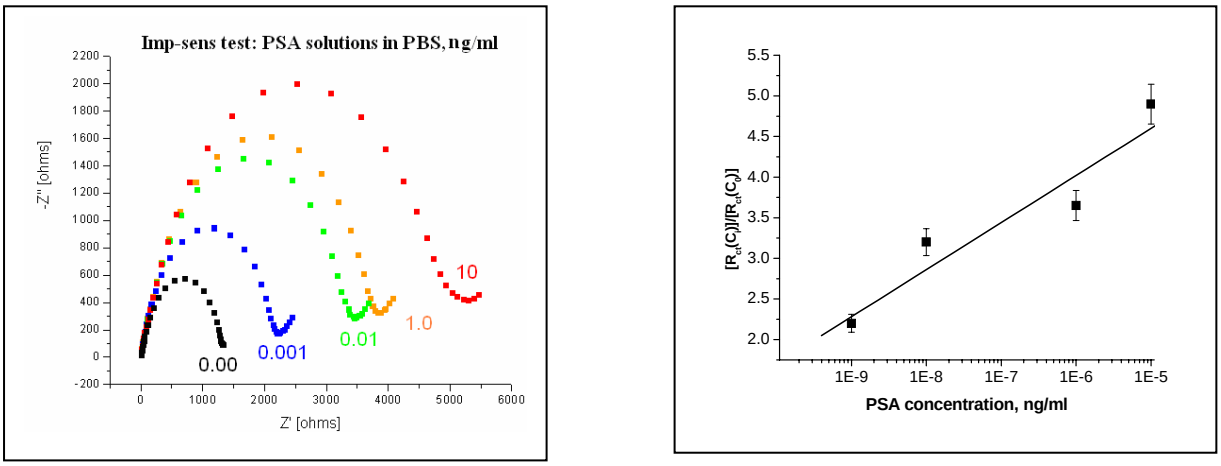

A B

Figure 22: Imp-sens initial test with PSA, diluted in PBS. A: EIS spectra; B. Normalized curve for data obtained from EIS studies for different PSA concentrations.

3.5.6. Sample collection and storage

Human serum/plasma samples, prospectively collected by Dr. Phelan's lab at Moffitt Cancer Center and participating clinics, were used in this study. These samples were obtained from African-American males, either positive for (cases), or having no clinical evidence (controls) of, PCa. There was no record of other cancers available for these patients. Informed consent was obtained from all subjects at time of blood draw. In the present work, researchers were not aware of any personal identifiers, associated with the human samples.

Samples were labeled, aliquoted and stored at deep freezer (-80^0 C) until further usage according to the Moffitt Cancer Center guidelines [41]. All procedures with the samples were completed within the 30 minutes since the blood draw. No sample have undergone more than 2 freeze-thaw cycles. All samples were tested for PSA and the values were recorded.

3.5.7. Imp-sens test with the PSA solutions in PBS

Imp-sens was initially utilized to detect PSA molecules in PBS in the concentration range 1pg/nl – 10 ng/ml (Fig. 23A). This range was chosen empirically, based on the interest for meeting both current needs in PSA sensitivity (usually up to 10 ng/ml in clinics) and establishing the lower detection threshold. For each concentration, the bio-electrode was incubated in PSA solution for 30 minutes, followed by PBS washing and EIS spectra recording using PBS (10 mM, pH 7.4) containing 5 mM $Fe(CN)_6^{3-/4-}$ as a redox probe. From Fig 3a, it is clear that R_{ct} (diameter of the Nyquist plots)

increases with increasing PSA concentration. The increas e in R_{ct} is attributed to the binding of PSA to i mmobilized anti-PSA on bio- electrode, producing a p acked lay er that decr eases the electron transfer fo r redox prob e. For sensing application relative change in EIS data have more significant information than ab solute value. Graph bet ween change in R_{ct} values and the logarithm of PSA co ncentrations reveals linear detection range for PSA con centrations in the range of 1pg/ml to 10 ng/ml (Figure 23B).

Though the im pedance of all electrodes fabr icated in the same batch can be ex pected to be the same, lack of industrial scale process control in the lab le ads to variations in i mpedance of individual electrode and antibody modified electrode. In order to confirm that o bserved change in im pedance wa s due to surface modification and not due to superim posed effects, all d ata was normaliz ed. For linear r ange detecti on, normalization was achieved by pl otting [charge transfer resistance for desired conc entration (R_{ct} (C_i))]/[charge transfer resi stance of blank EA/Mab/ DTSP/IDμE bio-electrode(R_{ct} (C_o))] versus logarithm of cortisol concentration (Fig 3b). After normalization, all electrodes with different impedance for bio-electrode with attached antibody exhibited similar response within the 4% error for each c oncentration. Fig 4b shows normalized data curve that can be characterized using R_{ct} (C_i)/R_{ct} (C_o) = 7.50 + 0.579 log C_{PSA} (g/ml). It reveals the linear range of 1pg/m l to 10 ng/m l with the correlation coefficient of 0.959. Furt her, to account for the variation in initi al impedance values for individual electrodes, all exper iments were carried out using a step-by-step approac h to increasing PSA concentration. Similar step-by-step concentration studies have been report ed by other resear chers and help to avoid superimposed effects of multi electrode measurement [42-45].

As is seen fr om the Figure 23B, the correlation coefficien t for the I mp-sens calibration curve is 0.959, suggesting a relatively weak linear trend. This effect was attributed to th e interfering effects of NSB which is a comm on obstacle in all bioassays, employing immunological affinity principles. Figure 23 dem onstrates the use of various bloc king techniques and their effects on NSB interference. Blocking buffers were obtained from Immunochemistry Techn ologies, LLC and used and stored according to m anufacturer's instructions . General Blocker (BB1) serve d as a general strength, and Neptune Block (BB2) served as an extra st rength blocking buffer. These buffers were specifically designed to be used in the ELISAs, including the sandwich ELISA.

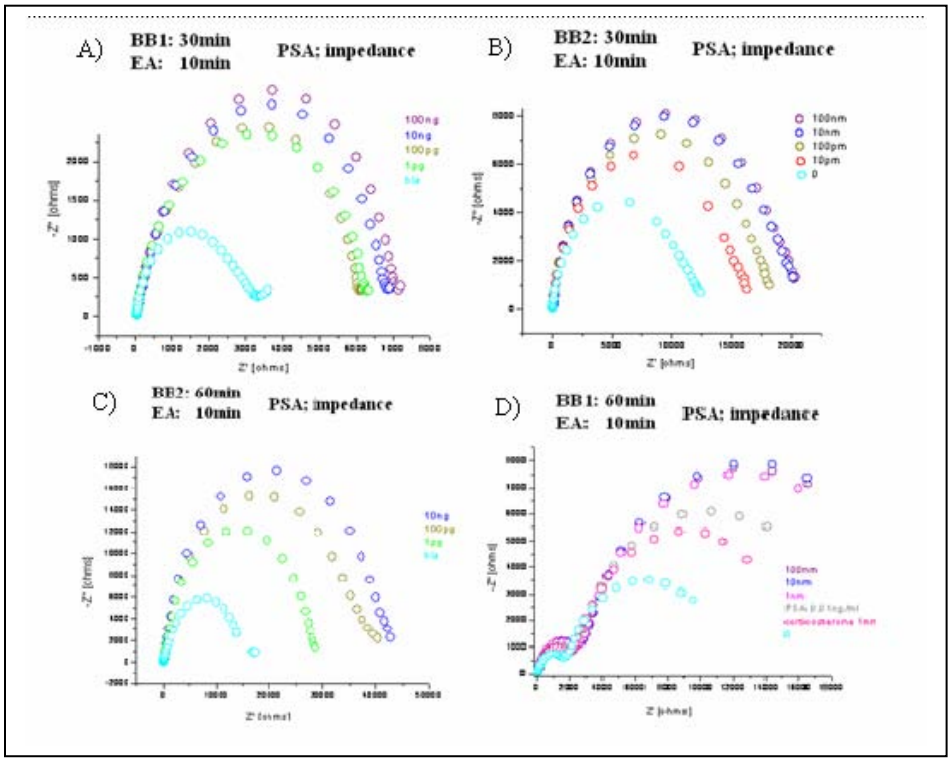

Figure 23: Imp-sens wit h PSA with varying blocking buffers and 30 m inute and 60 m inute tim e points show no effect on NSB intereference.
A: BB1 wash for 30 min and EA wash for 10 m in. B: BB2 was for 30 m in. and EA was for 10 min.
C: BB2 was for 60 m in. and EA wash for 10 min. D: BB1 was for 60 min. and EA was for 10 min.

Ethanolamine (EA) is wid ely used as a non-specific blocker in the electrochemical biosensors . It also has a capacity to remove any non-immunologically bound proteins that may have agglomerated on the surface. We studied the use of BB1

and BB2 for 30 and 60 minutes, followed by 10 minutes washing in 1% EA. It was revealed that the least blocking technique is the most effective (Figure 23).
The use of BB1, BB2, and EA as blocking agents was ineffective, as indicated by the curves corresponding to substantially different PSA concentrations producing similar or very close impedance signal (Z) (Figure 23). The NSB interference effect did not significantly change with introducing different blocking techniques (see Figure 23), including the use of extra strength blocking buffers and increased blocking times. Surprisingly, NSB issues were better controlled when real human serum/plasma sample was used.

3.5.8. Human plasma testing with Imp-sens

In the effort to better address the NSB issues, the real plasma sample with the lowest PSA concentration of 0.4 ng/ml, diluted 1000 times with PBS, was used as a diluent (we will further refer to this as simply a "diluent"). It is initially hypothesized that a human plasma sample, even when substantially diluted, will have enough proteins to block the initial electrode and minimize subsequent NSB during bioassays. At the same time, PSA concentration was kept low and equal which should not have interfered with the PSA detection. Using diluted plasma sample as a diluent and blocker allowed to mask major NSB issues and shift to actual complex human samples without the loss in sensitivity and selectivity. The diluent was subsequently spiked with different PSA concentrations. 1; 10 and 100 pg/ml of PSA were chosen as initial testing points, based on the previous results (Figure 24).

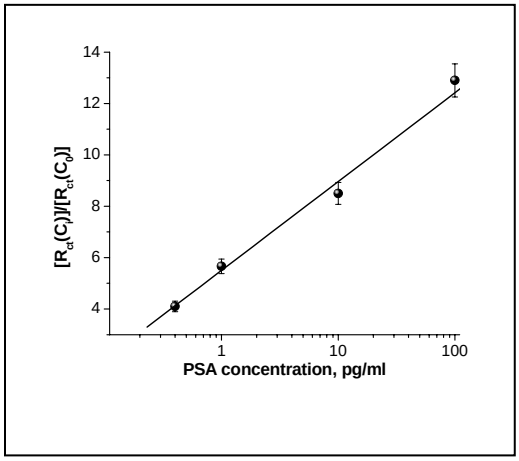

Figure 24: PSA sensing by impedance technique. BLK = electrode incubated with capture PSA antibody.

Providing that PSA concentration in base solution was 0.4pg/ml, the actual PSA values in the samples were 0.4; 1.4; 10.4; and 100.4; pg/ml. "Zero" or "blank" electrode impedance reading was obtained after the incubation with anti-PSA. As mentioned earlier, all samples were tested on the same electrode using the low to high concentration testing order. Similar studies were performed by other researchers and are convenient for the real time sensing. The results are shown on Figure 24. There is a clear dependence of the impedance resistance with increasing PSA concentration, indicating the PSA binding. Each step was resumed with the intense PBS washing to ensure complete removal of non-attached molecules.
An overall testing procedure schematic with Imp-sens, used in the experiment, was the following: 1. SAM formation on gold electrode (section # 2.4); 2. Anti-PSA incubation + wash + impedance reading (sections # 2.4 and 3.1); 3. Base solution ("blocker", 0.4 pg/ml PSA) incubation + wash + reading (section # 3.2.3); 4. 1 pg/ml incubation + wash + reading; 5. 10 pg/ml incubation + wash + reading; 6. 100 pg/ml incubation + wash + reading.

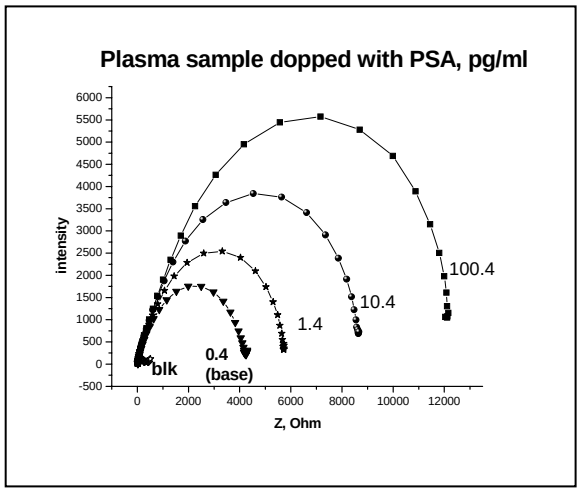

Figure 25: Normalized curve for data obtained from EIS studies for different PSA concentrations. 1000 times diluted human plasma sample was used as a blocker and a diluent to control NSB. Base (0.4 pg/ml) solution reading is shown instead and is taken as a zero. As indicated, there is a strong linear concentration dependence of the impedance increase in resistance with increased PSA concentration. The correlation coefficient for this experiment was 0.995 which is an indicator of a strong linear dependence.

3.5.9. Selective binding studies

Selectivity is a major and well-known pitfall in the biosensing techniques, based on the immunological principles. To ensure the selectivity of PSA binding, the cortisol antibody with increasing concentrations in PBS were tested on the electrodes, covered with capture anti-PSA. Anti-cortisol was used as a random protein which may contribute to nonselective binding. 0; 1; 10; 100 and 1000 pg/ml of anti-cortisol in PBS was used. The testing was done in exactly same conditions. The results are shown on Figure 26. There is a slight increase of resistance with increasing anti-cortisol concentrations, however, its intensity is very low, compared to PSA (15.5% highest increase compared to 312% highest increase for PSA), indicating that the NSB is in fact present, but is negligibly small. Further assay biochemistry optimizations may lower it even more.

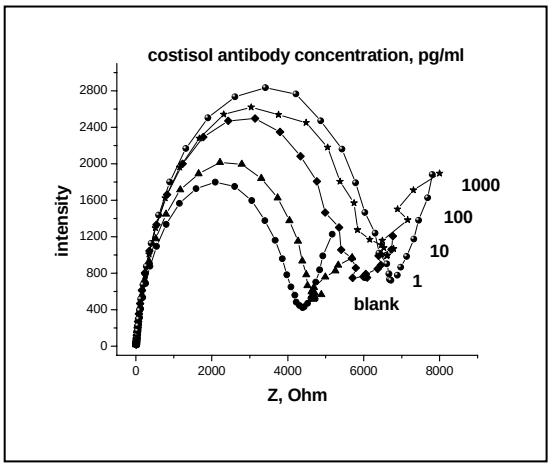

Figure 26: The interference studies of Imp-sens. Anti-cortisol binding on the bio-electrodes covered with anti-PSA.

3.6. Summary: Task 3 completed

3.7.Significance: Imp-sens, a novel portable impedimetric electrochemical immuno-sensor, can be used for an ultrasensitive and selective PSA detection. Imp-sens exhibits linear behavior in the concentration range 1pg/ml to 100 pg/ml, has low detection limit of 1 pg/ml which is at least 10 times lower than a standard commercially available, most sensitive PSA ELISA kit in the market. An average analysis time was 45 mins with Imp-sens. The sensor was found selective against cortisol antibodies in the concentrations 1 – 1000 pg/ml and was tested as a proof of concept with the human plasma sample, spiked with increasing PSA concentrations.

The main goal of this work was to establish a feasibility of using an Imp-sens as an inexpensive, reliable sensing device, suitable for point-of-care applications capable of working with complex bodily fluids like saliva, serum/plasma or urine. The sensor was therefore tested with a handful of samples and statistical analysis was out of the scope of this work. Achieving statistically significant validation of Imp-sens with a number of human serum/plasma samples is being the author's next task.

In the Future, Imp-sens concept will be further expanded to validate and characterize the sensor for PSA detection with statistically significant amount of samples, as well as utilizing it for detection of other potential PCa biomarkers.

Task 4. To derive optimal cutpoints for the sensitivity and specificity of the QD-conjugated biomarkers developed in Aims 2 to 3 individually, and in combination, for the early detection of prostate cancer in African-American men. (Months 26-36 according to Timeline). Approach: Assay the levels of the individual biomarkers in serum samples collected during PSA/DRE screening using a nested case- control approach. We will use logistic regression and Receiver Operator Curves to define the cutpoints that collectively define the optimal performance of the entire panel.

4.1. Summary: See above. Our sample size is rather small for detailed statistical analysis.

C. Key research accomplishments

1. Study recruitment.
2. Established database including demographic, health, risk factor and psychosocial data.
3. Established tissue collection including multiple aliquots of plasma and sera per patient and pellet for DNA extraction.
4. Exposure in the press regarding the study and press conference at the AACR meeting. The press coverage continues and our study was highlighted in the Department of Defense annual report.
5. Achieved funding for a further year of study using aptamer technology and microfluidic devices.
6. Determined the most reproducible nanotechnology is nanowire-integrated microfluidic devices.
7. Determined that all the chosen biomarkers except PSA are not suitable biomarkers so novel biomarkers must be identified.

D. Reportable outcomes

D.1. Press Release

Invited to attend a press conference in Disparities Research at the AACR annual 2008 meeting and the study was highlighted in the Department of Defense Prostate Cancer Research Program Annual Report and other journals and health magazines.

D.2. Publications:

1. TV Tochynska, A Diaz Cano, M Dybiec, S Ostapenko, M Morales Rodrigez, S Jiménez-Sandoval, Y Vorobiev, C Phelan, A Zajac, T Zhukov, T Sellers. Raman scattering and SEM study of bio-conjugated core-shell CdSe/ZnS quantum dots. *Phys Stat. Solid*. 2007; 4(2): 241-243.
2. M. Dybiec, G. Chornokur, and S. Ostapenko, A. Wolcott and J. Z. Zhang A. Zajac, C. Phelan, and T. Sellers. Photoluminescence spectroscopy of bioconjugated CdSe/ZnS quantum dots. *Appl. Phys. Lett.* 2007; 90(26): 263112-263115.
3. Ganna Chornokur, Sergei Ostapenko, Yusuf Emirov, Nadezhda Korsunska, Abraham Wolcott, Jin Zhang, Catherine Phelan, Abhilasha Nagaram, Thomas Sellers. Biologically Engineered Quantum Dots for Biomedical Applications. *MRS Proceedings*. 2008; 1095E**:** 1095-EE08-05.
4. G Chornokur, S Ostapenko, Yu Emirov, N E Korsunska, T Sellers and C Phelan. Spectroscopic behavior of bioconjugated quantum dots. *Semicond. Sci. Technol*. 2008; 23(7): 075045.
5. G. Chornokur, S. Ostapenko, E. Oleynik, C. Phelan, N. Korsunska, T. Kryshtab, J. Zhang, A. Wolcott and T. Sellers. Scanning Photoluminescent Spectroscopy of Bioconjugated Quantum Dots. *Superlattices and Microstructures*. 2008; 45(4-5): 240-248.

D.3. Oral presentations:

1. 'Early detection of prostate cancer in African-American men.' FPCN Brother-to-Brother meetings, Municipal library, Martin Luther King Blvd, Tampa. September 2006- Catherine Phelan
2. 'Prostate cancer in African-American men: Serum biomarkers for early detection using nanoparticles.' Moffitt Cancer Center Genitourinary Tumor Board. October 2006. Catherine Phelan.
3. 'Early detection of prostate cancer in African-American men.' FPCN Brother-to-Brother meetings, Municipal library, Martin Luther King Blvd, Tampa. March 2007 - Catherine Phelan
4. 'Prostate cancer in African-American men: Serum biomarkers for early detection using nanoparticles.' Moffitt Cancer Center Genitourinary Tumor Board. June 2007 - Catherine Phelan.
5. 'Nanoparticle-Conjugated Biomarkers for Early Detection of Prostate Cancer in African-American Men'. ImPaCT Invited speaker Sept. 2007 - Catherine Phelan.
6. 'Nanoparticle-conjugated biomarkers for early detection of prostate cancer in African-American men.' Grand Rounds in Population Sciences, Moffitt Cancer Center: October 25th 2007 - Catherine Phelan
7. 'Biomarkers' to Cancer Biology PhD students, Moffitt Cancer Center, November 8th, 2007 - Catherine Phelan.
8. 'Early detection of prostate cancer in African-American men.' FPCN Brother-to-Brother meetings, Municipal library, Martin Luther King Blvd, Tampa. February 2008 - Catherine Phelan
9. 'Early detection of prostate cancer in African American men.' Gastrointestinal and Genitourinary Current Therapies and Clinical Trials Agenda. March 28-29 2008 - Catherine Phelan
10. U. S. Department of State International Visitor Leadership Program, Moffitt Cancer Center. October 30, 2008 - Catherine Phelan
11. 'Biomarkers' to Cancer Biology PhD students, Moffitt Cancer Center. November 2008 - Catherine Phelan
12. 'Biomarkers' to Cancer Biology PhD students, Moffitt Cancer Center. October 2009 - Catherine Phelan

D.4. Abstracts and Poster presentations

1. Catherine M. Phelan, Thomas Sellers, Julio Pow-Sang, Alecsander Zajac, Abhilasha Nagaram, Jennifer Muller, Tatyana Zhukov, Raoul Salup, Sergei Ostapenko, Maciej Dybiec, Anna Chornokur and Jin Zhang. Nanoparticle-Conjugated Biomarkers for Early Detection of Prostate Cancer in African-American Men. Presented at:

Congressionally Directed Medical Research Programs Prostate Cancer Research Program 2007 IMPaCT Meeting,; September 5-8, 2007; Atlanta, Georgia.
2. G. Chornokur, S. Ostapenko, Yu. Emirov, A. Wolcott, J. Zhang, A. Nagaram, T. Sellers, and C. Phelan Biologically Engineered Quantum Dots for Biomedical Applications. Presented at: Materials Research Society meeting; March 25, 2008; San Francisco, California.
3. Catherine M. Phelan, Sergei Ostapenko, Anna Chornokur, Richard Tanner, Jin Zhang, Julio Pow-Sang, John Jack Steel, Thomas Sellers. Nanotechnologies and early detection of prostate cancer'. American Association of Cancer Research; April 16, 2008; San Diego, California.

D.5. Degrees obtained/contributed to by this study

1. Maciej Dybiec
   'Spatially Resolved Photoluminescence Spectroscopy of Quantum Dots'. A dissertation submitted in fulfillment of the requirements for the degree of Doctor of Philosophy, Department of Electrical Engineering, College of Engineering, University of South Florida, Completed June 2007. Main mentor: Sergei Ostapenko.

2. Ganna Chornokur:
   'Photoluminescence Spectroscopy of Bio-Conjugated Quantum Dots', Degree of Doctor of Philosophy, Department of Electrical Engineering, College of Engineering, University of South Florida - Completed Feb 2009. Main mentor: Sergei Ostapenko; Thesis committee member: Catherine Phelan

3. Marcus Marley:
   'Microfluidic devices and their application to early cancer detection'. Masters degree - Completed March 2008. Department of Electrical Engineering, College of Engineering, University of South Florida. Main mentor: William Lee; Thesis committee member: Catherine Phelan

D.5. Tissue or serum repositories – We have collected DNA, serum and plasma on all cases and controls. The specimens are stored in minus 80C freezers in the Tissue Procurement Facility at the Moffitt Cancer Center. Aliquots are retrieved on request. See Appendix 1.

D.6. Databases – Access database from the questionnaire and pathological data and psychosocial aspects to risk perception. Table 3 is based on a sub-portion of the total number of cases and controls.

D.7. Funding applied for based on work supported by this award

1. Cancer Research and Prevention Foundation – 'Quantum dot-conjugated biomarkers for early detection of breast cancer in Mexico –PI Catherine Phelan (2006)
2. Nanotechnology Sensors and Systems for Early Detection of Cancer – 'Microfluidic devices for early detection of breast cancer in Mexico - PI Sellers, Phelan PI of Pilot Study (Dec. 2007)
3. Lustgarten foundation – ' Enhanced detection of pancreatic cancer using advanced molecular probes –PI Phelan (2007)
4. NIH Health Disparities Center of Excellence P20. 'Aptamer-based microfluidic devices for early prostate cancer in African American men.' RO1 format PI – Catherine Phelan.
5. Moffitt Cancer Center/University of Florida Joint Cancer Center Funding Opportunity Advancing the Partnership (AP) Awards - PI Catherine Phelan – (Funded to July 2010) - $99,931

E. Conclusion

Implications of completed research: We have investigated emerging cutting-edge nanotechnologies, for early detection of prostate cancer in African-American men. Despite our initial enthusiasm for QDs as the nanotechnology of choice, we determined that QD technology is cost-prohibitive for use in a large population-based screening and lacks reproducibility. We investigated another type of nanotechnology - nanowire-integrated microfluidic devices and found these to function well for sub-ELISA level detection and will employ this technology in the future. Initially we chose six candidate biomarkers but showed they are unusable either due to technical difficulties in our hands or their levels did not show

differences between cases and controls or they decreased in concentration through increasing stage of disease. PSA is still the most optimal bio marker for prostat e cancer detection. So our final research (m anuscript in preparation) brings th ese two components together for the most optimal prostate cancer detection.
The samples collected in this study are essential for other studies in African-American men. We are planning to continue recruitment by expanding the collection Florida state-wide. Furthermore we are collaborating with other re searchers in a consortium known as 'Men of African Descent with Cancer of the Prostate -MADCaP' for future studies.

"so what section" – The novel, sensitive biom arkers generated in this study will be of vital im portance for early detection of prostate cancer in Afri can-American men to reduce the morbidity and m ortality from this disease. We are applying novel technologies. Further more, we ar e appl ying our knowledge and these tec hnologies for early de tection of ot her cancer types.

F. References

1. Warren C, Chan W, Nie S. Quantum dot bioconjugates for ultrasensitive nonisotopic detection. Science 1998; 281: 2016-18.
2. Human PSA ELISA Kit from Abazyme. Available from: URL: http://www.biocompare.com/itemdetails.asp?itemid=434262
3. Jurincic-Winkler C, Von der Kammer H, Horlbeck R, Klippel K-F, Pixberg H., Scheit K-H. Clinical evaluation of a new prostate-specific antigen sandwich ELISA which employs four monoclonal antibodies directed at different epitopes of prostate-specific antigen. Eur. Urol. 1993;24: 487-91.
4. Dybiec M, Chornokur G, Ostapenko S, Wolcott A, Zhang JZ, Zajac A, Phelan C and Sellers T. Photoluminescence spectroscopy of bioconjugated CdSe/ZnS quantum Dots. Appl Phys Lett 2007;90: 2631-12.
5. Chornokur G, Ostapenko S, Emirov Yu, Korsunska NE, Sellers T and Phelan C. Spectroscopic behavior of bioconjugated quantum dots. Semicond Sci Technol 2008;23: 075045-52.
6. Chornokur G, Ostapenko S, Emirov Yu, Korsunska NE, Wolcott A, Zhang J, Phelan C, Nagaram A, Sellers T. Biologically Engineered Quantum Dots for Biomedical Applications. MRS Proc 2008;1095E**:** 1095-EE08-05.
7. Borkovska L, Korsunska N, Krystab T, Pecherska E, Germash L, Ostapenko S, Chornokur G. Effect of conjugation with biomolecules on photoluminescence and structural characteristics of CdSe/ZnS quantum dots. Semiconductors 2009; 43(6).
8. Diaz Cano A, Torchynska TV, Dybiec M, Ostapenko S, Jiménez-Sandoval S, Vorobiev Y, Phelan CM, Zajac A, Zhukov T. Raman scattering and SEM study of bio-conjugated core-shell CdSe/ZnS quantum dots. Physica Status Solid 2007*;* 4: 241-3.
9. Dybiec M. Spatially Resolved Photoluminescence Spectroscopy of Quantum Dots [dissertation]. Tampa: University of South Florida; 2006.
10. Ramgir NS, Zajac A, Sekhar PK, Lee L, Zhukov T A, Bhansali S. Voltammetric Detection of Cancer Biomarkers Exemplified by Interleukin-10 and Osteopontin with Silica Nanowires J Phys Chem 2007; 111:13981-87.
11. Aravamudhan S, Kumar A, Mohapatra S, Bhansali S. Sensitive estimation of total cholesterol in blood using Au nanowires based micro-fluidic platform. Biosens Bioelectron 2007; 22:2289– 94.
12. Kumar A, Aravamudhan S, Gordic M, Bhansali S, Mohapatra SS. Ultrasensitive detection of cortisol with enzyme fragment complementation technology using functionalized nanowire. Biosens Bioelectron 2007; 22:2138–44.
13. Rahman RA, Lo C-M, Bhansali S. A MEMS Micro-Electrode Array Bio-sensor for Impedance Spectroscopy of Human Umbilical Vein Endothelial Cells. Sensors & Actuators B 2006; 118:115-20.
14. Ramgir NS, Zajac A, Sekhar PK, Lee L, Zhukov T, Bhansali S. Ultrasensitive Voltammetric Detection of IL-10, a Lung Cancer Biomarker, in Serum using SiO2 Nanowires Template. Sensors Lett 2007; 5:1-4.
15. Aravamudhan S, Kumar A, Mohapatra S, Bhansali S. Sensitive Estimation of Total Cholesterol in Blood using Au Nanowires based Micro-Fluidic Platform. Biosensors & Bioelectronics 2007; 22:2289-94.
16. Kumar A, Aravamudhan S, Gordic M, Bhansali S, Mohapatra SS. Ultra sensitive detection of cortisol with enzyme fragment complementation technology using functionalized nanowires Biosensors & Bioelectronics 2007; 22:2138-44.
17. Dhand C, Arya SK, Datta M, Malhotra BD. Polyaniline-carbon nanotube composite film for cholesterol biosensor. Anal Biochem 2008; 383: 194–9.
18. Ramgir N, Sekhar PK, Sun K, Bhansali S. Cortisol Detection in Saliva using Silica Nanowires as a Template for Enzyme Immunoassay. In: Proceedings of the 213th ECS Meeting: 2008 May 18-22; Phoenix, AZ, USA.
19. Radke SM, Alocilja EC. A high density microelectrode array biosensor for detection of E. coli O157: H7. Biosens Bioelectron 2005; 20:1662–7.
20. Qin Y, Bakker E. Elimination of Dimer Formation in In ^{III}Porphyrin-Based Anion-Selective Membranes by Covalent Attachment of the Ionophore. Anal Chem 2004; 76: 4379–86.
21. Alegret S. Integrated Analytical Systems. XXXIX; Elsevier B.V. Amsterdam 2003 (Chapter 1).
22. Arya SK, Solanki PR, Singh RP, Pandey MK, Datta M, Malhotra BD. Application of octadecanethiol self-assembled monolayer to cholesterol biosensor based on surface plasmon resonance technique. Talanta 2006; 69:918–26.

23. Oka K, Noguchi M, Kitam ura T, Shima S. Liquid chro matography and radioimmunoassay co mpared for determination of cor tisol and cor ticosterone in plasma after a dexa methasone suppression test**.** Clin Chem 1987; 33: 1639–42.
24. Appel D, Sc hmid R D, Dr agan CA, Bu reik M, Urla cher VB. A f luorimetric a ssay for cortisol. Anal Bio anal Ch em 2005: 383: 182–6.
25. Gatti R, Cap pelli E, Zecchin B, Antonelli G, Spinel la P, Mantero F, De Palo EF. Urinary high performance reverse phase chromatography cortisol and cortisone analyses before and at the end of a race in elite cyclists. Chromatography B 2005: 824, 51–6.
26. Jerkunica I, Sophianopoulos J, Sgoutas D. Im proved ultr afiltration m ethod for determ ining unbound cortisol in plasma. Clin Chem 1980; 26: 1734-7.
27. Vogeser M, Mohnle P, Briegel J. Free seru m cortisol: quan tification appl ying equilibrium dialysis or ul trafiltration and an automated immunoassay system. Clin Chem Lab Med 2007; 45: 521-5.
28. Cook NJ, Schaefer AL, Lepage P, and Jones SDM. Radioimmunoassay for Cortisol in Pig Saliva and Serum. J Agric Food Chem 1997; 45: 395-9
29. Schmalzing D, Nashabeh W, Yao XW, Mhatre R, Regnier FE, Afeyan NB, Fuchs M. Capillary Electrophoresis-Based Immunoassay for Cortisol in Serum. Anal Chem 1995; 67: 606-12.
30. Kaptein WA, Zwaagstra JJ, Venema K, Ruiters MHJ, Korf J. Con tinuous Ultraslow Microdialy sis and Ultrafiltration for Subcutan eous Sampling As Dem onstrated by Glucose and Lactate Me asurements in R ats. Anal Chem 1998; 70: 4696–700.
31. Sarkar M, Das BC, B ora BD, Kumar V, Mohan K, Mey er HHD, Prakash BS. Application of sensitive enzymeimmunoassay for determination of cortisol in blood plasma of y aks (*Poephagus grunniens* L.). Gen Co mp Endo 2007; 154: 85–90.
32. Mitchell JS, Lowe TE, In gram JR. Rapid ultrasensitive measurement of salivar y cortisol using nano-linker che mistry coupled with surface plasmon resonance detection. Analyst 2009; 134: 380–6
33. Bard AJ, Stratmann M, Unwin PR. Instrumentation and Electroanalytical Chemistry, vol. 3, Wiley-VCH, New Jersey, 2003 (Chapters 1–2).
34. Barsoukov E , MacDonald JR. I mpedance Spectroscopy : Theo ry, Experim ent and Applications, second ed., Wiley Interscience, New Jersey, 2005 (Chapter 1).
35. Sun K, Ramgir N, Bhansali S. An immunoelectrochemical sensor for salivary cortisol measurement. Sens Actuators B 2008 ; 133 : 533–7.
36. Katz E, Will ner I. Probing Biom olecular Interactio ns at Conductive and Semiconductive Surfaces by I mpedance Spectroscopy: Routes to Impedimetric Immunosensors, DNA-Sensors, and Enzyme Biosensors. Electroanalysis 2003; 15: 913–47.
37. Guan J, Miao Y, Zhang Q. Impedimetric biosensors. J Biosci Bioeng 2004; 97: 219–26.
38. Bott AW. Electrochemical techniques for the characterization of redox polymers. Curr Sep 2001; 19: 71–5.
39. Moffitt Cancer Center and Research Institute Official Website. Available from: URL: www.moffitt.org
40. Stevens RC, Soelberg SD, Near S, Furl ong CE. Detection of cort isol in saliva with a flow-filtered, porta ble surface plasmon resonance biosensor system. Anal Chem 2008; 80: 6747–51.
41. Hnaiein M, Hassen WM, Abdelghani A, Fournier-Wirth C, Coste J, Bessueill e F, Leonard D, Jaffrezic-Renault N. A conductometric i mmunosensor based o n f unctionalized magnetite nanoparticles for *E. coli* detection. Electroch em Comm 2008; 10:1152-4.
42. Su XL, Li Y. A QCM i mmunosensor for *Salmonella* detection with sim ultaneous measurements of resonan t frequency and motional resistance. Biosens Bioelectron 2005; 21: 840–8.
43. Huang Y, Bell MC, Suni II. Impedance Biosensor for Peanut Protein Ara h 1. Anal Chem 2008;80: 9157–61.
44. Lee YG, Chang KS. Application of a flow type quartz crystal microbalance immunosensor for real time determination of cattle bovine ephemeral fever virus in liquid. Talanta 2005; 65: 1335–42.
45. Lien TTN, Lam TD, An VTH, Hoang TV, Quang DT, Khieu DQ, Tsukahara T, Lee YH, Kim JS. Multi-wall carbon nanotubes (MWCNTs)-doped polypyrrole DNA biosensor for label-free detection of genetically modified organisms by QCM and EIS. Talanta 2010; 80: 1164-9.

phys. stat. sol. (c) **4**, No. 2, 241–243 (2007) / **DOI** 10.1002/pssc.200673249

Raman scattering and SEM study of bio-conjugated core-shell CdSe/ZnS quantum dots

T. V. Torchynska[*, 1], **A. Diaz Cano**[1], **M. Dybiec**[2], **S. Ostapenko**[2], **M. Morales Rodrigez**[3], **S. Jiménez-Sandoval**[4], **Y. Vorobiev**[4], **C. Phelan**[5], **A. Zajac**[5], **T. Zhukov**[5], and **T. Sellers**[5]

[1] SEPI – Instituto Politécnico Nacional, México D. F. 07738, México
[2] University of South Florida, 4202 E. Fowler Ave, Tampa, FL, USA
[3] Universidad Autónoma Metropolitana, Ud. Azcapotzalco, México D. F., México
[4] CINVESTAV, Unidad Querétaro, 76230 Querétaro, México
[5] H. Lee Moffitt Cancer Center and Research Institute, Tampa, FL, USA

Received 30 July 2006, accepted 18 August 2006
Published online 7 February 2007

PACS 68.37.Hk, 73.21.La, 78.30.Fs, 78.67.Hc

Core-shell CdSe/ZnS quantum dots are promising as bio-luminescent markers: being conjugated to bio molecules (proteins), they serve as luminescence tags in antigen-antibody biochemical reaction. This presents a possibility to detect, for example, the variation of the protein biomarkers to promote the early cancer diagnosis. We studied the effect of bio molecules conjugated to QDs using Raman scattering spectra, and found that in some cases the conjugation leads to noticeable variation of these spectra, so that the detection of bio molecules could be done more accurately. An explanation of the effect is proposed.

1 Introduction

The nanometer-scale II-VI semiconductors quantum dots (QDs) have unique optical properties such as photoluminescence (PL) with sufficiently high quantum efficiency in surface passivated core-shell structures [1]. A particularly interesting case is the CdSe/ZnS core/shell structures, where a large band-gap material (ZnS) serves as a surface passivating layer and as a barrier assisting the electron-hole confinement in the CdSe core [2]. It has been reported [3] that these QDs can be used as bio-luminescent markers varying the PL intensity when coupled to different bio molecules and thus indicating changes in quantity of these molecules. The attempts were made to employ this effect for diagnosis of various diseases, including ovarian, lung, and prostate cancers, which are associated with altered expression of cancer-related protein and DNA markers in living tissue or cells whose detection is crucial for early stage diagnose. For example, clinical study described in [3] has shown that detection of enhanced level of osteopontin in circulating blood allows accurate early detection of this disease [3, 4]. Another example is PSA (Prostate-Specific Antigen), which is a protein produced by the cells of the prostate gland, and its level increases in case of the prostate cancer or some other serious prostate diseases [5].

A novel approach is based on spatially resolved PL spectroscopy by using QDs bio-conjugated to specific antibodies (IgG proteins). Concurrently, it is important to look for other effects of the QDs bio-conjugation which could offer additional information on structure of the bio-conjugated QDs along with the proof of actual bio-conjugation, which is questionable in many cases. Here we present the results of Raman light scattering investigation in CdSe/ZnS QDs conjugated to two different types of antibodies.

[*] Corresponding author: e-mail: ttorch@esfm.ipn.mx, Phone: 52 55 5752 6008, Fax: 52 55 5752 6008

It is shown that in one case the conjugation leads to appearance of new lines in the Raman spectrum thus giving an opportunity to more accurate spectroscopic confirmation of the bio-conjugation.

2 Results and discussion

The commercially available core-shell CdSe/ZnS quantum dots were used in a form of colloidal particles diluted with phosphate buffer (PBS) in a 1:200 volumetric ratio [6]. Samples of QDs (bio conjugated and non-conjugated) in the form of an 5 mm-size spot were dried on a polished surface of crystalline Si substrate to ensure a low level of light scattering background. The proteins used for conjugation were mouse monoclonal anti human Osteopontin antibody (mab), and mouse anti PSA (Prostate-Specific Antigen) mab.

Raman scattering spectra were measured at room temperature in a Lab Ram-Dilor micro Raman spectrometer using a He-Ne laser (632.8 nm) as an excitation source with a power of 20 mW in backscattering configuration. The SEM images were obtained with PHILIPS XL30 ESEM.

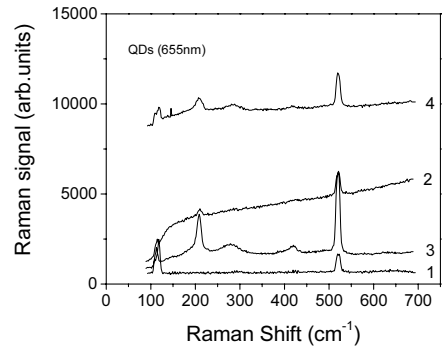

Fig. 1 Raman spectrum of non-conjugated (1, 2) QDs and conjugated with Osteopontin molecules (3, 4).

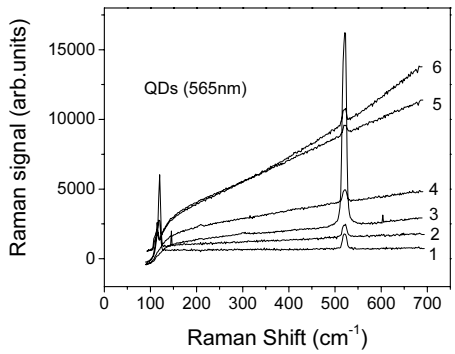

Fig. 2 Raman spectrum of non-conjugated (1, 2, 3) QDs and conjugated with PSA molecules (4, 5, 6).

Figure 1 presents the Raman spectra of QDs, designed for light emission with the PL wavelength peak at 655 nm, non-conjugated (curves 1, 2) and conjugated (curves 3, 4) with anti human Osteopontin antibody molecules. The sharp peak at 521 cm^{-1} represents the LO phonon Raman signal of the Si substrate and that at 114 cm^{-1} is of instrumental origin. As can be seen, the spectrum of pure non-conjugated QDs has no other features. In contrary, the spectrum of bio-conjugated QDs exhibits three additional bands – at 208.6, 278.4 and 418.0 cm^{-1}. The strongest band at 208.6 cm^{-1} corresponds to the optical phonon of QD core material – CdSe and its overtone is observed at 418.0 cm^{-1}, while the band at 278.4 cm^{-1} can be interpreted as the TO mode of the ZnS shell.

Figure 2 shows Raman scattering spectra for another type of QDs (the PL wavelength at 565 nm) conjugated with other bio-molecules – anti-PSA antibody. Both, non-conjugated and conjugated samples are identical and show no additional lines. This differs from the previous case of bio-conjugated anti-Osteopontin antibody. We also noticed that Raman spectra of the bio-conjugated QDs, as a rule, are characterized by a broad background signal due to diffused light scattering.

Figures 3 and 4 present Scanning Electron Microscopy (SEM) images of non-conjugated and conjugated QDs on Si substrate. It is obvious that even in a micron scale these two images are quite different: the percentage of area covered with conjugated QDs is much larger than that corresponding to pure QDs. The corresponding antibody molecules are quite large (thousands of atoms) and are capable of providing strong enough interactions with QDs (which actually starts from the conjugation itself).

We may suggest that in pure QDs the Raman lines of the QD material are weak due to a small volume of nano-sized particles, whereas the presence of anti-Osteopontin mab greatly enhances the optical phonon signal originated from the core-shell CdSe/ZnS QDs. Optical field enhancement near the surface of illuminated nanoparticles can be observed as surface enhanced Raman scattering (SERS) or surface enhanced infrared absorption (SEIRA) [7–10].

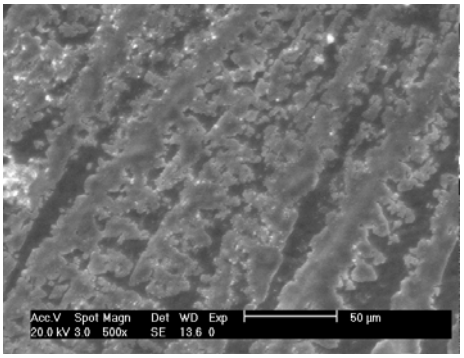

Fig. 3 SEM images of Si substrate covered with conjugated QDs.

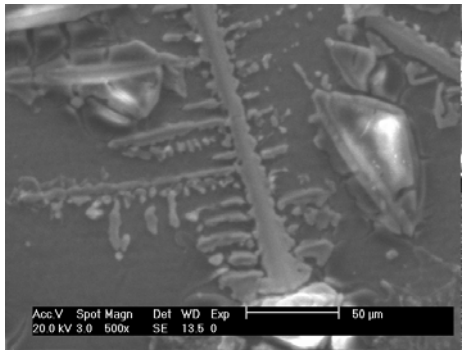

Fig. 4 SEM images of Si substrate covered with non-conjugated QDs.

Typically, locally enhanced electric field in SERS is attributed to the plasmon resonance at the interface of metallic nanoparticles. As a result a plasmon-polariton resonance occurs when a system of metallic nanoparticles and studied structures is illuminated at a proper wavelength.

The surface electric field enhancement due to the realization of another resonance conditions such as phonon or exciton resonances has been established as well [11, 12]. For example in [12] the enhanced IR absorption due to phonon-resonance mechanism is demonstrated for anthracene coating polar dielectric nanoparticles of SiC and Al_2O_3. An enhancement factor greater than 100 was measured near the surface of polar SiC particles at the realization of SiC surface phonon-polariton resonance. Thus, in general phonons, plasmons or exitons can satisfy resonance conditions for maximum local electric field enhancement.

In our case, Raman enhancement is observed only for CdSe/ZnS QDs conjugated with anti human Osteopontin mab and has negative effect for QDs conjugated with anti-PSA antibody. The actual mechanism of interaction between QDs and different bio molecules has to be studied in more details to address the issue why some molecules promote the enhanced Raman intensity while others do not. It is quite possible that here we observe conditions when QDs with different size/structure (655nm and 565 nm) interact with antibody molecules of different primary and secondary spatial structure, that eventually affects the position of QDs in conjugate complex and modulate its optical properties. The results obtained could be useful in the application of QDs mentioned as biomarkers for cancer diagnostic purposes.

Acknowledgement This research was funded in part by the Department of Defense Prostate Cancer Research Program, grant No. PC050873 as well as by CONACYT, Mexico, project U42436 and SIP-IPN.

References

[1] M. A. Hines et al., J. Phys. Chem. **100**, 468 (1996).
[2] M. Bruchez et al., Science **281**, 2013 (1998).
[3] H. I. Pass, D. Lott, F. Leonardo et al., The New England J. of Medicine **353**, 1564 (2005).
[4] D. Agrawal, T. Chen, R. Irby et al., J. Natl. Cancer Inst. **94**, 513 (2002).
[5] I. M. Thompson, D. K. Pauler, P. J. Goodman et al., The New England J. of Medicine **350**, 2239 (2004).
[6] www.qdots.com
[7] A. Campion and P. Kambhampati, Chem. Soc. Rev. **27**, 241 (1998).
[8] F. J. García-Rodriguez et al., J. Raman Spectrosc. **29**, 763 (1998).
[9] R. F. Aroca, D. J. Ross, and C. Domingo, Appl. Spectrosc. **58**, 324A (2004).
[10] A. Znagwill, Physics at Surfaces (Cambridge University Press, Cambridge, N. Y., 1996), pp. 330–333.
[11] P. K. Aravind and H. Metiu, Surf. Sci. **124**, 506 (1983).
[12] M. S. Anderson, Appl. Phys. Lett. **83**, 2964 (2003).

Photoluminescence spectroscopy of bioconjugated CdSe/ZnS quantum dots

M. Dybiec, G. Chornokur, and S. Ostapenko[a)]
Nanomaterials and Nanomanufacturing Research Center, University of South Florida, Tampa, Florida 33620

A. Wolcott and J. Z. Zhang
Department of Chemistry and Biochemistry, University of California, Santa Cruz, California 95064

A. Zajac, C. Phelan, and T. Sellers
H. Lee Moffitt Cancer Center and Research Institute, Tampa, Florida 33620

D. Gerion
Physics and Advanced Technology, Lawrence Livermore National Laboratory, Livermore, California 94550

(Received 6 April 2007; accepted 5 June 2007; published online 26 June 2007)

The authors performed scanning photoluminescence (PL) spectroscopy on CdSe/ZnS core/shell quantum dots (QDs) bioconjugated to Interleukin 10 (IL10) antibody. The influence of IL10 on the QD photoluminescence spectra was explored on samples dried on solid substrates at various temperatures. A "blue" up to 15 nm spectral shift of the PL maximum was observed on the bioconjugated QDs. The spectral shift is strongly increased after samples annealing above room temperature. A mechanism of the observed effect is attributed to changes in the QD electronic energy levels caused by local electric or stress field or chemical reactions which occurred on the QD surface. © *2007 American Institute of Physics*. [DOI: 10.1063/1.2752537]

Semiconductor nanoparticles or quantum dots (QDs) such as CdSe–ZnS core-shell structures exhibit particle-size dependent tunable photoluminescence (PL) with narrow emission bandwidths of 30–45 nm that span the visible spectrum and broad absorption and PL excitation spectra that allow simultaneous excitation of several particle sizes at a single excitation wavelength. QDs have high PL quantum yield ranging from 10% to 50% depending on nanocrystal quality and surface passivation while exhibiting a high resistance to photodegradation.[1] The ability to decorate the QD surface with specific functional groups [thiols, amines, poly(ethylene glycol), etc.] is a critical step in producing efficient QD bioconjugates.[2] Bioconjugation of proteins to QD surfaces can be achieved directly via electrostatic interaction or through covalent bonds via functional groups on the QD surface with different linker molecules.[3] At this time the full impact of the bioconjugation process on the luminescent/spectral properties of QDs is not fully understood. One key function of QD bioconjugates is to fluoresce readily and remain stable in biological conditions in order to allow for efficient detection. Most studies of QD-biological systems rely primarily on the overall PL intensity of a stained material either with QDs or fluorescent dyes.[4] These measurements are prone to errors that may arise from unwashed dyes or nonconjugated QDs in solution. Spectroscopic confirmation of a bioconjugation with additional features such as spectral shift of emission maxima or change in the peak full width at half maximum (FWHM) would greatly improve the overall precision and detection limits of immunofluorescent assays. A recent study of the multiplexed CdSe/ZnS QDs bioconjugated with various antibodies indicated that the quantum dot PL band spectral shift is observed within a few nanometers range; however, no detailed study of this effect was performed.[5] In our experimental study a specific ovarian cancer antibody Interleukin 10 (IL10) was selected as a protein conjugated to QDs. Screening tests for rare diseases such as ovarian cancer must have high sensitivity and specificity. Motivated by the scientific merit of inflammatory cytokines as biomarkers for ovarian cancer and the recent report in which IL10 was not detectable,[6] we sought to evaluate whether QD bioconjugation methodology could overcome this deficiency. More experiments are currently in progress to justify this approach.

Commercial 605, 655, and 705 nm CdSe/ZnS core-shell QDs covered with a polymer were obtained from Invitrogen Inc. The QDs were conjugated to the IL 10 (antihuman IL10, rat IgG2a) molecule from Serotec (Raleigh, NC, stock concentration of 1 mg/ml, clone JES3-12G8, code MCA2250). Bioconjugation of the QDs with the antibody was confirmed with concentration dependence of the PL intensity versus known antigen concentration, the so-called calibration curve, with the microarray technique.[7] PL studies were also performed on the experimental set of silanized CdSe/ZnS QDs whose procedure is detailed by Gerion *et al.*[3] Subsequent synthesis of CdSe cores as well as epitaxial growth of ZnS shells in trioctylphosphine oxide (TOPO) was published previously.[1]

For all experiments the nonconjugated fraction of the same size QDs was used as a reference. Experimental samples represented spots of a particular nonconjugated and conjugated solution (~100 μl) deposited on a crystalline Si wafer. Before initial PL study the spots were dried in the atmospheric ambience at room temperature for approximately 1 h. Conjugated and nonconjugated spots of approximately 3 mm in diameter were placed on the same Si wafer for a spectroscopic PL mapping with spatial resolution of 0.2 mm to produce a set of up to 70 separate PL spectra for each dried spot. We should point out that drying of the bio-

[a)]Electronic mail: ostapenk@eng.usf.edu

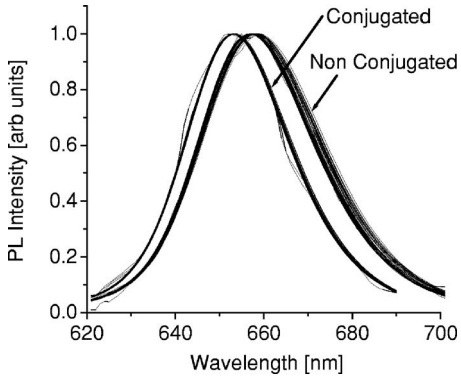

FIG. 1. Normalized spectra of CdSe/ZnS quantum dots with principal emission maxima around 655 nm (nonconjugated) and same quantum dots after IL10 antibody attachment (conjugated). Spectra were collected at 70 points within two dried sample spots, one for conjugated and another for nonconjugated. The PL spectra per group are plotted on top of each to show a spread within the individual group.

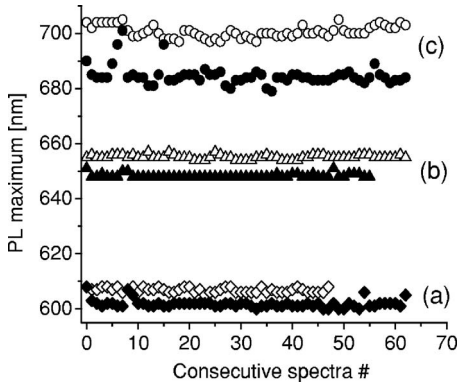

FIG. 2. Peak position of the PL maximum measured on nonconjugated (open shapes) and conjugated with IL10 antibody molecule (close shapes). CdSe/ZnS core-shell QDs of three different sizes with maxima at (a) 605 nm, (b) 655 nm, and (c) 705 nm are shown. Spectral shift caused by the conjugation was observed for majority of measured PL spectra that were collected for each sample in the PL mapping mode.

conjugated QD samples on various solid substrates is a well-documented alternative for PL study of liquid QD samples.[5,8] For the shift enhancement experiments, conjugated and reference samples were annealed in a temperature stabilized oven at air ambient atmosphere at various temperatures up to 245 °C. It is realized that high-temperature processing may produce a decomposition of the protein structure. However, it was used to facilitate PL shift process for exploration purposes. The kinetics of the annealing process was monitored using PL spectra at room temperature.

The scanning PL spectroscopy was performed at room temperature with the use of a 325 nm cw HeCd laser as the excitation source with the laser power density of $\sim 2\ \mathrm{W/cm^2}$. We initially assured that the light-induced degradation and enhancement effects caused by UV laser do not contribute to the PL mapping.[9] Silicon wafers with deposited QD samples were mounted on a computer controlled *X-Y* moving stage with the smallest step of 0.1 mm. Typical mapping area was $3\times 3\ \mathrm{mm^2}$ square with the step of 0.2 mm. The PL spectrum was dispersed by a SPEX 500M spectrometer and recorded by cooled photomultiplier tube coupled with a lock-in amplifier. Low temperature PL spectra were recorded using closed cycle helium cryostat with temperature stabilization.

In Fig. 1 we present intensity normalized PL spectra of commercial nonconjugated QD655 with emission maxima at 658 nm and the same QDs conjugated to IL10 molecules. We observed that the principal PL maximum is blueshifted by approximately 5 nm in the conjugated compared to nonconjugated QD sample. Spectroscopic PL mapping provides a statistically valid confirmation that the blueshift is observed for the entire conjugated spot and not at individual local areas. This PL shift persists at temperatures down to 20 K, though PL maxima of both samples shift synchronously due to CdSe band gap increase. On the other hand, the shift magnitude is different for QDs of various core sizes; it is more pronounced for QDs with larger CdSe core with longer emission wavelength. In Fig. 2 we show three different QD samples conjugated to the same type IL10 molecules. The blueshift was observed for all conjugated samples with the absolute shift magnitude increasing gradually with the QD core size with the largest blueshift of 15 nm on 705 nm QDs.

It has been further observed that the spectral shift is increasing with time of sample storage (aging) in dark at room temperature and can approach 40 nm within 7 days. At this point the spectral shift can be clearly observed as a change of the PL color between conjugated and nonconjugated spots under the 325 nm laser line. It occurred that for the samples that have annealed above room temperature, the process exhibited as the PL spectral shift is facilitated noticeably. Figure 3 shows the kinetic curves of the PL spectral shift versus annealing time at different temperatures over a period of 12 h. At annealing temperatures of 140 and 190 °C, the kinetic curves show an exponential growth with saturation of the relative PL spectral shift allowing for an estimate of the time constant of this process at 5 and 8 h for 190 and 140 °C, respectively. The spectral shift rate was much higher for 250 °C annealing temperature (τ=0.4 h) while for 115 °C observable shift change does not show full exponential saturation level even after 12 h. The time constants at different temperatures allowed us to calculate activation energy of the process E_{act}=0.38 eV using the following standard equation:

$$\tau^{-1} = \tau_0^{-1} \exp(-E_{\mathrm{act}}/k_B T), \tag{1}$$

where k_B is the Boltzmann constant and T is the annealing absolute temperature. Apart from the PL spectral shift, we noticed a gradual reduction of the PL intensity and approximately threefold PL peak broadening (i.e., increasing of the FWHM) in the conjugated samples subjected to temperature

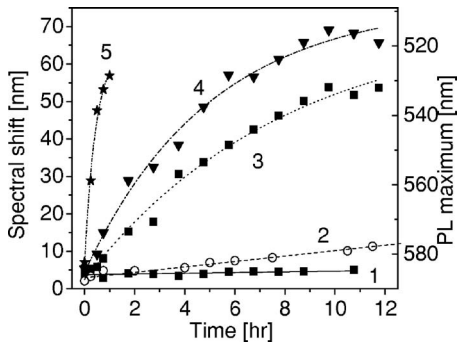

FIG. 3. Kinetics of the PL spectral shift enhancement in the bioconjugated sample due to annealing at different temperatures: 1, room; 2, 115 °C; 3, 140 °C; 4, 190 °C; and 5, 250 °C. Nonconjugated QD samples (not shown) retain a PL band spectral position within experimental accuracy of ~1 nm with results identical to points (1) on this graph.

annealing. In contrast, the nonconjugated reference QD samples are stable at the same annealing conditions with respect to the peak position, intensity, and FWHM values.

Based on the experimental data, we suggest that the initial (before sample aging) PL spectral shift due to bioconjugation is related to the QD surface area and the number of biomolecules attached to the QD surface. Larger magnitude of the spectral shift for larger QDs (longer emission wavelength) is possibly associated with their larger surface area per particle and larger number of molecules which can be bound to the QD. The attachment of biomolecules occurs via electrostatic or covalent forces; therefore, a distribution of these molecules on the QD surface imposes net electric field across the QD core. This electric field may contribute to the spectral shift of emission maxima via Stark effect that causes changes in the QD exciton levels. The PL spectral shift of up to 12 nm has previously been observed by applying external electric field to single CdSe nanocrystals.[10] Storage of the bioconjugated samples at room temperature or annealed at higher temperatures can promote rearrangement of the conjugated biomolecules due to the slow drying process of the IL10 molecules, leading to increased electric field and enhanced spectral shift. The effects of different ambient atmosphere (oxygen, water) and photoexcitation on the PL spectral characteristics of the CdSe core nanocrystals have been reported.[11] We should notice that the magnitude of spectral shift observed in Ref. 11 did not exceed 10 nm, which is substantially smaller than the spectral shift in the bioconjugated QDs in our study. For estimation purposes, we can compare the 10 nm (or 29 meV) initial PL spectral shift observed in this study on 655QD/IL10 bioconjugates (Fig. 2) with the Coulomb energy due to electrostatic interaction between charged point defects separated by the QD radius ($\sim$3 nm for 655 nm QDs). This Coulomb interaction yields the value of 37 meV in the medium having a dielectric constant of CdSe ($\varepsilon=9.0$). Realizing the simplicity of this approximation, we may conclude that the electric field effect can account for the observed spectral shift.

Alternatively, the PL shift with aging can be interpreted as a stress field applied to the QD levels in a process of drying of the bioconjugated QDs deposited on a solid substrate. There is yet another possible explanation that is related to chemical changes at the surface of the QDs that could affect the effective size of the particle as well as the density and distribution of surface trap states. During aging or annealing, chemical changes at or near the QD surface could take place due to reactions involving residual water, oxygen, or other species remaining on the surface from the synthesis process. Such changes, including local *p*H, are known to have significant potential effect on the PL properties of the QDs.[12,13] If this explanation is correct, the chemical changes must have taken place at the interface of the core and the shell since the effect is primarily on the PL properties of the CdSe core. This indicates that the ZnS shell is likely porous and allows small molecules or ions to reach the CdSe core surface. To further test the different possibilities, additional experiments with various types of biomolecules are currently in progress. As a preliminary result which is a subject of a separate manuscript, we found that both initial PL spectral shift and its temperature stimulated kinetics differ noticeably with variation of the biomolecule origin.

We anticipate that chemical structure and shape of the IL10 molecules can be substantially modified after QD annealing used in this study for the purpose of speeding up and enhancing the PL spectral shift in bioconjugated QDs. However, this annealing can be performed after completion of the antigen-antibody reaction which is used for cancer diagnostics. A spectral shift of the entire antigen-antibody-QD complex can be a highly sensitive and specific spectroscopic fingerprint for early detection of the cancer related antigens.

The work was supported by NSF award DMI-0523163 and the Department of Defense award PC050873. One of the authors (J.Z.Z.) is grateful to NSF (ECS-0401206) and DOE (DE-05ER46232A00) for financial support. The authors thank Tatyana Zhukov and Deborah Ortiz for their assistance in part of the bioconjugation experiment.

[1] B. O. Dabbousi, J. Rodriguez Viejo, F. V. Mikulec, J. R. Heine, H. Mattoussi, R. Ober, K. F. Jensen, and M. G. Bawendi, J. Phys. Chem. B **101**, 9463 (1997).
[2] A. Wolcott, D. Gerion, M. Visconte, J. Sun, A. Schwartzberg, S. W. Chen, and J. Z. Zhang, J. Phys. Chem. B **110**, 5779 (2006).
[3] D. Gerion, F. Pinaud, S. C. Williams, W. J. Parak, D. Zanchet, S. Weiss, and A. P. Alivisatos, J. Phys. Chem. B **105**, 8861 (2001).
[4] B. Dubertret, P. Skourides, D. J. Norris, V. Noireaux, A. H. Brivanlou, and A. Libchaber, Science **298**, 1759 (2002).
[5] E. R. Goldman, A. R. Clapp, G. P. Anderson, H. T. Uyeda, J. M. Mauro, I. L. Medintz, and H. Mattoussi, Anal. Chem. **76**, 684 (2004).
[6] E. Gorelik, D. P. Landsittel, A. M. Marrangoni, F. Modugno, L. Velikokhatnaya, M. T. Winans, W. L. Bigbee, R. B. Herberman, and A. E. Lokshin, Cancer Epidemiol. Biomarkers Prev. **14**, 981 (2005).
[7] *Protein Microarrays*, edited by M. Schena (Jones and Bartlett, Boston, 2005), xv, p. 496.
[8] D. Y. Kong Z. L. Wang C. K. Lin Z. W. Quan, Y. Y. Li, and J. Lin, Nanotechnology **18**, 075601 (2007).
[9] N. E. Korsunska, M. Dybiec, L. Zhukov, S. Ostapenko, and T. Zhukov, Semicond. Sci. Technol. **20**, 876 (2005).
[10] S. A. Empedocles and M. G. Bawendi, Science **278**, 2114 (1997).
[11] A. Y. Nazzal, X. Y. Wang, L. H. Qu, W. Yu, Y. J. Wang, X. G. Peng, and M. Xiao, J. Phys. Chem. B **108**, 5507 (2004).
[12] S. R. Cordero, P. J. Carson, R. A. Estabrook, G. F. Strouse, and S. K. Buratto, J. Phys. Chem. B **104**, 12137 (2000).
[13] T. W. Roberti, N. J. Cherepy, and J. Z. Zhang, J. Chem. Phys. **108**, 2143 (1998).

Mater. Res. Soc. Symp. Proc. Vol. 1095 © 2008 Materials Research Society 1095-EE08-05

Biologically Engineered Quantum Dots for Biomedical Applications

Ganna Chornokur[1], Sergei Ostapenko[1], Yusuf Emirov[1], Nadezhda Korsunska[2], Abraham Wolcott[3], Jin Zhang[3], Catherine Phelan[4], Abhilasha Nagaram[4], and Thomas Sellers[4]

[1]Nanomaterials and Nanomanufacturing Research Center, University of South Florida, ENB 118, 4202 E. Fowler Ave, Tampa, FL, 33620

[2]Institute of Semiconductor Physics, Ukrainian Academy of Sciences, pr. Nauki 45, Kiev, Ukraine

[3]University of California Santa Cruz, Santa Cruz, CA, 95064

[4]H. Lee Moffitt Cancer Center and Research Institute, Tampa, FL, 33620

ABSTRACT

We report on a short-wavelength, "blue" spectral shift of the photoluminescence (PL) spectrum in CdSeTe/ZnS core/shell quantum dots (QDs) caused by bioconjugation with several monoclonal cancer related antibodies (ABs). Scanning PL spectroscopy was performed on samples dried on solid substrates at various temperatures. The influence of the AB chemical origin on the PL spectral shift was observed. The conjugation QD-AB reaction was confirmed using the agarose gel electrophoresis technique. The spectral shift is strongly increased and the process facilitated when the samples are dried above room temperature. The PL spectroscopic mapping revealed a profile of the PL spectral shift across the dried QD-AB spot. Transmission Electron Microscopy analyses of the samples were performed to reveal the shape and size of individual QDs. A mechanism of the "blue" shift is attributed to changes in the QD electronic energy levels caused by local stress field applied to the bio-conjugated QD.

INTRODUCTION

Cancer is a major cause of illness and death in the US [1]. Clinical outcome of cancer is strongly related to the stage, at which the malignancy is detected, however, most solid tumors are detectable with standard diagnostic methods during a late phase of disease when it may have already metastasized. Therefore, there is a critical need to develop sensitive probes for early cancer detection.

Quantum dots (QDs) represent state-of-the-art nano-scale devices that exhibit promising results toward the development of a sensitive probe for screening cancer markers. It's anticipated that QDs could be successfully used for the purpose of early cancer detection to substitute organic dyes in many biological techniques including ELISA (Enzyme-Linked ImmunoSorbent Assay) which provides low detection limits for target biomolecules due to high sensitivities which can detect, for instance, PSA antigen concentrations as low as 1 ng/ml [2]. Our recent experiments demonstrated that PL spectra of QDs are changed by the bio-conjugation [3]. This is revealed as a "blue" or short wavelength spectral shift of the PL maximum, which can be clearly observed as a color change of the dried bio-conjugated sample. This PL spectroscopic feature of the bio-conjugated QDs may serve as a fingerprint of the bio-conjugation reaction. Ultimately, this will dramatically improve sensitivity of the cancer antigen detection using QDs because a background PL from the non-conjugated QDs can be spectrally separated.

EXPERIMENT

Commercial 605, 655, and 705 nm CdSe/ZnS core-shell PEGylated QDs covered with a polymer were obtained from Invitrogen Inc. Commercial monoclonal ABs were obtained as follows: IL-10 – Serotec Inc, IL-6 – Sigma Aldrich Inc, OPG – Imgenex Corp., CAV-1 and P53 – Abcam Inc, PSA - Chemicon International Inc. The conjugation procedure was performed using commercially available 705nm QD conjugation kit by Invitrogen Inc [4].The conjugation procedure is described step by step in the Qdot® 705 Antibody Conjugation Kit , made by Invitrogen [4].

In all experiments the non-conjugated fraction of the same size QDs was used as a reference. For the shift enhancement experiments, conjugated and reference samples were dried in a temperature stabilized oven in air ambient atmosphere at 50°C. The detailed schematic and description of the PL system and sample preparation procedure could be found elsewhere [3]. TEM experiments were carried out at the Transmission Electron Microscope Tecnai T20 with the line resolution of 1.2 A and electronic images captured using Orius 831 7 MP CCD camera. TEM analysis of pure and conjugated 705nm QDs revealed an ellipsoid shape approximately 11x6 nm +/- 0.5nm (figure 1).

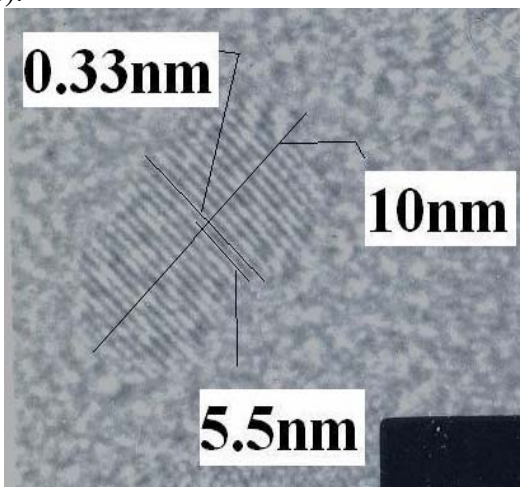

Figure 1. TEM image of the individual 705nm CdSeTe/ZnS core/shell quantum dot.

Agarose gel electrophoresis technique was performed using genetic analysis grade agarose and Tris-Borate-EDTA buffer (TBE) 10X stock solution, purchased from Fisher Scientific. Horizontal electrophoresis batch purchased from Owl Separation Systems Inc, rated as 0-150V, 0-100mA, was used to run the gel with the X0.5 EDTA as a running buffer. The running buffer was prepared from stock EDTA solution by dilution with distilled water. The organic dye Fluorescamine (4-phenylspiro[furan-2(3*H*),1'-phthalan]-3,3'-dione, [5]) was purchased from Invitrogen Inc. The fluorescamine bulk 1% solution was prepared by diluting the fluorescamine powder in acetone, and stored at 4C in the dark. To make a sample, 5uL of AB solution was mixed with 5ul TBE buffer at pH 7.4, following by the addition of 2uL 1% solution of Fluorescamine in acetone, and mixed for 30 seconds [6]. Non-conjugated QDs were tracked in the electrophoresis study using their own luminescence emission without adding fluorescamine. The retarded movement of bioconjugate (figure 2, wells 1 and 5 versus wells 2 and 6) was interpreted as a proof of successful conjugation procedure.

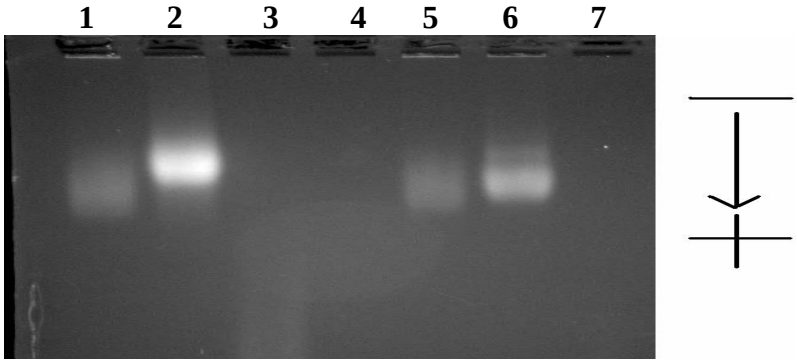

Figure 2. Agarose gel electrophoresis photograph, 2% agarose gel, 1.5V, 120 mins running time, 0.5xTBE running buffer. Wells are as follows: (1) non-conjugated 705nm QDs; (2) PSA conjugated to 705nm QDs; (3) PSA pure protein + Fluorescamine, (4) empty, (5) non-conjugated 705nm QDs, (6) IL6 conjugated to 705nm QDs, and (7) IL6 pure protein + Fluorescamine.

RESULTS AND DISCUSSION

"Blue" Spectral Shift

Typical results of the PL spectrum "blue" shift between non-conjugated and conjugated samples on silicon substrates is presented in figure 3.

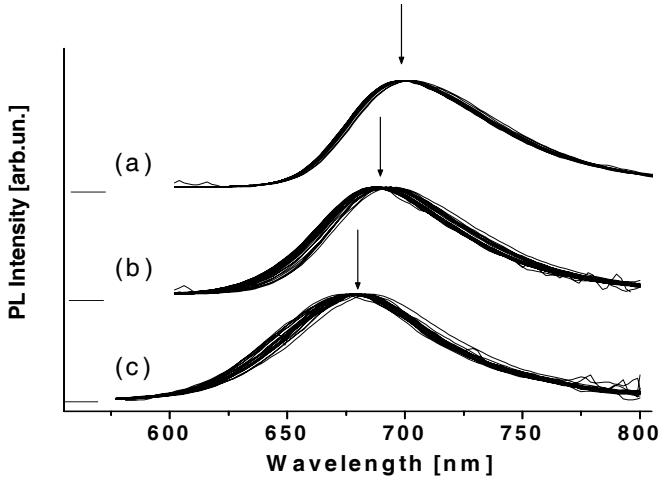

Figure 3. (a) Non-conjugated (a) and 705QD-CAV-1 bio-conjugated (b) samples after 30 minutes drying on Si substrate at room temperature. (c) – same conjugated sample after 3 days of drying at ambient atmosphere and room temperature. Multiple PL spectra are measured using the PL mapping technique.

Increase of the initial 5 to 7 nm shift up to 25 nm occurred during sample drying at room temperature in ambient atmosphere. The "blue" shift, which occurs in the middle areas of the spots, develops quickly, and reaches ~ 25nm in three days of storage at the 50C and at room ambience (figure 3). In addition, drying at 50C in various environments (vacuum, oxygen, argon and nitrogen) was performed, and no difference with control sample dried at ambient atmosphere

at the same temperature (50^0C) was found. Based on these results, we conclude that chemical interaction of the QD-AB with gas molecules play negligible role in the observed effect.

Spectroscopic PL mapping

In order to track variations in the blue spectral shift across the sample, PL spectral mapping was performed. First we noticed that after the sample deposition on the substrate and initial 30 minutes drying, the PL intensity shows a radial gradient profile with higher PL ring area at the spot periphery and reduced PL intensity in the central part. Similar PL intensity profile is maintained after 3 days sample drying (figure 4A), however various regions exhibit different rate of the PL intensity reduction due to drying as presented in figure 4C. Analysis of the PL spectra measured in different individual spots revealed a distinct and repeatable blue shift pattern across the sample which we assigned as a "plate-shape" pattern. It means that the "blue" spectral shift is more pronounced in the center of the spot and reduced in the periphery as shown in figures 4B. Consistently with data of the room temperature drying we also observed a strong enhancement of the PL shift which is quantified in figure 4D as two line scans of the PL peak position measured across the center of the sample. This effect is very pronounced on the conjugated dried samples and shows very small negligible gradient from the center to periphery in non-conjugated control QD samples dried at identical conditions. We will discuss two different mechanisms which can account for the "blue" PL shift in bio-conjugated QDs.

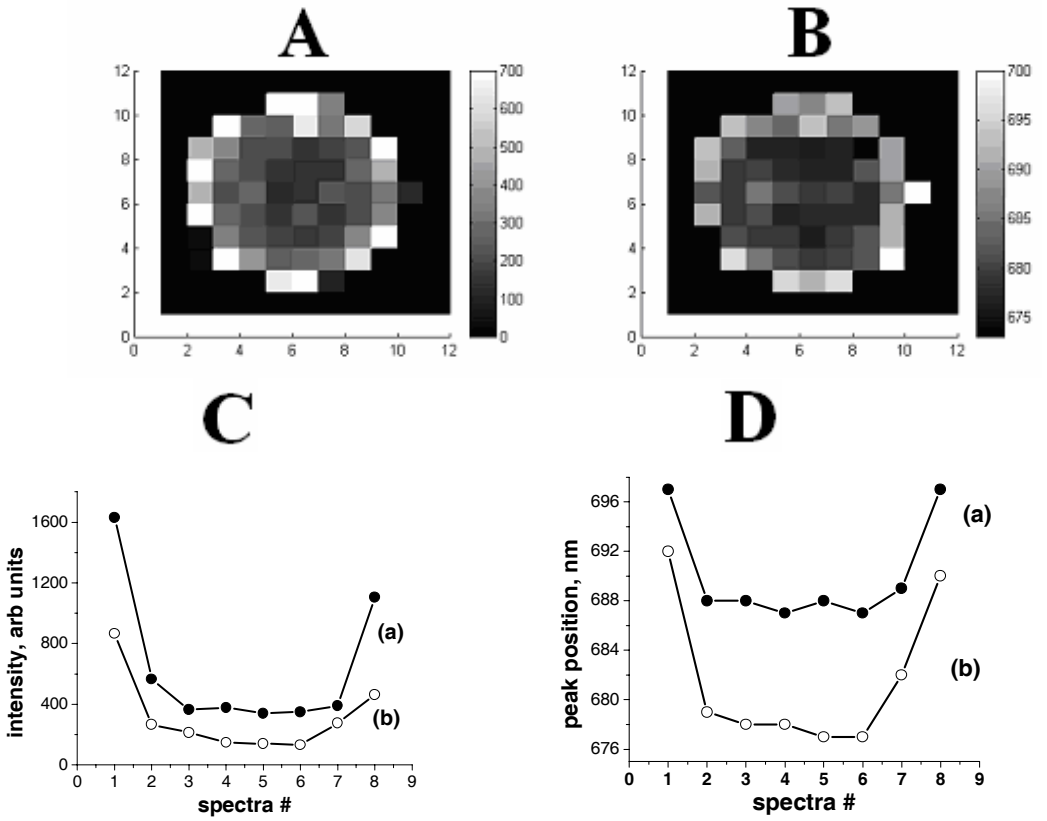

Figure 4. Maps of stored for 3 days at 50^oC conjugated sample: A – PL intensity; B – PL peak position. The linescans of (a) fresh and (b) stored for three days at 50^oC conjugated sample: C – PL intensity: D – PL peak position.

Compression stress

It is experimentally observed and theoretically explained that compression stress applied to II-VI compounds with embedded nano-scale objects having quantum confined wave function provides a high-energy shift of the exciton transitions [7]. Our experiments demonstrate a substantial role of elastic stress in the observed PL "blue" shift. One of critical results is a negligible PL shift in conjugated and non-conjugated QDs diluted in the buffer solution or immersed into the agarose gel. This must be compared to a substantial PL shift in identical bio-conjugated QDs dried on solid substrates at room or elevated temperatures. This mechanism is also consistent with the PL experiments on QDs dried on various substrates. The largest shift up to 36 nm is found on crystalline Si and SiC while a negligibly small shift on grids covered with amorphous carbon film and on the plane rubber substrate. These observations evidence that elastic properties of the substrate play important role. A direct confirmation of the stress model was recently received using X-ray diffraction in similar QDs bio-conjugated with IL-10 antigen and dried on silicon [8]. In this study a substantial increase of compression stress and corresponding compressive strain was directly measured. The increase of strain from 7.9e(-4) up to 9.6E(-3) was accompanied by 6 nm PL spectral shift. We conjecture that stress effect is the most probable mechanism for the observed blue PL shift.

Electric field

We notice that the appearance of the extra charge in the ensemble of non-oriented QDs is expected to lead to the "red" PL shift due to a quadratic Stark effect [9]. At the same time compensation (reduction) of the initial charge which may be caused by bio-conjugation and drying processes can explain that even in the case of Stark effect the PL shift will be in opposite i.e. "blue" direction, which is observed in our experiments. Therefore, we would like to discuss this in more details. Electric field applied to the QDs can be changed due to conjugation with charged or polar bio-molecules. We expect that this feature will be quite similar in the liquid or dried phase which is in contrast with our data. Additionally, electric field should be affected by various gas environments due to absorption of gas molecules [10]. However, our data on the sample drying in different gas environment such as oxygen, nitrogen, argon and vacuum, are in a strong contrast with this process, i.e. PL spectral shift is independent on drying conditions performed at the same temperature. The PL shift is also not affected by light illumination and observed in a sample after storage in dark. Finally, the electric field may be changed after drying due to evaporation of water molecules form the buffer solution and water ions attached directly to bio-molecules. This, however, would rather increase a net charge on the QD, and therefore lead to the "red" PL shift. All this consideration still can not rule out electric field effect as an alternative to the stress mechanism.

The second interesting feature we observed is a "plate" shape profile of the PL shift in dried bio-conjugated QDs (figures 4). According to our data, the largest PL shift is observed in the sample central part with gradual reduction to the periphery. This feature can be interpreted as a radial reduction of stress in dried sample from its center to the edge. This would explain similar but much smaller radial profile in non-conjugated sample. On the other hand, other explanation is quite feasible. As we documented in figures 4A and 4C the PL intensity also shows this type of non-homogeneity; the highest PL intensity at the spot periphery and the smallest in center.

This intensity profile can be attributed to diffusion of the QDs to the sample periphery. Taking into account that bio-conjugated sample contains some fraction of non-conjugated QDs we conclude that periphery region is enriched with non-conjugated QDs which is revealed as smaller "blue" PL shift at the periphery. This process is explained by a higher mobility of non-conjugated QDs compared to bio-conjugated as confirmed by our gel electrophoreses study.

CONCLUSIONS

Short wavelength, "blue" PL spectral shift is observed on 705QDs, bioconjugated to six different monoclonal cancer antibodies on the samples deposited on solid substrates and dried at room and elevated temperatures up to 50^{o}C. We found that the PL shift is developed faster at higher temperature. The heterogeneous pattern of the shift of dried bioconjugated QD spot ("plate-shape" effect) is observed and interpreted as enrichment of periphery region in dried sport with non-conjugated QDs. The most probable mechanism behind the PL shift effect is attributed to increased stress field applied to QDs from the conjugated bio-molecules. The results of this research could lead to critical improvements of the cancer antibody detection concentration threshold using QD luminescent tagging technique.

ACKNOWLEDGMENTS

The work was supported by National Science Foundation award DMI-0523163, Department of Defense award PC050873 and by Ministry of Education and Science of Ukraine project M/207-2007.

REFERENCES

1. National Vital Statistics Report 2007 **55** (19)
2. Human PSA ELISA Kit from Abazyme: http://www.biocompare.com/itemdetails.asp?itemid=434262
3. Dybiec M, Chornokur G, Ostapenko S, Wolcott A, Zhang JZ, Zajac A, Phelan C and Sellers T 2007 Photoluminescence spectroscopy of bioconjugated CdSe/ZnS quantum Dots *Appl. Phys Lett* **90** 263112
4. Official Invitrogen website: http://www.invitrogen.com
5. Udenfriend S, Stein S, Böhlen P, DairmanW, Leimgruber W and Weigele M 1972 Fluorescamine: a reagent for assay of amino acids, peptides, proteins, and primary amines in the picomole range *Science, New Series* **178**(4063) 871-72.
6. Skelley AM and Mathies RA 2003 Chiral separation of fluorescamine-labeled amino acids using microfabricated capillary electrophoresis devices for extraterrestrial exploration *J Chromatography A* **1021** 191–99
7. Shahzad K, Olego DJ and Van de Walle CJ 1988 Optical characterization and band offsets in ZnSe-ZnSxSe1-x strained-layer superlattices *Phys.Rev.B* **38** 1417
8. Borkovska L, Korsunska N, Krystab T, Pecherska E, Germash L, Ostapenko S and Chornokur G In press The influence of bioconjugation on photoluminescence and structural characteristics of quantum dots CdSe/ZnS *Semiconductors*
9. Empedocles SA and Bawendi MG 1997 *Science* **278** 2114 – 39
10. Oda M, Tsukamoto J, Hasegawa A, Iwami N, Nishiura K, Hagiwara I, Ando N, Horiuchi H and Tani T 2006 Photoluminescence of CdSe/ZnS/TOPO nanocrystals expanded on silica glass substrates: adsorption and desorption effects of polar molecules on nanocrystal surfaces *J.Lumin*. **570** 110-20

Spectroscopic behavior of bioconjugated quantum dots

2008 Semicond. Sci. Technol. 23 075045

(http://iopscience.iop.org/0268-1242/23/7/075045)

Semicond. Sci. Technol. **23** (2008) 075045 (7pp) doi:10.1088/0268-1242/23/7/075045

Spectroscopic behavior of bioconjugated quantum dots

G Chornokur[1], S Ostapenko[1], Yu Emirov[1], N E Korsunska[2], T Sellers[3] and C Phelan[3]

[1] Nanomaterials and Nanomanufacturing Research Center, University of South Florida, Tampa, FL 33620, USA
[2] Institute of Semiconductor Physics, Ukrainian Academy of Sciences, pr. Nauki 45, Kiev, Ukraine
[3] H. Lee Moffitt Cancer Center and Research Institute, Tampa, FL 33620, USA

Received 14 March 2008, in final form 2 May 2008
Published 4 June 2008
Online at stacks.iop.org/SST/23/075045

Abstract
We report on a short-wavelength, 'blue' spectral shift of the photoluminescence (PL) spectrum in CdSeTe/ZnS core/shell quantum dots (QDs) caused by bioconjugation with several monoclonal cancer-related antibodies (ABs). Scanning PL spectroscopy was performed on samples dried on solid substrates at various temperatures. The influence of the AB chemical origin on the PL spectral shift was observed. The QD–AB conjugation reaction was confirmed using the agarose gel electrophoresis technique. The spectral shift was strongly increased and the process facilitated when the samples were dried above room temperature. The PL spectroscopic mapping revealed a profile of the PL spectral shift across the dried QD–AB spot. A mechanism of the blue shift is attributed to changes in the QD electronic energy levels caused by a local stress applied to the bioconjugated QD.

1. Introduction

Cancer is a major cause of illness and death in the United States, second after heart diseases in 2004 [1]; approximately, half a million people die because of cancer in the United States alone every year. An estimated 3–35% of all cancer deaths could be avoided through early detection [2]. Clinical outcome of cancer is strongly related to the stage at which malignancy is detected, especially for breast cancer in women and prostate cancer in men [3]. Most solid tumors, however, are detectable with standard diagnostic methods during a late phase of disease when it may have already metastasized. Therefore, there is a critical need to develop sensitive probes for early cancer detection.

Quantum dots (QDs) represent state-of-the-art nano-scale devices that exhibit promising results toward the development of a sensitive probe for screening cancer markers. Currently, QDs are successfully used for *in vitro* and *in vivo* imaging of tumors [4, 5], immunochemistry [6, 7], DNA hybridization [8–10], cell imaging [11–16] and potential photodynamic therapy [17]. QDs possess inherent advantages over organic fluorophores [18], such as SYPRO protein stains [19] or fluorescamine [20, 21], and are a possible replacement in biomedical imaging applications [22, 23]. QDs can absorb a wide spectral range of quantum energies above the core material band gap, which excites the photoluminescence (PL) in a relatively narrow PL band with 20–50 nm bandwidth. In contrast, most molecular dyes can absorb only a narrow band of quantum energies separated from the PL maximum by a Stoke's shift. Furthermore, dye molecules emit at a much wider band of wavelengths compared to QDs. As a result, to distinguish separate features it is necessary to use different molecular dyes, each with its own required excitation wavelength. In the case of QDs, the emission wavelength depends on the QD size; therefore, the QDs made of the same semiconductor material but varying in size can all be excited by the same light source (provided the above band-gap energy is used), but then emit distinctly at different PL bands [18].

Given the complexity of cancer, the value of using multiple markers simultaneously as a panel has been shown empirically [24]. However, the efforts to apply this approach are still at very early stages [25, 26]. It is anticipated that QDs could be successfully used as substitutes for organic dyes in early cancer detection in many biological techniques including ELISA (enzyme-linked immunosorbent assay), which provides low detection limits for target biomolecules due to high sensitivities which can detect, for instance, PSA antigen concentrations as low as 1 ng ml^{-1} [27]. One of the

current problems in QD usage for biomedical applications is that bioconjugation reactions may be incomplete and result in residual non-conjugated QDs. A photoluminescent signal from these non-conjugated QDs will superimpose with conjugated QDs and lead to false positive events in cancer antigen detection, thereby reducing the method's sensitivity. Our recent experiments demonstrated that PL spectra of QDs are changed by bioconjugation [28]. This is manifested as a blue or short-wavelength spectral shift of the PL maximum, which can be clearly observed as a color change of the dried bioconjugated sample. This unique spectroscopic feature of the bioconjugated QDs may serve as a fingerprint of the bioconjugation reaction. Ultimately, this will dramatically improve sensitivity of cancer antigen detection using QDs because a background PL from the non-conjugated QDs can be spectrally separated.

In this paper, we report on a PL spectroscopic study of the blue spectral shift for QDs, conjugated to various monoclonal ABs, in which the samples are dried at different temperatures. The agarose gel electrophoresis technique with the organic dye fluorescamine is employed to assure the quality of the conjugate. A positive correlation of the blue spectral shift magnitude and molecular weight of the AB molecule is found. A spatial profile of the blue spectral shift across the dried sample is observed, described, and hypotheses explaining it are presented.

2. Materials and methods

2.1. QDs, ABs and conjugation

Commercial 605, 655 and 705 nm CdSe/ZnS and CdSeTe/ZnS core-shell PEGylated QDs covered with a polymer were obtained from Invitrogen Inc. Commercial monoclonal ABs were obtained as follows: IL-10—Serotec Inc, IL-6—Sigma Aldrich Inc., OPG—Imgenex Corp., CAV-1 and P53—Abcam Inc., PSA—Chemicon International Inc. The conjugation procedure was performed using a commercially available 705 nm QD conjugation kit from Invitrogen Inc. [29].

The main steps of the conjugation are as follows.

(1) Activation of 705 nm QDs with the SMCC to introduce thiol-reactive groups and reduction of the ABs with DCC (dithiothreitol), which is used for the reduction of disulfide bonds and maintaining monothiols in a reduced state.

(2) Desalting of both reagents after step 1 using the desalting columns.

(3) Mixing the reagents to let them conjugate (through the disulphide reduction and sulfhydryl-amino coupling).

(4) Concentration of the conjugate, formed in step 3, using the ultra-filtration vials with centrifugation for 12–15 min at ∼7000 rpm.

(5) Draining of the concentrated conjugate through the separation column to get rid of the non-conjugated ABs.

2.2. Samples and PL measurement

In all experiments, the non-conjugated portion of same-sized QDs was used as a reference. Individual droplets of the non-conjugated and conjugated solutions of the 3 μl volume were deposited on the unpolished surface of the same crystalline Si wafer. Before the initial PL study, the droplets were dried in atmospheric ambience at room temperature for approximately 30 min forming clear spots on the silicon surface. Conjugated and non-conjugated spots approximately 3 mm in diameter were used for spectroscopic PL mapping with a spatial resolution of 0.2 mm to produce a set of up to 120 individual PL spectra for each dried spot. We should point out that drying of the bioconjugated QD samples on various solid substrates is a well-documented alternative for the PL study of liquid QD samples [30, 31]. For the shift enhancement experiments, conjugated and reference samples were dried in a temperature-stabilized oven in air ambient atmosphere at 50 °C. This temperature has quite a substantial influence on the rate of the PL spectral shift. The kinetics of the drying process was monitored using PL spectra at room temperature.

The scanning PL spectroscopy was performed at room temperature using a 325 nm cw HeCd laser as the excitation source. Silicon wafers with deposited QD spots were mounted on a computer-controlled *X*–*Y* moving stage with a smallest step of 0.1 mm. The typical mapping area was 3 mm × 3 mm with a step of 0.25 mm. The PL spectrum was dispersed by a SPEX 500M spectrometer and recorded by a cooled photomultiplier tube coupled with a lock-in amplifier. A detailed schematic and description of the PL system can be found elsewhere [28]. TEM experiments were carried out at a Tecnai T20 transmission electron microscope with a line resolution of 1.2 A and electronic images captured using an Orius 831 7 MP CCD camera. The TEM analysis of pure and conjugated 705 nm QDs was conducted. It revealed an ellipsoid shape approximately 11 nm × 6 nm ± 0.5 nm with a diffraction pattern identifying the $CdSe_{0.6}Te_{0.4}$ ternary compound of the QD core material (figure 1).

2.3. Agarose gel electrophoresis with fluorescamine

The agarose gel electrophoresis technique was performed using genetic analysis grade agarose and Tris-borate–EDTA buffer (TBE) 10× stock solution purchased from Fisher Scientific. A horizontal electrophoresis batch purchased from Owl Separation Systems Inc., rated as 0–150 V, 0–100 mA, was used to run the gel with ×0.5 EDTA as a running buffer. The running buffer was prepared from the stock EDTA solution by dilution with distilled water. The organic dye fluorescamine (4-phenylspiro[furan-2(3*H*),1′-phthalan]-3,3′-dione, [21]) was purchased from Invitrogen Inc. The fluorescamine bulk 1% solution was prepared by diluting the fluorescamine powder in acetone, and stored at 4 °C in the dark. To make a sample, 5 μl of AB solution was mixed with 5 μl of TBE buffer at pH 7.4, followed by the addition of 2 μl 1% solution of fluorescamine in acetone, and mixed for 30 s [20]. The sample was then left exposed to air for approximately 30 min to let the acetone evaporate. To prevent the protein from denaturing under the influence of acetone, the

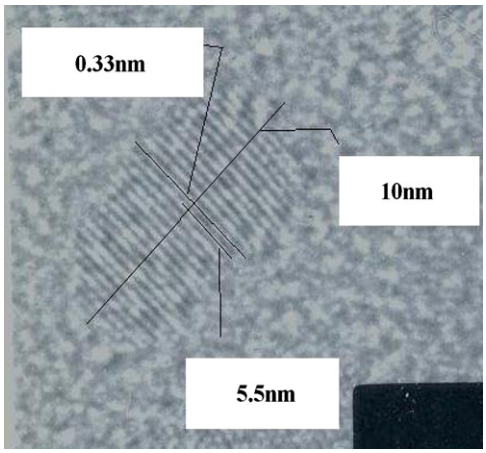

Figure 1. TEM image of the individual 705 nm CdSeTe/ZnS core/shell quantum dot. Analysis performed using the diffraction parameters of both CdSeTe and ZnS ([32] and [33], respectively) indicated that inter-atomic layer distances are 3.50 A ± 0.2 A, and with 100:1 probability that the diffraction lines belong to the $CdSe_{0.6}Te_{0.4}$ core material. The core has a cubic structure with (0, 0, 2) Miller indices.

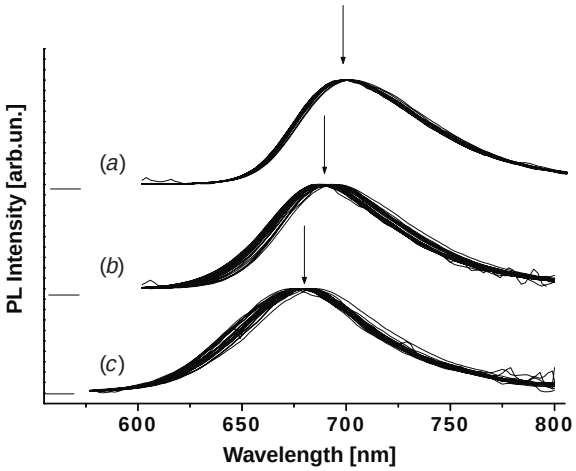

Figure 2. Non-conjugated (*a*) and 705QD-CAV-1 bioconjugated (*b*) samples after 30 min of drying on the Si substrate at room temperature. (*c*) Same conjugated samples after 3 days of drying at ambient atmosphere at 50 °C. Multiple PL spectra are measured using the PL mapping technique.

samples were stored continuously on ice (∼2–4 °C) until the gel procedure was started. Non-conjugated QDs were tracked in the electrophoresis study using their own luminescence emission without adding fluorescamine.

3. Results

3.1. Dependence of the blue spectral shift on the AB chemical origin

We started with PL spectroscopy of pure and conjugated QDs immersed in a liquid buffer medium. These PL spectra are practically identical both in terms of the PL peak position and bandwidth. Similar data on QDs in liquids were published previously [34]. Similarly, no spectral difference was observed between conjugated and non-conjugated QDs when they were located in a gel during electrophoresis experiments (see below). We found a difference between QDs deposited on solid substrates (Si, SiC) compared to plain rubber or metal copper grid covered with an amorphous carbon layer (TEM sample holder). In the last two substrates, we did not see a spectral shift both after sample deposition and after 50 °C drying up to 11 days. In contrast, both solid substrates (Si and SiC) behaved similarly with a clear and reproducible PL shift. These observations are critical to understand the role of elastic stress applied to the QDs after drying on a solid substrate.

It was reported previously that the PL spectrum of variously sized QDs bioconjugated with the IL-10 AB and deposited on silicon show a blue PL spectral shift in comparison to identical non-conjugated QDs [28]. We extended this study to other types of cancer-related ABs. In this experiment the identical type and size of QDs with the PL maximum at 705 ± 2 nm were used. This QD selection was motivated by the fact that the initial spectral shift observed after ∼30 min sample drying in QD-IL-10 conjugates gradually increases with the PL band wavelength, i.e. is directly related to the QD size [28].

Typical results of the PL spectrum blue shift between non-conjugated and conjugated samples dried on silicon substrates are presented in figure 2. Increase of the initial 5–7 nm shift up to 25 nm occurred during sample drying at room temperature in ambient atmosphere. The blue shift develops quickly and reaches ∼25 nm in 3 days of storage at 50 °C and room ambience (figure 2). In addition, drying at 50 °C in various environments (vacuum, oxygen, argon and nitrogen) was performed, and no difference with the control sample dried at ambient atmosphere at the same temperature was found. Based on these results, we conclude that the chemical interaction of the QD–AB with gas molecules plays a negligible role in the observed effect. This will be further elaborated in section 4.

The bioconjugation and subsequent PL spectroscopic analysis was performed on six monoclonal ABs currently being considered as cancer biomarkers. They are IL-6, IL-10, PSA, P53, OPG and CAV-1. The 705 nm QDs, conjugated to each of ABs, mentioned above, exhibited a blue spectral shift. This PL shift had different magnitudes, with the IL-6 giving the smallest shift, and OPG, the largest, approaching 36 nm after 11 days of room temperature sample storage (figure 3).

The different magnitudes of the blue spectral shift for different ABs are observed in samples dried at room or higher temperatures. For instance, we previously observed an approximately 40 nm spectral shift for the IL-10 AB after 12 days of drying at room temperature or after annealing at 140 °C for 12 h [28]. In figure 4, we present data of the maximum PL spectral shift for different ABs after room temperature drying correlated with the AB molecular weight. The AB molecules with larger molecular weight show a larger blue shift of the conjugated 705 nm QDs. For instance, molecular weight of the IL-6 AB molecule is 22–26 kDa [35], while the OPG AB

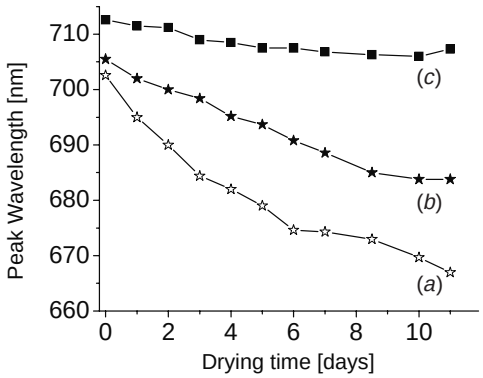

Figure 3. Blue spectral shift developed for 11 days of sample drying at room temperature. (*a*) 705 nm QDs conjugated to OPG AB, (*b*) 705 nm QDs conjugated to IL-6 AB and (*c*) non-conjugated 705 nm QDs used as controls.

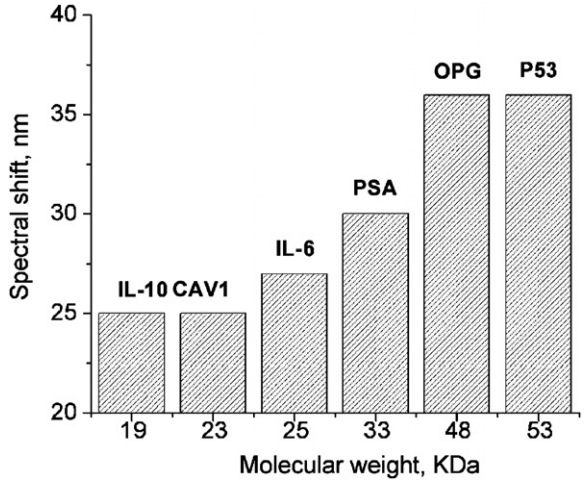

Figure 4. Dependence of the QD blue spectral shift on the molecular weight of the AB molecule used for bioconjugation. The samples were deposited on silicon and dried at room temperature for 11 days.

molecule weights 48 kDa [36], which corresponds to 27 and 36 nm PL shifts, respectively.

Also, as can be seen from figure 3, the spectral shift is developed for 11 days of storage at room temperature. A larger shift can be achieved with longer drying time or at higher temperature [28]. We noticed that control non-conjugated, 705 nm QDs also exhibit a small blue spectral shift which ranges from 2 to 5 nm in different experiments with an illustrative example in figure 3.

3.2. Spectroscopic PL mapping

In order to track variations in the blue spectral shift across the sample, PL spectral mapping was performed. First we noticed that after sample deposition on the substrate and the initial 30 min of drying, the PL intensity shows a radial gradient profile with higher PL at the ring area at the spot periphery and reduced PL intensity in the central part. A similar PL intensity profile is maintained after 3 days of sample drying (figure 5(*a*)). Various regions, however, exhibit different rates of PL intensity reduction due to drying, as presented in figure 5(*c*). Analysis of the PL spectra measured on different individual spots revealed a characteristic blue PL shift pattern across the sample, which we assigned as a 'plate-shape' pattern. This means that the blue spectral shift is more pronounced in the center of the spot and reduced in the periphery, as shown in figure 5(*b*). Consistent with data of the room temperature drying, we also observed a strong enhancement of the PL shift which is quantified in figure 5(*d*) as two linescans of the PL peak position measured across the center of the sample. This effect is very pronounced on the conjugated dried samples and shows a very small gradient from the center to periphery in non-conjugated control QD samples dried at identical conditions. We concentrate here on the conjugated samples only.

The observed 'plate-shape' effect is important, because it provides a method to obtain a maximum blue spectral shift, concentrated in a central area of the deposited sample. Its origin and mechanism will be discussed below.

3.3. Agarose gel electrophoresis

Agarose gel electrophoresis represents an easy, inexpensive and reliable method to verify the conjugation of QDs to different monoclonal ABs. According to Invitrogen [29], one QD molecule, covered with all layers, has a molecular weight about 750 kDa, which is larger in comparison to AB molecules in the weight range of 20–55 kDa. One QD molecule could attach two to three AB molecules [29]; therefore, we should see a difference in the electric field drift and separation of the 750 kDa pure QDs and 800–850 kDa conjugated QDs. This task requires careful optimization of experimental conditions to improve the separation distance in gel. Specifically, we used a 2% agarose gel, applying voltages up to 1.5 V and running time up to 2 h. In figure 6 the agarose gel image is shown after 120 min of running time. Here the retardation in movement between the pure 705 nm QDs and conjugated 705 nm QDs is evident (compare wells 1 and 2; 5 and 6). In this image, pure ABs mixed with fluorescamine (wells 3 and 7) have already run out of the gel, and only the trace PL from them could be seen in well 3. We observed also that two different ABs, PSA and IL-6, move with different velocities in the gel experiment as illustrated in figure 6 (wells 2 and 6). According to [37], the molecular weight of the PSA molecule is 32–33 kDa, while the weight of IL-6 is 22–28 kDa [35]. It is logical to assume that QDs conjugated to the IL-6 molecule will move faster than those conjugated to PSA because of the size difference. This hypothesis is confirmed: PSA movement (2) is retarded in comparison to IL-6 movement (6). Also, the trace of the PSA + fluorescamine PL is visible in well 3, while no PL could be observed in well 7, which contains a pure IL-6 + fluorescamine mixture. Therefore, the separation capacity of the agarose gel is high enough for this type of application.

4. Discussion

In this section, we address and discuss two major findings observed in the experimental part. The first is a blue PL

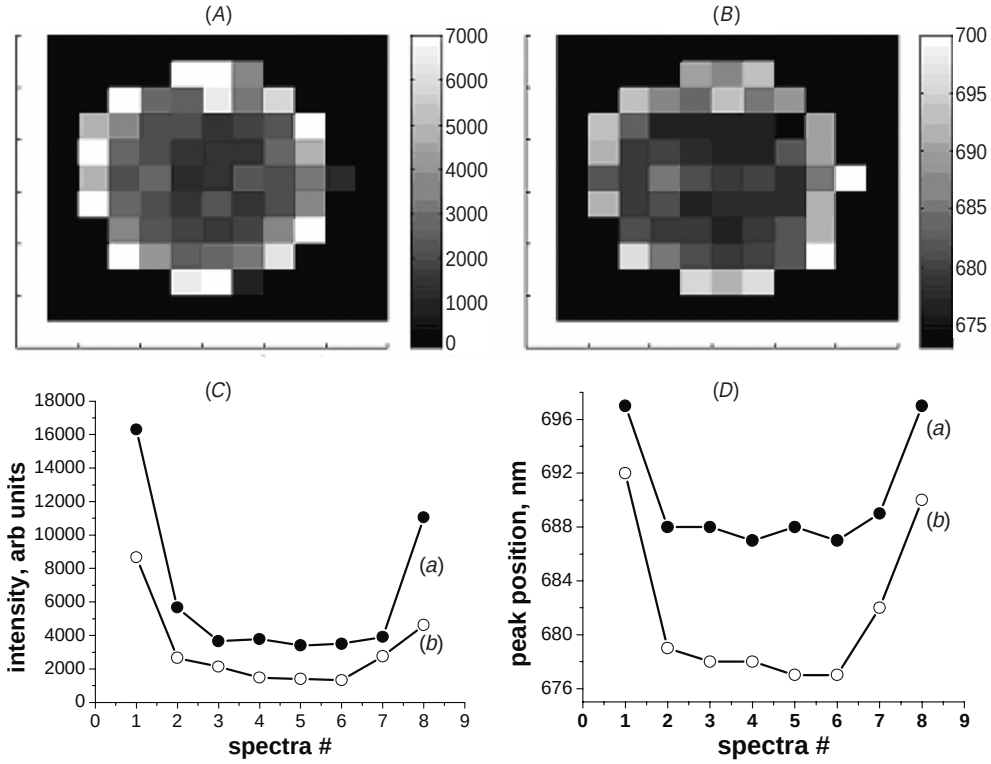

Figure 5. Photoluminescence (PL) maps of a conjugated sample stored for 3 days at 50 °C: A—PL intensity; B—PL peak position. The linescans of the conjugated sample (*a*) dried for 30 min and (*b*) stored for 3 days at 50 °C: C—PL intensity, D—PL peak position.

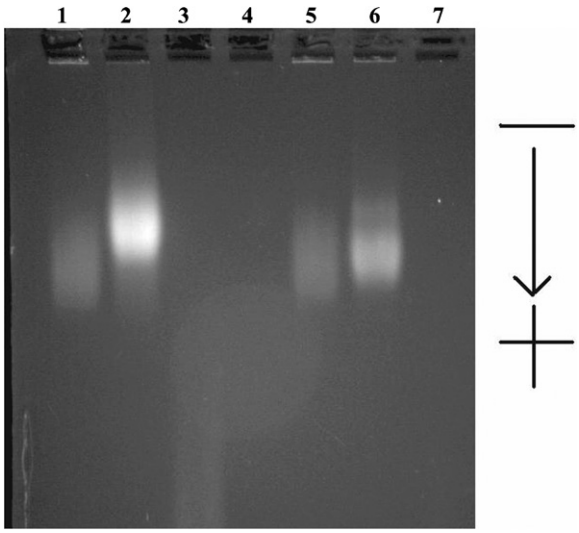

Figure 6. Agarose gel electrophoresis photograph, 2% agarose gel, 1.5 V, 120 min of running time, 0.5× TBE running buffer. Wells are as follows: (1) non-conjugated 705nm QDs, (2) PSA conjugated to 705 nm QDs, (3) PSA pure protein + fluorescamine, (4) empty, (5) non-conjugated 705 nm QDs, (6) IL-6 conjugated to 705 nm QDs and (7) IL-6 pure protein + fluorescamine.

spectral shift of the bioconjugated QDs deposited on solid substrates compared to identical but non-conjugated QDs and the enhancement of this shift with drying time at elevated temperatures. The second is a distribution of the blue shift across the dried spot as revealed by a spectroscopic PL mapping. It is obvious that various physical and chemical processes in the bulk, interface and surface of a QD can modify the QD's excited states exhibited in the PL band spectral shift. We will discuss two different mechanisms, which can account for the blue PL shift in bioconjugated QDs. The first mechanism is the elastic field applied to conjugated QDs caused by compressions that build up after drying the spot on a solid substrate. The second mechanism is a variation of the local electric field applied to the QD electronic levels caused by bioconjugation with charged or polar molecules that resulted in changes of the QD surface charge.

4.1. Compression stress

It is experimentally observed and theoretically explained that compression stress applied to II–VI compounds with embedded nano-scale objects having quantum-confined wavefunctions provides a high-energy shift of the exciton transitions [38]. A typical example is represented by a super-lattice structure with quantum wells stressed due to lattice mismatch between the well and barrier materials, such as ZnSeTe/ZnS_xSe_{1-x} quantum well/barrier structure. The objects in our study can be modeled as a similar system with stress originated at the interface between dried QD sample and a solid substrate, such as a silicon wafer. One can assume that stress is applied to the QDs caused by the change of the QD sample volume due to a slow drying process. Presumably the surface tension between the substrate and the drying sample is a driving force to generate this stress field.

Our experiments demonstrate a substantial role of elastic stress in the observed PL blue shift. One of the critical results

is a negligible PL shift in conjugated and non-conjugated QDs diluted in the buffer solution or immersed in the agarose gel. This must be compared to a substantial PL shift in identical bioconjugated QDs dried on solid substrates at room or elevated temperatures. This mechanism is also consistent with the PL experiments on QDs dried on various substrates. The largest shift, up to 36 nm, is found on crystalline Si and SiC while a negligibly small shift on grids covered with amorphous carbon film and on the plain rubber substrate. These observations evidence that the elastic properties of the substrate play an important role in determining the elastic stress on the QD. We suggest that compressive stress is applied to dried bioconjugated QD samples at the interface between the substrate and a dried droplet. To support this hypothesis, TEM analysis of pure and conjugated 705 nm QDs was conducted. It revealed an ellipsoid shape approximately 11 nm $\times$ 6 nm as illustrated in figure 1. Further TEM analyses of bioconjugated QDs are planned in order to reveal possible changes in the shape and/or size of bioconjugated QDs, caused by compression stress.

A direct confirmation of the stress model was recently received using X-ray diffraction in similar QDs bioconjugated with IL-10 antigen and dried on silicon [39]. In this study, a substantial increase of compression stress and corresponding compressive strain was directly measured. The increase of strain from 7.9E(−4) up to 9.6E(−3) was accompanied by a 6 nm PL spectral shift. We conclude here that the stress effect is the most probable mechanism for the observed blue PL shift.

4.2. Electric field

We will also discuss the potential role of electric field variation on the observed PL shift. The influence of electric field was intensively studied and discussed in publications on QDs [40, 41]. The following arguments, however, are generally in contradiction with the electric field model in our case, but we will discuss them as an alternative to the stress mechanism. We notice that the appearance of the extra charge in the ensemble of non-oriented QDs is expected to lead to the 'red' PL shift due to a quadratic Stark effect [40]. At the same time, a compensation (reduction) of the initial charge which may be caused by bioconjugation and drying processes can explain that the PL shift will be in opposite, i.e. blue direction. Therefore, we would like to discuss this in more details. The electric field applied to the QDs can be changed due to conjugation with charged or polar biomolecules. We expect that this feature will be quite similar in the liquid or dried phase, which is in contrast with our data. Additionally, the electric field should be affected by various gas environments due to photo-absorption of gas molecules [42]. However, our data on the sample drying in oxygen, nitrogen, argon and vacuum are in a strong contrast with this process, i.e. PL spectral shift is independent of drying conditions performed at the same temperature. The PL shift is also not affected by light illumination and observed in a sample after storage in darkness. Finally, the electric field may be changed after drying due to evaporation of water molecules from the buffer solution and water ions attached directly to the biomolecules. This, however, would rather increase a net charge on the QD, and therefore lead to the 'red' PL shift. All these considerations still cannot rule out the electric field effect as an alternative to the stress mechanism.

The second interesting feature we observed is a 'plate-shape' profile of the PL shift in dried bioconjugated QDs (figure 5). According to our data, the largest PL shift is observed in the spot's central part with gradual reduction toward the periphery. This feature can be interpreted as a radial reduction of stress in a dried sample from its center to the edge. This would explain the similar but much smaller radial profile in a non-conjugated sample. On the other hand, another explanation is quite feasible. As we documented in figures 5(*a*) and (*c*), the PL intensity also shows this type of non-homogeneity; the highest PL intensity is at the spot periphery and the smallest at the center. This intensity profile can be attributed to the diffusion of the QDs to the sample periphery during drying. Taking into account that the bioconjugated sample contains some fraction of non-conjugated QDs we may suggest that the periphery region is enriched with non-conjugated QDs, which is revealed as a smaller blue PL shift at the periphery. This process is explained by a higher mobility of non-conjugated QDs compared to bioconjugated, as confirmed by our gel electrophoreses study.

5. Conclusions

A short-wavelength, blue PL spectral shift is observed on 705 nm QDs bioconjugated to six different monoclonal cancer ABs on samples deposited on solid substrates and dried at room and elevated temperatures up to 50 °C. We found that the PL shift is developed faster at higher temperatures. The positive correlation between the AB's molecular weight and the magnitude of the PL shift is shown. The heterogeneous pattern of the shift of the dried bioconjugated QD spot ('plate-shape' effect) is observed and interpreted as the effect of surface tension distribution across the dried sample or as an enrichment of the periphery region in a dried spot with non-conjugated QDs. The agarose gel electrophoresis technique verifies the success of the bioconjugation procedure, and optimum conditions (agarose concentration and running time) are proposed to achieve the best separation between the bands of pure and bioconjugated QDs. The most probable mechanism behind the PL shift effect is attributed to the increased stress field applied to QDs from the conjugated biomolecules. The results of this research could lead to critical improvements for *in vitro* cancer antigen detection concentration threshold using the QD luminescent tagging technique.

Acknowledgments

The work was supported by National Science Foundation award DMI-0523163, Department of Defense award PC050873 and by Ministry of Education and Science of Ukraine project M/207-2007.

References

[1] National Center for Health Statistics 2007 *National Vital Statistics Report* vol 56, no 5 (http://www.cdc.gov/nchs/products.html)

[2] Colditz G A, Sellers T A and Trapido E 2006 Epidemiology—identifying the causes and preventability of cancer *Nat. Rev. Cancer* **6** 75

[3] Smith S, Dave S, True Nie L and Gao X 2006 Multicolor quantum dots for molecular diagnostics of cancer *Expert Rev. Mol. Diagn.* **6** 231–44

[4] So M-K, Hu C, Loening A M, Gambhir S S and Rao J 2006 Self illuminating quantum dot conjugates for in vivo imaging *Nature Biotechnol.* **24** 339

[5] Rhyner M N, Smith A M, Gao X, Mao H, Yang L and Nie S 2006 Quantum dots and multifunctional nanoparticles: new contrast agents for tumor imaging *Nanomedicine* **1** 1–9

[6] Xing Y, Shaudry Q and Shen S 2007 Bioconjugated quantum dots for multiplexed and quantitative immunochemistry *Nature Protoc.* **2** 1152

[7] Goldman E R, Medintz I L and Mattoussi H 2006 Luminescent quantum dots in immunoassays *Anal. Bioanal. Chem.* **384** 560

[8] Pathak S, Choi S K, Arnheim N and Thompson M E 2001 *J. Am. Chem. Soc.* **123** 4103

[9] Xiao Y and Barker P E 2004 *Nucleic Acids Res.* **32** 28

[10] Crut A, Geron-Landre B, Bonnet I, Bonneau S, Desbiolles P and Escude C 2005 *Nucleic Acids Res.* **33** 98

[11] Chan W C W and Nie S 1998 *Science* **281** 2016

[12] Bruchez Jr, Moronne M, Gin P, Weiss S and Alivisatos A P 1998 *Science* **281** 2013

[13] Lidke D S, Nagy P, Heintzmann R, Arndt-Jovin D-J, Post N J, Grecco H E, Jares-Erijman E A and Jovin T M 2004 *Nature Biotechnol.* **22** 198

[14] Dubertret B, Skourides P, Norris D J, Noireaux V, Brivanlou A H and Libchaber A 2002 *Science* **298** 1759

[15] Han M, Gao X, Su J Z and Nie S 2001 *Nat. Biotechnol.* **19** 631

[16] Jaiswal J K, Mattoussi H, Mauro J M and Simon S M 2003 *Nature Biotechnol.* **21** 47

[17] Wu X, Liu H, Liu J, Haley K N, Treadway J A, Larson J P, Ge N, Peale F and Bruchez M P 2003 *Nature Biotechnol.* **21** 41

[18] Goodsell D S 2004 *Bionanotechnology: Lessons from Nature* (Hoboken, NJ: Wiley-Liss)

[19] SYPRO® Orange Protein Gel Stain Instruction Manual: http://www.bio.indiana.edu/~ybelab/procedures/SyproOrange.pdf

[20] Skelley A M and Mathies R A 2003 Chiral separation of fluorescamine-labeled amino acids using microfabricated capillary electrophoresis devices for extraterrestrial exploration *J. Chromatogr.* A **1021** 191–99

[21] Udenfriend S, Stein S, Böhlen P, Dairman W, Leimgruber W and Weigele M 1972 Fluorescamine: a reagent for assay of amino acids, peptides, proteins, and primary amines in the picomole range *Science* **178** 871–72

[22] Gerion D, Pinaud F, Williams S C, Parak W J, Zanchet D, Weiss S and Alivisatos A P 2001 Synthesis and properties of biocompatible water-soluble silica-coated CdSe/ZnS semiconductor quantum dots *J. Phys. Chem.* B **105** 8861–71

[23] Warren C, Chan W and Nie S 1998 Quantum dot bioconjugates for ultrasensitive nonisotopic detection *Science* **281** 2016–18

[24] Visintin I *et al* 2008 Diagnostic markers for early detection of ovarian cancer *Clin. Cancer Res.* **14** 1065–72

[25] Bailey R E, Smith A M and Nie S 2004 Quantum dots in biology and medicine *Physica* E **25** 1–12

[26] Chan W C W, Maxwell D J, Gao X, Bailey R E, Han M and Nie S 2002 Luminescent quantum dots for multiplexed biological detection and imaging *Curr. Opin. Biotech.* **13** 40–6

[27] Human PSA ELISA Kit from Abazyme: http://www.biocompare.com/itemdetails.asp?itemid=434262

[28] Dybiec M, Chornokur G, Ostapenko S, Wolcott A, Zhang J Z, Zajac A, Phelan C and Sellers T 2007 Photoluminescence spectroscopy of bioconjugated CdSe/ZnS quantum dots *Appl. Phys. Lett.* **90** 263112

[29] http://www.invitrogen.com

[30] Gaponik N, Talapin D V, Rogach A L, Hoppe K, Shevchenko E V, Kornowski A, Eychmuller A and Weller H 2002 *J. Phys. Chem.* B **106** 7177–85

[31] Michalet X, Pinaud F F, Bentolila L A, Tsay J M, Doose S, Li J J, Sundaresan G, Wu A M, Gambhir S S and Weiss S 2005 *Science* **307** 538–44

[32] Razik N, Al-Barakati G and Al-Heneti S 1990 *Powder Diffr.* **5** 206

[33] Mardix S and Brafman O 1967 *Acta Crystallogr.* **23** 501

[34] Mattousi H, Mauro J M, Goldman E R, Anderson G P, Sundar V C, Mikulec F V and Bawendi M G 2000 Self-assembly of CdSe-ZnS quantum dot bioconjugates using an engineered recombinant protein *J. Am. Chem. Soc.* **122** 12142–50

[35] Official LabCorp website: http://www.labcorp.com/datasets/labcorp/html/chapter/mono/sr019300htm

[36] Official GenWayBio Corp website: http://www.genwaybio.com/product_info.php?products_id=190896&osCsid=9j8vmvqtmqei0uggeoqr3ic3b7

[37] Sarvestani E K, Khezri A, Vessal M and Ghaderi A 1999 A simplified and reproducible two-step method for the purification of prostate-specific antigen *Iran. Biomed. J.* **3** 87–91

[38] Shahzad K, Olego D J and Van de Walle C J 1988 Optical characterization and band offsets in ZnSe-ZnS_xSe_{1-x} strained-layer superlattices *Phys. Rev. B* **38** 1417

[39] Borkovska L, Korsunska N, Krystab T, Pecherska E, Germash L, Ostapenko S and Chornokur G 2008 The influence of bioconjugation on photoluminescence and structural characteristics of quantum dots CdSe/ZnS *Semiconductors* at press

[40] Empedocles S A and Bawendi M G 1997 *Science* **278** 2114–39

[41] Empedocles S A, Neuhauser R, Shimizu K and Bawendi M J 1999 *Adv. Mater.* **11** 1243

[42] Oda M, Tsukamoto J, Hasegawa A, Iwami N, Nishiura K, Hagiwara I, Ando N, Horiuchi H and Tani T 2006 Photoluminescence of CdSe/ZnS/TOPO nanocrystals expanded on silica glass substrates: adsorption and desorption effects of polar molecules on nanocrystal surfaces *J. Lumin.* **570** 110–20

Superlattices and Microstructures 45 (2009) 240–248

Contents lists available at ScienceDirect

Superlattices and Microstructures

journal homepage: www.elsevier.com/locate/superlattices

Scanning photoluminescent spectroscopy of bioconjugated quantum dots

G. Chornokur [a,*], S. Ostapenko [a], E. Oleynik [a], C. Phelan [b], N. Korsunska [c], T. Kryshtab [d], J. Zhang [e], A. Wolcott [e], T. Sellers [b]

[a] *Nanomaterials and Nanomanufacturing Research Center, University of South Florida, Tampa, FL 33620, USA*

[b] *H. Lee Moffitt Cancer Center and Research Institute, Tampa, FL 33620, USA*

[c] *Institute of Semiconductor Physics, Ukrainian Academy of Sciences, Kiev, Ukraine*

[d] *National Polytechnics University, Mexico-07338, Mexico*

[e] *University of California at Santa Cruz, Santa Cruz, CA 95064, USA*

ARTICLE INFO

Article history:
Available online 6 January 2009

Keywords:
Quantum dots
Photoluminescence
Cancer
Antigen
Antibody

ABSTRACT

We report on the application of the bio-conjugated quantum dots (QDs) for a "sandwich" enzyme-linked immunosorbent assay (ELISA) cancer testing technique. Quantum dot ELISA detection of the cancer PSA antigen at concentrations as low as 0.01 ng/ml which is ~50 times lower than the classic "sandwich" ELISA was demonstrated. Scanning photoluminescence (PL) spectroscopy was performed on dried ELISA wells and the results compared with the same QD samples dried on a solid substrate. We confirmed a "blue" up to 37 nm PL spectral shift in a case of QDs conjugated to PSA antibodies. Increasing of the "blue" spectral shift was observed at lower PSA antigen concentrations. The results can be used to improve sensitivity of "sandwich" ELISA cancer antigen detection.

Published by Elsevier Ltd

1. Introduction

Cancer is a major cause of illness and death in the United States, second after heart diseases in 2004 [1]; approximately, half a million people die because of cancer in the United States alone every year. An estimated 3%–35% of all cancer deaths could be avoided through early detection [2]. The clinical outcome of cancer is strongly related to the stage at which malignancy is detected, especially for breast cancer in women and prostate cancer in men [3]. Most solid tumors, however,

* Corresponding author. Tel.: +1 813 846 3897.
E-mail address: gchornok@mail.usf.edu (G. Chornokur).

0749-6036/$ – see front matter. Published by Elsevier Ltd
doi:10.1016/j.spmi.2008.11.029

are detectable with standard diagnostic methods during a late phase of disease when it may have already metastasized. Therefore, there is a critical need to develop sensitive probes for early cancer detection. Quantum dots (QDs) represent state-of-the-art nano-scale devices that exhibit promising results toward the development of a sensitive probe for screening cancer markers. Currently, QDs are successfully used for *in vitro* and *in vivo* imaging of tumors [4,5], immunochemistry [6,7], DNA hybridization [8–10], cell imaging [11–16] and potential photodynamic therapy [17]. QDs possess inherent advantages over organic fluorophores [18], such as SYPRO protein stains [19] or fluorescamine [20,21], and are a possible replacement in biomedical imaging applications [22–24]. It is anticipated that QDs could be successfully used as substitutes for organic dyes in early cancer detection and forensic analyses in many biological techniques including ELISA (enzyme-linked immunosorbent assay), which provides low detection limits for target biomolecules due to high sensitivities which can detect, for instance, PSA AG concentrations as low as 1 ng/ml [25].

An enzyme-linked immunosorbent assay (ELISA) against PSA already exists in a commercial form, and has been employed for the analyses of large clinical materials [26].

Currently, there is much data available on the threshold of PSA AG detection for "sandwich"-ELISA with organic dyes, but many ELISA kits manifest this threshold to be at 1 ng/ml [25], which is usually low enough for early cancer detection, but "sandwich" ELISA with QDs could possibly detect as low as 0.01 ng/ml of PSA AG, which may be very useful in forensic analysis, dealing with sexual assaults. In this case, forensic scientists may deal with the smallest traces of semen liquids which require extremely sensitive methods of PSA detection [27,28]. Therefore, the need to lower PSA detection thresholds is evident.

One of the current problems in QD usage for biomedical applications is that bioconjugation reactions may be incomplete and result in residual non-conjugated QDs in the same bio-conjugated solution. Our recent experiments demonstrated that the PL spectra of QDs are changed by bioconjugation [29–31]. This is manifested as a blue or short-wavelength spectral shift of the PL maximum, which can be clearly observed as a color change of the dried bioconjugated sample. This unique spectroscopic feature of the bioconjugated QDs may serve as a fingerprint of the bioconjugation reaction. Ultimately, this will dramatically improve the sensitivity of biomolecule detection using QDs because a background PL from the non-conjugated QDs can be spectrally separated. In this paper, we report on PL spectroscopic study of the dried "sandwich" ELISA wells, utilizing QDs to detect PSA AG at the concentration range of 0.01–1.0 ng/ml. The agarose gel electrophoresis technique with the organic dye fluorescamine is employed to assure the quality of the conjugate, used for "sandwich"-ELISA technique. A "blue" spectral shift magnitude was found to be larger for ELISA "sandwiches" in comparison with the same bio-conjugated QDs, dried on a flat silicon substrate. This effect can be attributed to the elevated stress applied to the individual QD, involved into the "sandwich" formation, as well as more or less efficient, but probably not complete, nonconjugated QD elimination caused by the washing procedure. The PL signal from the bio-conjugated QDs was found in all wells, containing AG, with different concentration but was undetectable in the control well without AG. It is expected that the results can provide strong benefits for early cancer detection and forensic technology.

2. Materials and methods

2.1. QDs, ABs, conjugation and agarose gel electrophoresis

Commercial 705 nm CdSeTe/ZnS core-shell PEGylated (with covalently coupled Polyethylene glycol molecules on top in order to produce non-ionic surfactants) QDs covered with a polymer were obtained from Invitrogen Inc. Commercial monoclonal PSA ABs and AGs were obtained from Millipore Inc. The conjugation procedure was performed using a commercially available 705 nm QD conjugation kit [32]. The main steps of this procedure are also described elsewhere [30,31]. Uncoated polystyrene ELISA wells were purchased from NUNC company (part of Thermo Fisher Scientific). All buffers in stock solutions (coating, blocking and washing) were purchased from Immunochemistry Technologies LLC.

The agarose gel electrophoresis technique with fluorescamine was employed to verify the conjugation reaction. It was in detail explained in our previous works [30,31].

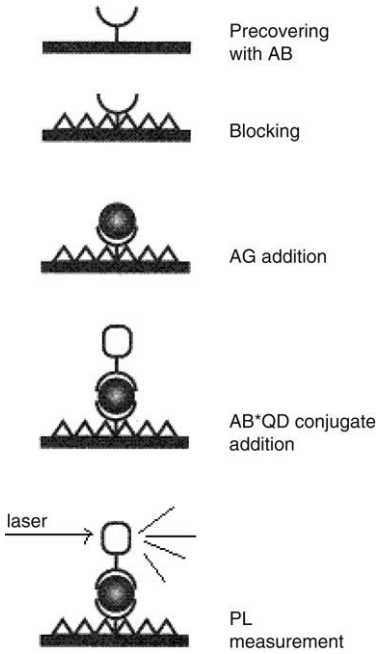

Fig. 1. "Sandwich"—ELISA method schematic. Modified, original taken from [33].

2.2. ELISA experiment

The scheme of the "sandwich"—ELISA method is shown in Fig. 1.

Wells were coated with capture PSA AB by adding 50 μl of 5X diluted coating buffer mixed with AB in concentration 7.5 μg/ml. The amount of coating AB was taken in excess to provide a complete coverage of bonding sites. The wells were then covered with aluminum foil to prevent light exposure and incubated for 20 h at room temperature (RT) under constant slow rotation. After that coated wells were washed 3 times with washing buffer and incubated with blocking buffer (300 μl/well) at the same conditions to ensure blocking of all unused sites on the well, available for further protein bonding. This stage was also followed with 3-times washing, and immediately proceeded to AG solution addition. 50 μl of PSA AG solution was added to wells #2–4 in the following concentrations: well #2–1.0 ng/ml; well #3–0.1 ng/ml; well #4–0.01 ng/ml; and well #5 was a control – pure PBS (pH 7.4) added, no AG. Well #1 was loaded with 5 μl pure nonconjugated 705 nm QD solution and let dry in air. The wells #2 to #5 were incubated in the same conditions for 12 h, washed 3 times with washing buffer, and the 50 μl of 2X diluted AB*QD solution was added immediately, incubated for 12 h at the same conditions, washed 3 times and let dry in air until further spectroscopic analysis. The 2X dilution of a conjugate with QD incubation buffer was used in an effort to lower expenses, associated with the experiment. QD*AB conjugated is very concentrated in ABs (300 μg/ml of AB in the stock solution, used for conjugation [31]), therefore, they are taken in excess even if the conjugate is diluted 2 times. QD concentration could also be a limited factor in an effort to use diluted conjugate for ELISA. We assume however that further dilution is possible and research in this direction is currently in progress.

2.3. Samples and PL measurement

After the final washing, ELISA wells were dried in air at room ambience for up to 120 min, and then each well was stored in a clear plastic box in order to minimize contamination of the wells. In order to eliminate a contribution of conjugated QDs which may occasionally be attached to the walls of the

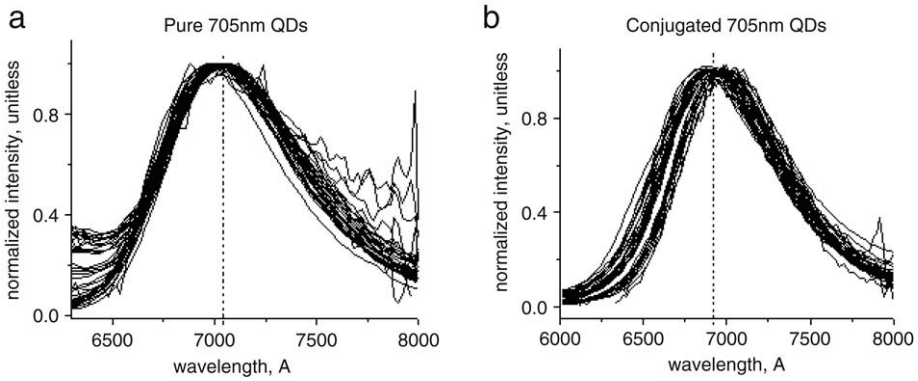

Fig. 2. Normalized PL spectra from the spectroscopic mapping on non-conjugated 705 nm QDs (a) and bio-conjugated with PSA antibody 705 nm QDs (b), dried on a silicon substrate. Dashed lines correspond to the PL peak positions averaged across the sample area.

well and have no relation to the "sandwich" formation, the bottom was separated from the walls using a clean heated blade which allowed an accurate cut. Spectroscopic measurements were conducted with ELISA bottoms only. We realize that this procedure is complicated and hardly to use as described in clinics, but it is quite suitable for the main purposes of this work — to research the possibility of forming a "sandwich" with conjugated QDs, using lower AG concentrations, and studying the scanning PL spectroscopy of bioconjugated QDs, involved in the "sandwich" formation.

In all experiments, the conjugated and non-conjugated portion of same-sized QDs was used as a reference. Individual droplets of the nonconjugated and conjugated solutions of the 3 μl volume were deposited on the unpolished surface of the crystalline Si wafer. Before the initial PL study, the droplets were dried in atmospheric ambience at room temperature forming clear spots on the silicon surface.

Both ELISA sample and dried QD spots deposited on silicon were used for spectroscopic PL mapping with a smallest step of 0.5 mm to produce a set of up to 100 individual PL spectra for each well and spot. The scanning PL spectroscopy was performed at room temperature using a 488 nm Ar laser with power density of 70 W/cm^2 as the excitation source. ELISA samples or silicon wafers with deposited QD spots were mounted on a computer-controlled X–Y moving stage. The typical mapping area was 8 mm × 8 mm for ELISA wells, and 3.5 mm × 3.5 mm for dried QD samples. The PL spectrum was dispersed by a SPEX 500M spectrometer and recorded by a cooled photomultiplier coupled with a lock-in amplifier. A detailed schematic and description of the PL system can be found elsewhere [29].

3. Results and discussion

3.1. PL spectral mapping on ELISA samples

In order to accurately measure, record and analyze the PL signal across the samples, a spectroscopic mapping technique was employed. PL spectra, obtained in the process of the spectral mapping of ELISA wells, were compared with the spectra, obtained from identical batch of nonconjugated and conjugated QDs, dried on the silicon substrate. The results are shown in Fig. 2.

It was shown in our previous works [29–31], that the "blue" spectral shift of different magnitudes on dried bioconjugated QDs was observed on different QDs and different antibody molecules. The positive "blue" shift magnitude correlation with the antibody molecular weight was also found [30]. In this work, the spectral mapping procedure revealed a non-uniform peak position across the dried spot of the bioconjugated QDs ranging from 682 nm in the central part of the sample up to 706 nm at the periphery. This pattern was observed previously and assigned to a "plate-shape" effect [30]. We will discuss below in more detail.

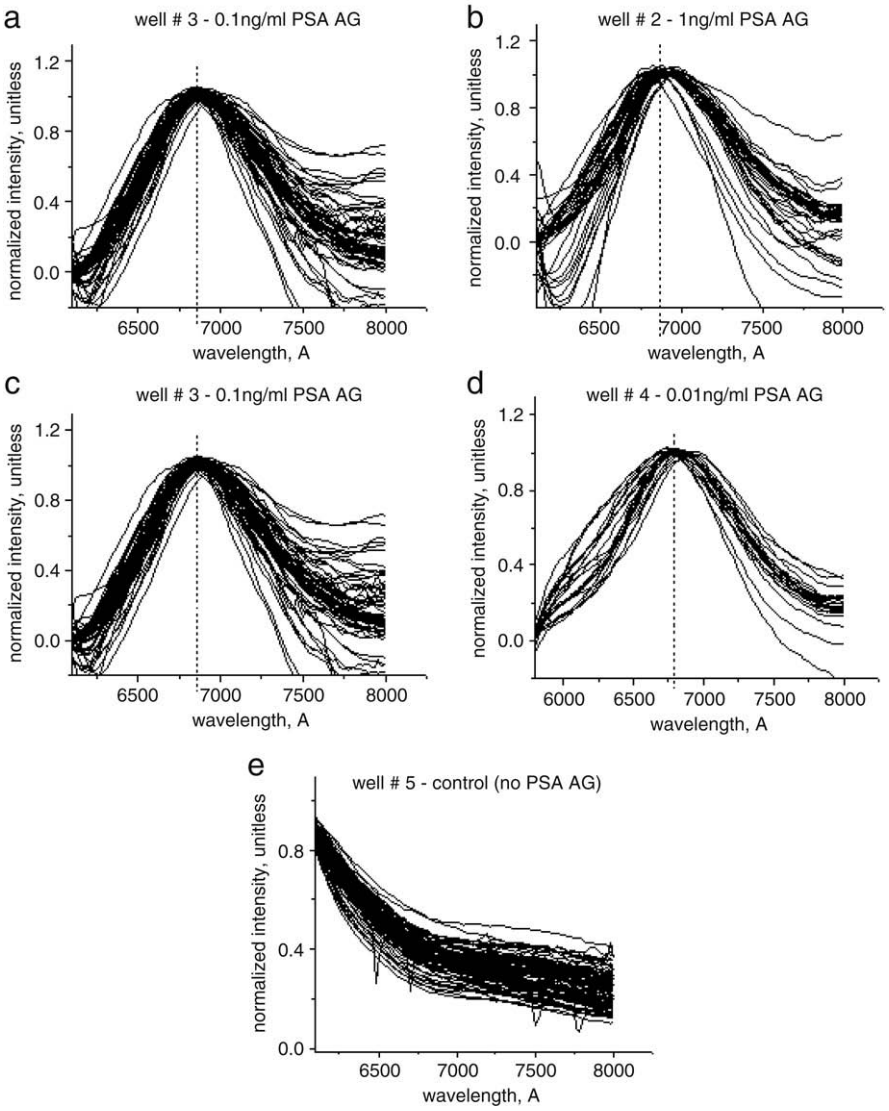

Fig. 3. Normalized PL spectra measured on ELISA wells #1–5 (a–e, respectively). Dashed lines correspond to the average PL peak positions.

Spectra, obtained from ELISA wells are shown in Fig. 3.

It is obvious that all wells, containing AG (b–d) provide the PL spectrum that matches with the QD luminescence. In contrast, the control well #5 without PSA AG shows a negligible PL peak intensity in the range of 575–800 nm, although was loaded with the same amount of conjugated QDs and undergone identical washing regime. Clearly, the AB*QD conjugate in the well #5 did not form a "sandwich" because of the PSA AG absence, and was therefore washed out. We point out that a residual optical signal observed in the well #5, is a spectroscopic tail of 488 nm laser line, scattered by the plastic well, and therefore has no relation to the QD luminescence. Well #1 was included in the experiment in order to compare the "blue" spectral shift of conjugated QDs in comparison to nonconjugated. Well #1 was precovered with primary AB in the same way as all other wells, but did

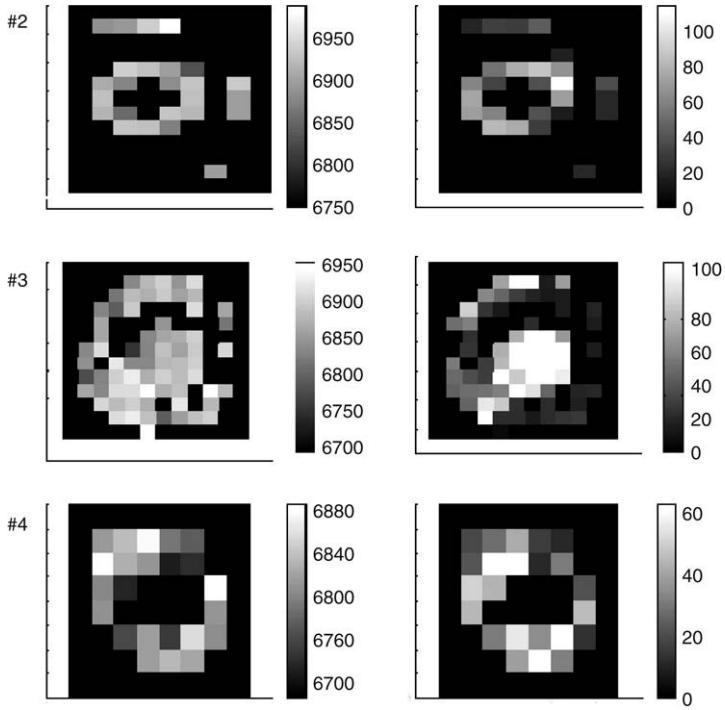

Fig. 4. Spectral maps of the ELISA wells #2–4. Left column — peak positions in A, right column — corresponding intensities [arb units].

not undergo any washing cycles, therefore, the PL spectral peak position of nonconjugated QDs, dried on the plastic ELISA well, could be taken from the well #1.

All ELISA wells, which contained PSA AG, have a PL signal from the conjugated QDs, involved in the "sandwich" formation. It was obvious that PL intensity and PL peak spectral position are not uniform across the well area, and this nonuniformity was tracked with the PL spectroscopic mapping procedure. The spectral maps of the #2–4 ELISA wells are shown in Fig. 4.

The spectral map of the well #1 is not informative (because nonconjugated QDs were simply dried in the well), while the well #5 does not exhibit a measurable PL intensity from the 705 nm PL band. The well #4 (with the smallest AG concentration of 0.01 ng/ml) shows the QD PL peaks mostly at the periphery area, the wells #2 at the center, and the well #3 all over the sample. This inhomogeneity can be attributed to a non-uniform capture of the PSA AG molecules by the capturing antibodies, when forming a sandwich structure.

In this experiment using the PL spectral mapping technique we observed a new effect, as a dependence of the "blue" spectral shift versus the AG concentration. In Fig. 5 the average peak positions, along with the standard deviations, are presented.

The average PL peak position is shifted to the short wavelengths with decreased AG concentrations, and its standard deviations are also increased with decreased AG concentrations. The average peak positions, along with their standard deviations, are as follows in wells #1–4: 7080 (+−10); 6900 (+−32); 6870 (+−40); 6810 (+−52). Additional research in the effort to confirm this interesting effect is currently in progress.

3.2. "Plate-shape" effect and residual nonconjugated QDs

As was described in our previous works [30,31], the authors found a so-called "plate-shape" effect on the QD samples dried on the solid surface (silicon). This effect was especially pronounced in

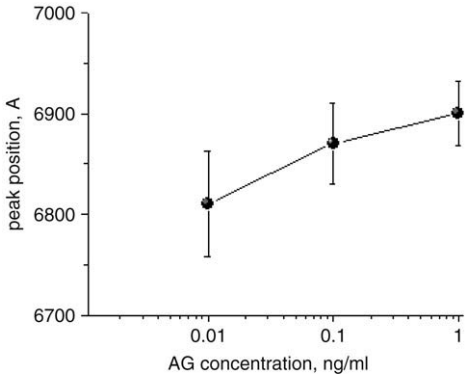

Fig. 5. Average spectroscopic peak (close to 705 nm) positions and their standard deviations (presented as error bars) of the ELISA samples with different AG concentrations.

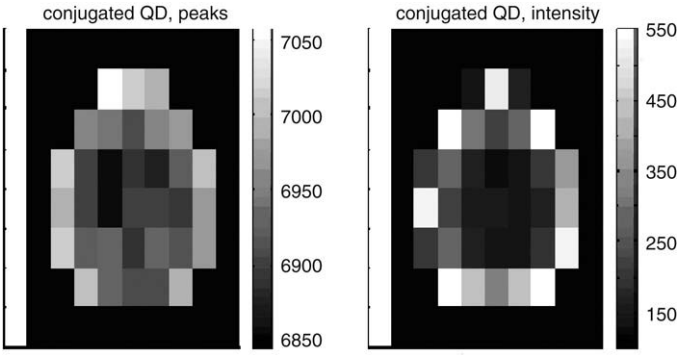

Fig. 6. Spectroscopic peak position (a) and PL intensity (b) maps of 705 nm QD sample, conjugated to PSA AB, dried on a clear silicon chip. Lighter areas correspond to elevated intensity/peak position values.

Table 1
Average peak positions for different conjugated samples and their magnitudes.

Sample	Average PL peak position (nm)	PL peak range (nm)
Conj dried on Si	694	**682–706**
Well #2	690	687–693
Well #3	687	675–694
Well #4	681	671–691

conjugated samples. It means the different intensity and peak profiles across the area of a dried sample, with both intensity and peak positions being elevated in the periphery region and decreased in the center. The typical ''plate-shape'' effect for 705 nm QD, conjugated to PSA AB, dried on the clear silicon chip, is shown on the Fig. 6.

The authors attributed this effect to either increased stress applied to QDs in the center, which may change their shape/size, or to the increased concentration of nonconjugated QDs in the periphery region, which is caused by their increased mobility because of their small size in comparison with heavy and bulky conjugated QDs. In the effort to approve one of these hypotheses, an average peak position values along with their ranges were analyzed for ELISA wells #2–4 and conjugated sample, presented in Fig. 6. The results are shown in the Table 1.

From the Table 1 it is clear that the upper limit of the sample, dried on the silicon surface, is 110–130 A elevated in comparison with any of the ELISA wells. And what is even more important,

is that the upper limit of the dried on Si chip conjugated sample surely lies on the very periphery (Fig. 6(a)) and corresponds to the wavelength of emission of pure, 705 nm QD sample, deposited on the silicon surface [30,31]. This helps to draw the conclusion that because only conjugated QDs take part in the ELISA "sandwich" formation, nonconjugated QDs, small fraction of which is always present in a conjugate, are washed away and do not interfere with the PL from conjugated QDs. However, when a small droplet of conjugate is deposited on silicon, the nonconjugated fraction of QDs contributes to the PL signal. This observation is important, because allows one to separate and eliminate the residual nonconjugation QDs, and their PL signal which may interfere with conjugated QDs and cause false positive results. It is also important, because serves as an additional proof that the PL, coming from ELISA wells, is the PL of conjugated 705 nm QDs, involved into the "sandwich" formation, and not the residual QDs, got stuck in the plastic.

4. Conclusions

"Sandwich" ELISA bimolecular tool enhanced with conjugated 705 nm QDs instead of commonly used luminescent dyes was employed to detect a PSA AG in the concentration range from 0.01 to 1.0 ng/ml. Three ELISA wells with AG concentrations 1.0, 0.1 and 0.01 ng/ml shows the PL peak, originated from the conjugated QDs in the sandwich structure with corresponding AG (PSA). The control well without AG molecules shows a negligible QD PL intensity. A short-wavelength, blue PL spectral shift was observed on all ELISA wells, utilizing conjugated QDs, and the values of this spectral shift (13–37 nm) were enhanced in comparison with the same QDs, conjugated to PSA AB, dried on a silicon substrate (2–26 nm). This fact was attributed to effective washing of nonconjugated QDs from the ELISA wells, which are always present in a conjugate mixture and therefore contribute to an average PL of the dried QD samples. In addition, a negative correlation was observed between an average "blue" PL spectral position and AG concentration. The origin of this effect is under investigation and presumably attributed to a decrease of elastic stress at higher AG concentrtaions. If confirmed, this will benefit the ultralow limits of detection for biomolecules, because "blue" spectral shift will increase with AG concentration decreasing, making it easier to distinguish between PL coming from "sandwiches" and possible traces of nonconjugated QDs or other contaminants at ultralow concentrations of a target molecule. This effect will also be useful in predicting the unknown biomolecule concentration based on the spectral shift position alone, eliminating a need for PL intensity assessment. The results of this research could lead to critical improvements for *in vitro* cancer antigen detection sensitivity using the QD luminescent tagging technique.

Acknowledgments

The work was supported by National Science Foundation award DMI-0523163, Department of Defense award PC050873 and by Ministry of Education and Science of Ukraine project M/207-2007.

References

[1] National Vital Statistics Report 55 (19) (2007).
[2] G.A. Colditz, T.A. Sellers, E. Trapido, Epidemiology–identifying the causes and preventability of cancer, Nat. Rev. Cancer 6 (2006) 75.
[3] S. Smith, S. Dave, Nie L. True, X. Gao, Multicolor quantum dots for molecular diagnostics of cancer, Expert Rev. M. Diag. 6 (2) (2006) 231–244.
[4] M.-K. So, C. Hu, A.M. Loening, S.S. Gambhir, J. Rao, Self illuminating quantum dot conjugates for in vivo imaging, Nat. Biotechnol. 24 (3) (2006) 339.
[5] M.N. Rhyner, A.M. Smith, X. Gao, H. Mao, L. Yang, S. Nie, Quantum dots and multifunctional nanoparticles: New contrast agents for tumor imaging, Nanomedicine 1 (2) (2006) 1–9.
[6] Y. Xing, Q. Shaudry, S. Shen, Bioconjugated quantum dots for multiplexed and quantitative immunochemistry, Nature Protocols 2 (5) (2007) 1152.
[7] E.R. Goldman, I.L. Medintz, H. Mattoussi, Luminescent quantum dots in immunoassays, Anal. Bioanal. Chem. 384 (3) (2006) 560.
[8] S. Pathak, S.K. Choi, N. Arnheim, M.E. Thompson, J. Amer. Chem. Soc. 123 (2001) 4103.
[9] Y. Xiao, P.E. Barker, Nucleic Acids Res. 32 (2004) 28.
[10] A. Crut, B. Geron-Landre, I. Bonnet, S. Bonneau, P. Desbiolles, C. Escude, Nucleic Acids Res. 33 (2005) 98.

[11] W.C.W. Chan, S. Nie, Science 281 (1998) 2016.
[12] Bruchez Jr., M. Moronne, P. Gin, S. Weiss, A.P. Alivisatos, Science 281 (1998) 2013.
[13] D.S. Lidke, P. Nagy, R. Heintzmann, D.-J. Arndt-Jovin, N.J. Post, H.E. Grecco, E.A. Jares-Erijman, T.M. Jovin, Nat. Biotechnol. 22 (2004) 198.
[14] B. Dubertret, P. Skourides, D.J. Norris, V. Noireaux, A.H. Brivanlou, A. Libchaber, Science 298 (2002) 1759.
[15] M. Han, X. Gao, J.Z. Su, S. Nie, Nat. Biotechnol. 19 (2001) 631.
[16] J.K. Jaiswal, H. Mattoussi, J.M. Mauro, S.M. Simon, Nat. Biotechnol. 21 (2003) 47.
[17] X. Wu, H. Liu, J. Liu, K.N. Haley, J.A. Treadway, J.P. Larson, N. Ge, F. Peale, M.P. Bruchez, Nat. Biotechnol. 21 (2003) 41.
[18] D.S. Goodsell, Bionanotechnology: Lessons from Nature, Wiley-Liss, Inc., New Jersey, 2004.
[19] SYPRO® Orange Protein Gel Stain Instruction Manual, http://www.bio.indiana.edu/~ybelab/procedures/SyproOrange.pdf.
[20] A.M. Skelley, R.A. Mathies, Chiral separation of fluorescamine-labeled amino acids using microfabricated capillary electrophoresis devices for extraterrestrial exploration, J. Chromatogr. A 1021 (2003) 191–199.
[21] S. Udenfriend, S. Stein, P. Böhlen, W. Dairman, W. Leimgruber, M. Weigele, Fluorescamine: A reagent for assay of amino acids, peptides, proteins, and primary amines in the picomole range, Science, New Series 178 (4063) (1972) 871–872.
[22] D. Gerion, F. Pinaud, S.C. Williams, W.J. Parak, D. Zanchet, S. Weiss, A.P. Alivisatos, Synthesis and properties of biocompatible water-soluble silica-coated CdSe/ZnS semiconductor quantum dots, J. Phys. Chem. B 105 (2001) 8861–8871.
[23] C. Warren, W. Chan, S. Nie, Quantum dot bioconjugates for ultrasensitive nonisotopic detection, Science 281 (1998) 2016–2018.
[24] A. Wolcott, D. Gerion, M. Visconte, J. Sun, A. Schwartzberg, S.W. Chen, J.Z. Zhang, J. Phys. Chem. B 110 (11) (2006) 5779–5789.
[25] Human PSA ELISA Kit from Abazyme, http://www.biocompare.com/itemdetails.asp?itemid=434262.
[26] C. Jurincic-Winkler, H. Von der Kammer, R. Horlbeck, K.-F. Klippel, H.U. Pixberg, K.-H. Scheit, Clinical evaluation of a new prostate-specific antigen sandwich ELISA which employs four monoclonal antibodies directed at different epitopes of prostate-specific antigen, Eur. Urol. 24 (4) (1993) 487–491.
[27] A.F. Dekairelle, B. Hoste, Application of a Y-STR-pentaplex PCR (DYS19, DYS389I and II, DYS390 and DYS393) to sexual assault cases, Forensic Sci. Int. 118 (2–3) (2001) 122–125.
[28] Itaru Sato, Morihisa Sagi, Atsuya Ishiwari, Hironori Nishijima, Emi Ito, Toshiji Mukai, Use of the SMITEST PSA card to identify the presence of prostate-specific antigen in semen and male urine, Forensic Sci. Int. 127 (2002) 71–74.
[29] M. Dybiec, G. Chornokur, S. Ostapenko, A. Wolcott, J.Z. Zhang, A. Zajac, C. Phelan, T. Sellers, Photoluminescence spectroscopy of bioconjugated CdSe/ZnS quantum dots, Appl. Phys. Lett. 90 (2007) 263112.
[30] G. Chornokur, S. Ostapenko, Yu Emirov, N.E. Korsunska, T. Sellers, C. Phelan, Spectroscopic behavior of bioconjugated quantum dots, Semicond. Sci. Technol. 23 (2008) 075045.
[31] Ganna Chornokur, Sergei Ostapenko, Yusuf Emirov, Nadezhda Korsunska, Abraham Wolcott, Jin Zhang, Catherine Phelan, Abhilasha Nagaram, Thomas Sellers, Biologically Engineered Quantum Dots for Biomedical Applications, in: MRS Proceedings, vol. 1095E, 1095-EE08-05, 2008.
[32] www.invitrogen.com.
[33] Chikako Suzuki, Hiroshi Ueda, Kouhei Tsumoto, Walt C. Mahoney, Izumi Kumagai, Teruyuki Nagamune, Open sandwich ELISA with Vh/Vl -alkaline phosphatase fusion proteins, J. Immunol. Methods 224 (1999) 171–184.